CHAPTER IV

RESULT AND DISCUSSION

This chapter describes the experimental results of two major areas of experiment were undertaken, firstly in regard to the use of waste sugar sediment as a component of Autoclaved Aerated Concrete. The result of the replacement of sand and lime in the concrete mix with the waste sugar sediment resulted in a concrete material that displayed significant improvements in compressive strength, and some improvement in the thermal transfer properties of the new material; Improved AAC.

Secondly, the results regarding the effectiveness of PCM coating, especially on the Improved AAC, were compared with uncoated building materials; brick, concrete block, and commercial autoclaved aerated concrete. This chapter therefore included both techno-economic and environmental analysis regarding the waste sugar sediment use and effect, and the insulative and thermal transfer effects of using PCM. A comparison of the economics and the evaluation of life cycle assessment of the Improved AAC was also investigated.

Technique analysis

Analysis results of optimal proportion for autoclaved aerated concrete

The variation between sand and sugar sediment (AAC-S)

In the first process (the substitution of fine sand by sugar sediment; AAC-S), the density with a variation of the sugar sediment contents is shown in Figure 25 and Table 9. The density of AAC-S was quite stable when the content of sugar sediment increased. The density was between 570 and 620 kg/m^3 when the content of sugar sediment was between 0 and 50 % by weight as shown in Table . All density values were claimed in quality class of 4 (510-800 kg/m^3), which is based on the Thai Industrial Standard 1505-1998.

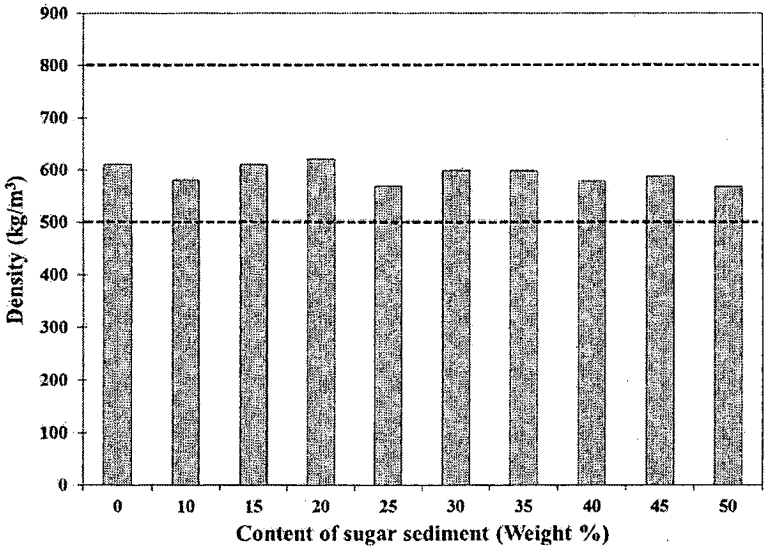

Figure 25 The density of AAC-S with various contents of sugar sediment.

The humidity with a variation of sugar sediment contents is shown in Figure 26 and Table 9. The humidity of AAC-S was not quite stable when the content of sugar sediment increased. The humidity was between 23 and 27% when the content of sugar sediment was between 0 and 50 % by weight as shown in Table 9.

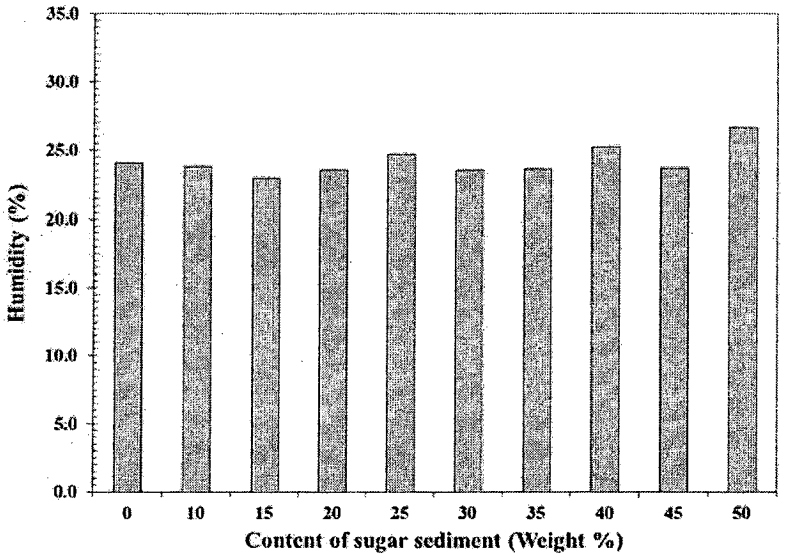

Figure 26 The humidity of AAC-S with different contents of sugar sediment

The water absorption and open porous volume with a variation of sugar sediment contents is shown in Figure 27 and Table 9. Water absorption of AAC-S remained stable even with the increase of the sugar sediment content. The water absorption was in the range of 380 and 400 kg/m^3 when the content of sugar sediment was between 0 and 50 % by weight as shown in Figure 27 (a) and Table 9. The open porous volume with a variation of sugar sediment contents is shown in Figure 27 (b) and Table 9. The open porous volume of AAC-S was not quite stable when the content of sugar sediment increased. The open porous volume was between 259 and 287 cm^3 when the content of sugar sediment was between 0 and 50 % by weight as shown in Table 9. It was observed that the maximum open porous volume was around 287 cm^3 was found at the sample of AAC-S40.

The compressive strength and the flexural strength with a variation of the sugar sediment contents are shown in Figure 28 and Table 9. In this first process (the substitution of fine sand by sugar sediment; AAC-S), the compressive strength increased and reached its highest at the sugar sediment content of 30 % by weight (AAC-S30) and then dropped in value when the sugar sediment content was higher than 30 % by weight, as shown in Figure 28 (a) and Table 9. The maximum compressive strength was around 5.9×10^6 N/m^2 obtained from the sample with the sugar sediment content of 30 % by weight (AAC-S30). The maximum compressive strength was claimed in quality class of 4 ($\geq 5 \times 10^6$ and $< 6 \times 10^6$ N/m^2), which also based on the Thai Industrial Standard 1505-1998. The flexural strength also obtained its highest at the sugar sediment content of 30 % by weight (AAC-S30) and then dropped in value when the sugar sediment content was higher than 30 % by weight, as shown in Figure 28 (b) and Table 9. The maximum flexural strength was around 1.81×10^6 N/mm^2 obtained from the sample with the sugar sediment content of 30 % by weight (AAC-S30). This value was claimed in quality class of 4 (30-40% of the compressive strength), which also based on the Thai Industrial Standard 1505-1998.

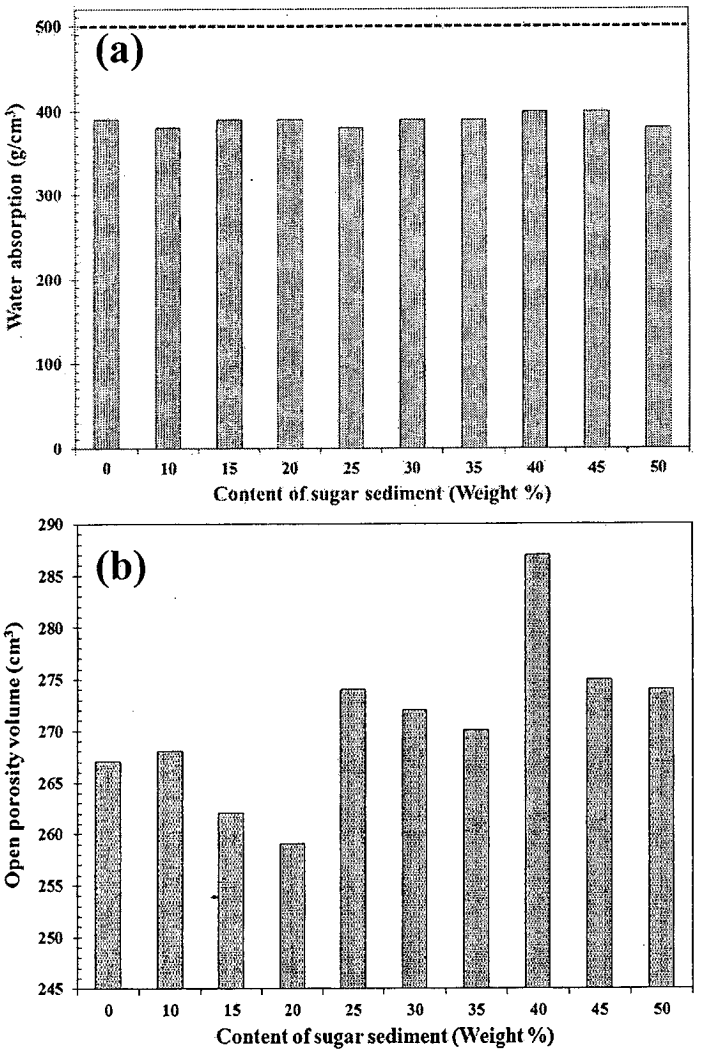

Figure 27 (a) The water absorption ratio and (b) the open porous volume of AAC-S with different sugar sediment contents.

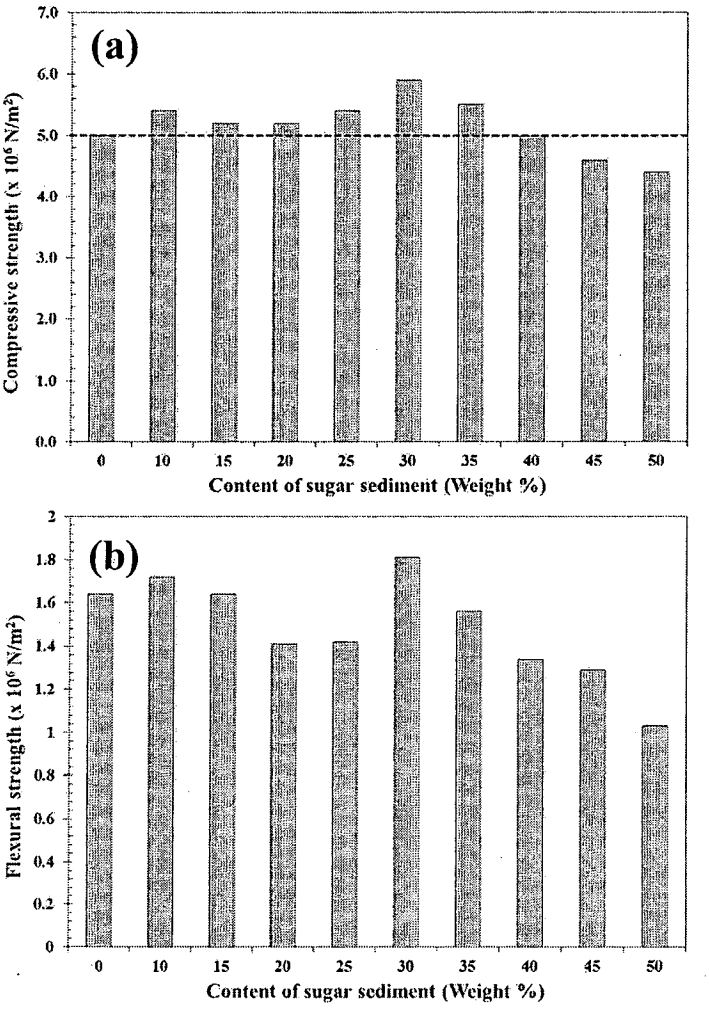

Figure 28 (a) The compressive strength and (b) the flexural strength of AAC-S with different contents of sugar sediment.

Table 9 The average density, humidity, water absorption, open porosity volume, compressive strength and flexural strength of AAC-S with the variation between sand and sugar sediment.

Characteristic properties of tested sample	Content of the sugar sediment (Weight %)									
	0	10	15	20	25	30	35	40	45	50
Density (kg/m^3)	610	580	610	620	570	600	600	580	590	570
Humidity (%)	24.1	23.8	23.0	23.6	24.7	23.6	23.7	25.3	23.8	26.7

Table 9 (cont.)

Characteristic properties of tested sample	Content of the sugar sediment (Weight %)									
	0	10	15	20	25	30	35	40	45	50
Water absorption (kg/m^3)	390	380	390	390	380	390	390	400	400	380
Open porosity volume (cm^3)	267	268	262	259	274	272	270	287	275	274
Compressive strength ($x\ 10^6\ N/m^2$)	5.0	5.4	5.2	5.2	5.4	5.9	5.5	5.0	4.6	4.4
Flexural strength ($x\ 10^6\ N/m^2$)	1.64	1.72	1.64	1.41	1.42	1.81	1.56	1.34	1.29	1.03

The variation between lime and sugar sediment (AAC-L)

In the second process (the substitution of lime by sugar sediment; AAC-L), the density with a variation of the sugar sediment contents is shown in Figure 29 and Table 10. The density of AAC-L was slightly decreased when the content of sugar sediment increased. The density was between 610 and 540 kg/m^3 when the content of sugar sediment was between 0 and 30 % by weight as shown in Table 10. All density values were claimed in quality class of 4 (510-800 g/cm^3), which is based on the Thai Industrial Standard 1505-1998.

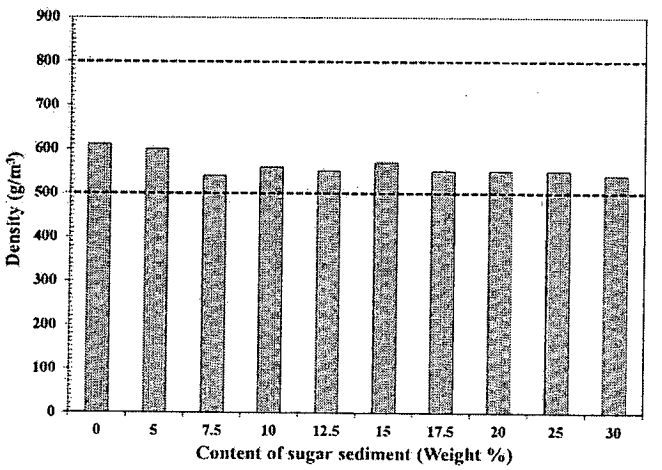

Figure 29 The density of AAC-L with various contents of sugar sediment.

The humidity with a variation of sugar sediment contents is shown in Figure 30 and Table 10. The humidity of AAC-L tended to increase and reached its highest at the sugar sediment content of 30 % by weight (AAC-L17.5) and then dropped in value when the sugar sediment content was higher than 17.5 % by weight, as shown in Figure 30. The humidity was between 24.1 and 27.8 % when the content of sugar sediment was between 0 and 30 % by weight as shown in Table 10. The maximum humidity was around 27.8 % obtained from the sample with the sugar sediment content of 17.5 % by weight (AAC-L17.5).

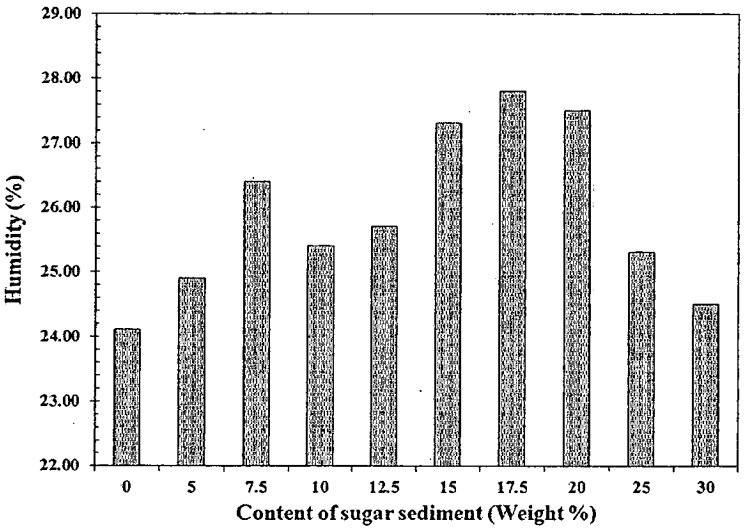

Figure 30 The humidity of AAC-L with different contents of sugar sediment

The water absorption and open porous volume with a variation of sugar sediment contents is shown in Figure 31 and Table 10. Water absorption of AAC-L remained stable even with the increase of the sugar sediment content. The water absorption was in the range of 380 and 430 kg/m^3 when the content of sugar sediment was between 0 and 30 % by weight as shown in Figure 31 (a) and Table 10. The maximum water absorption was around 430 kg/m^3 obtained from the sample with the sugar sediment content of 15 % by weight (AAC-L15). The open porous volume with a variation of sugar sediment contents is shown in Figure 31 (b) and Table 10. The open porous volume of AAC-L was not quite stable when the content of sugar sediment increased. The open porous volume was between 266 and 315 cm^3 when the

content of sugar sediment was between 0 and 30 % by weight as shown in Table 10. It was observed that the maximum open porous volume was around 315 cm^3 was found at the sample of AAC-L30.

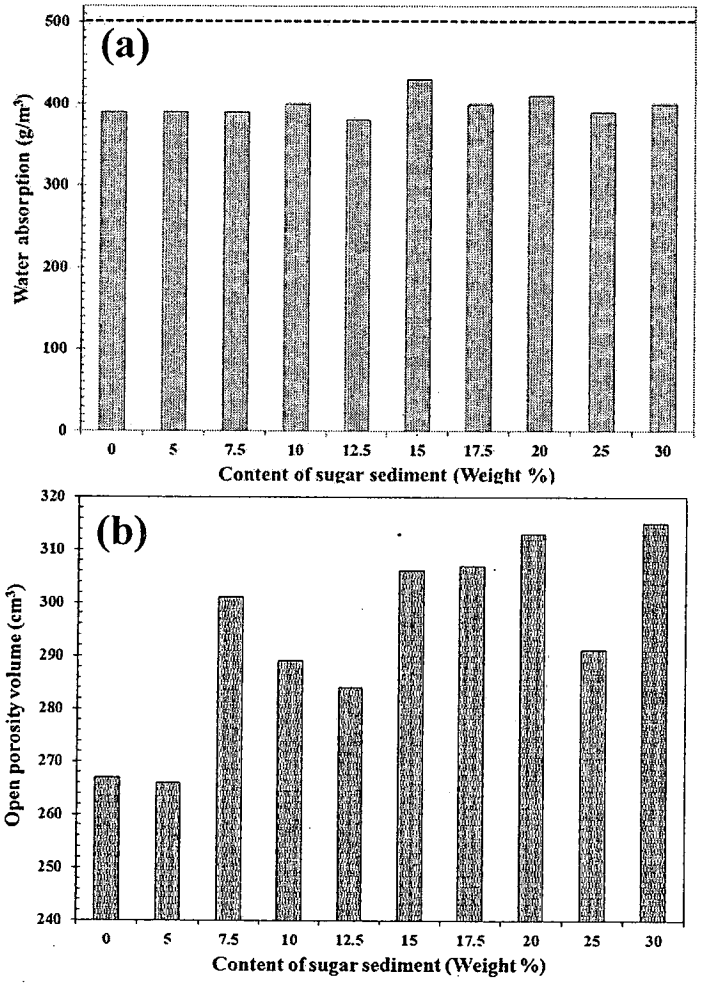

Figure 31 (a) The water absorption ratio and (b) the open porous volume of AAC-L with different sugar sediment contents.

The compressive strength and the flexural strength with a variation of the sugar sediment contents and lime are shown in Figure 32 and Table 10. In this second process (the substitution of lime by sugar sediment; AAC-L), the compressive strength increased and reached its highest at the sugar sediment content of 7.5 % by weight (AAC-L7.5) and then dropped in value when the sugar sediment content was higher than 7.5 % by weight, as shown in Figure 32 (a) and Table 10. The maximum

compressive strength was around 5.2 x 10^6 N/m^2 obtained from the sample with the sugar sediment content of 7.5% by weight (AAC-L7.5). The maximum compressive strength was claimed in quality class of 4 ($\geq$ 5 x 10^6 and < 6 x 10^6 N/m^2), which also based on the Thai Industrial Standard 1505-1998. The flexural strength of AAC-L was not quite stable when the content of sugar sediment increased as shown in Figure 32 (b) and Table 10. The maximum flexural strength was around 2.10 x 10^6 N/m^2 obtained from the sample with the sugar sediment content of 15 % by weight (AAC-L15). This value was not claimed in quality class of 4 (30-40% of the compressive strength) because the compressive strength of this composition was not in quality class of 4 ($\geq$ 5 x 10^6 and < 6 x 10^6 N/m^2). While, the flexural strength of AAC-L7.5 was around 1.95 x 10^6 N/m^2 which also based on the Thai Industrial Standard 1505-1998.

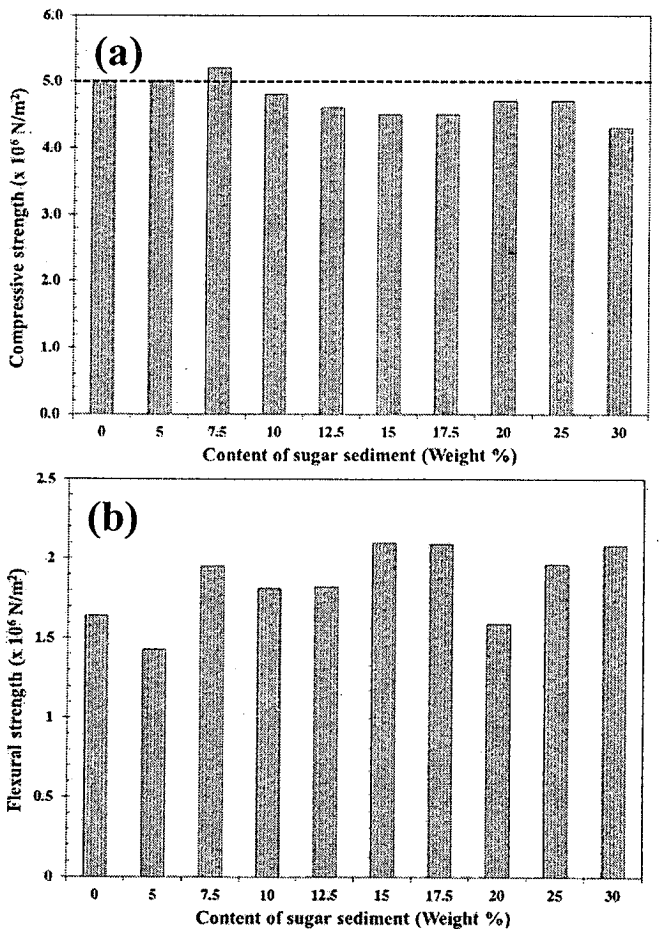

Figure 32 (a) The compressive strength and (b) the flexural strength of AAC-L with different contents of sugar sediment.

Table 10 The average density, humidity, water absorption, open porosity volume, compressive strength and flexural strength of AAC-L with the variation between lime and sugar sediment.

Characteristic properties of tested sample	Content of the sugar sediment (Weight %)									
	0	5	7.5	10	12.5	15	17.5	20	25	30
Density (kg/m^3)	610	600	540	560	550	570	550	550	550	540
Humidity (%)	24.1	24.9	26.4	25.4	25.7	27.3	27.8	27.5	25.3	24.5
Water absorption (kg/m^3)	390	390	390	400	380	430	400	410	390	400
Open porosity volume (cm^3)	267	266	301	289	284	306	307	313	291	315
Compressive strength (x 10^6 N/m^2)	5.0	4.5	5.2	4.8	4.6	4.5	4.5	4.7	4.7	4.3
Flexural strength (x 10^6 N/m^2)	1.64	1.43	1.95	1.81	1.82	2.10	2.09	1.59	1.96	2.08

The variation between sand/sugar sediment and fine recycling powder (AAC-SSR)

In the third process (the substitution of fine sand and sugar sediment by recycling powder; AAC-SSR), the density with a variation of the recycling powder contents is shown in Figure 33 and Table 11. The density of AAC-SSR tended to increase and reached its highest at the recycling powder content of 10-25 % by weight (AAC-SSR10, AAC-SSR15, AAC-SSR20 and AAC-SSR25) and then dropped in value when the recycling powder content was higher than 25 % by weight, as shown in Figure 33. The density was between 590 and 640 kg/m^3 when the content of recycling powder was between 0 and 45 % by weight as shown in Table 11. All density values were claimed in quality class of 4 (510-800 kg/m^3), which is based on the Thai Industrial Standard 1505-1998.

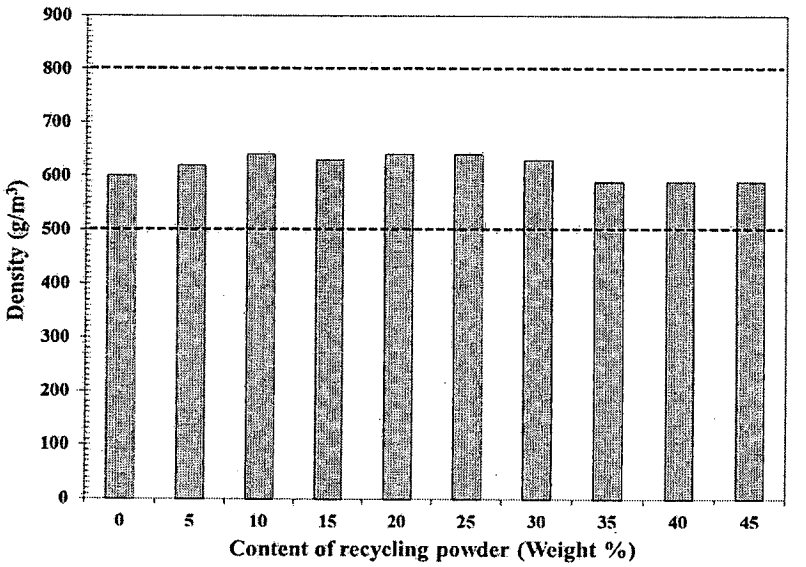

Figure 33 The density of AAC-SSR with various contents of fine recycling powder.

The humidity with a variation of the recycling powder contents is shown in Figure 34 and Table 11. The humidity of AAC-SSR tended to increase when there was an increase of the recycling powder contents. The humidity was between 21.6 and 29.0 % when the content of the recycling powder was between 0 and 45 % by weight as shown in Figure 34. The maximum humidity was around 29.0 % obtained from the sample with the recycling powder content of 45 % by weight (AAC-SSR45).

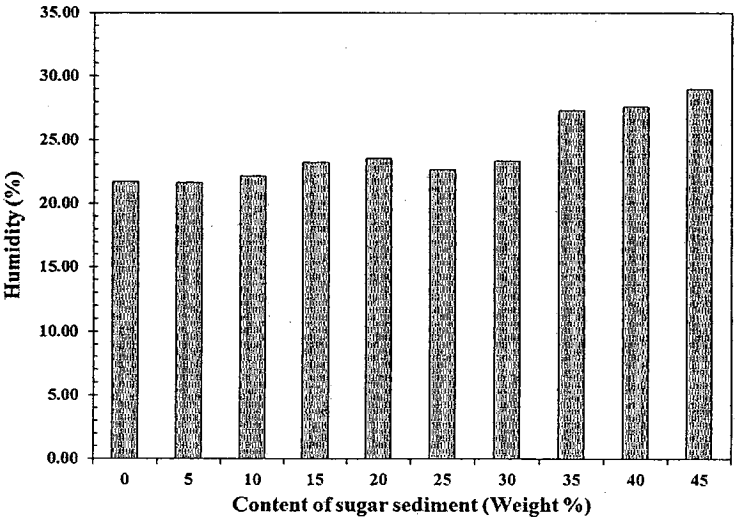

Figure 34 The humidity of AAC-SSR with different contents of fine recycling powder.

The water absorption and open porous volume with a variation of the recycling powder contents is shown in Figure 35 and Table 11. Water absorption of AAC-SSR tended to increase with the increase of the recycling powder content. The water absorption was in the range of 370 and 450 kg/m^3 when the content of the recycling powder was between 0 and 45 % by weight as shown in Figure 35 (a) and Table 11. The maximum water absorption was around 450 kg/m^3 obtained from the sample with the recycling powder content of 45 % by weight (AAC-SSR45). The open porous volume with a variation of the recycling powder contents is shown in Figure 35 (b) and Table 11. The open porous volume of AAC-SSR had similarly trend with the water absorption when the content of the recycling powder increased. The open porous volume was between 235 and 313 cm^3 when the content of the recycling powder was between 0 and 45 % by weight as shown in Table 11. It was observed that the maximum open porous volume was around 313 cm^3 was found at the sample of AAC-SSR45.

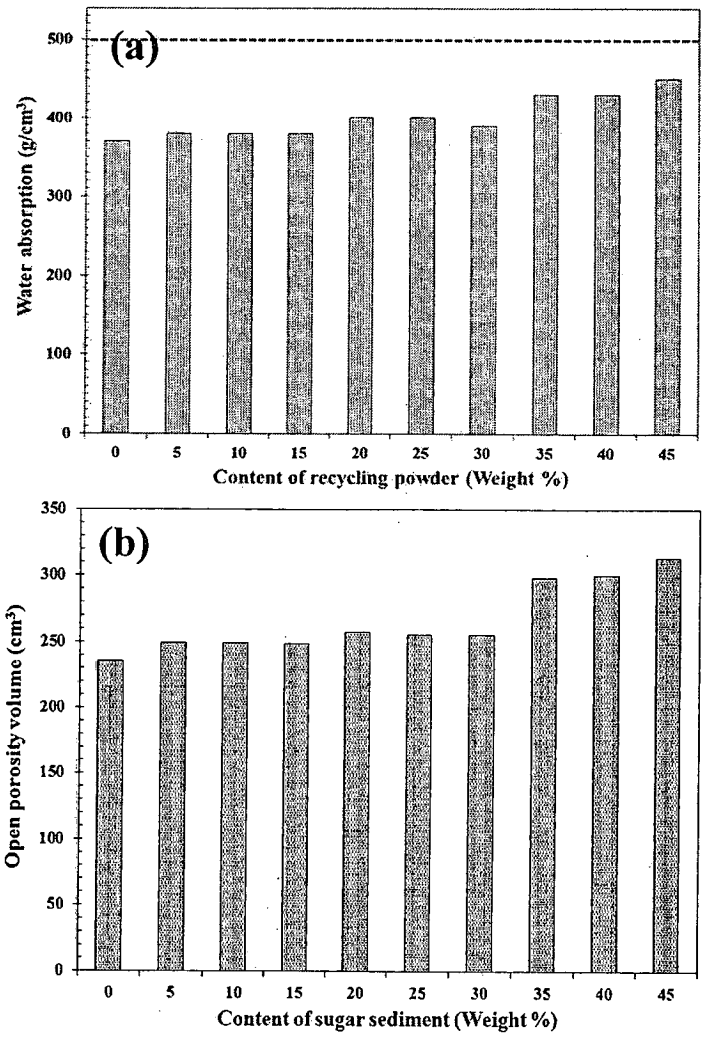

Figure 35 (a) The water absorption ratio and (b) the open porous volume of AAC-SSR with different fine recycling powder contents.

The compressive strength and the flexural strength with a variation of the recycling powder contents are shown in Figure 36 and Table 11. In this third process (the substitution of fine sand/sugar sediment by recycling powder; AAC-SSR), the maximum compressive strength was around 6.1 x 10^6 N/m^2 was found at the recycling powder content of 0 % by weight (AAC-SSR0). Subsequently, the compressive strength decreased extremely when the recycling powder content of 5 % by weight was added. Further, the compressive strength increased and reached its highest at the recycling powder content of 20 % by weight (AAC-SSR20) and then dropped in value

when the recycling powder content was higher than 20 % by weight, as shown in Figure 36 (a) and Table 11. The maximum compressive strength (6.1 x 10^6 N/m^2) was claimed in quality class of 4 ($\geq$ 5 x 10^6 and < 6 x 10^6 N/m^2), which also based on the Thai Industrial Standard 1505-1998. The flexural strength of AAC-SSR was not quite stable when the content of recycling powder contents increased as shown in Figure 36 (b) and Table 11. The maximum flexural strength was around 2.89 x 10^6 N/m^2 obtained from the sample with the recycling powder content of 40 % by weight (AAC-SSR45). For the flexural strength of AAC-SSR0, it was around 2.61 x 10^6 N/m^2. This value was claimed in quality class of 4 (30-40% of the compressive strength), which also based on the Thai Industrial Standard 1505-1998.

Table 11 The average density, humidity, water absorption, open porosity volume, compressive strength and flexural strength of AAC-SSR with the variation among sand, sugar sediment and fine recycling powder.

Characteristic properties of tested sample	Content of the fine recycling powder (Weight %)									
	0	5	10	15	20	25	30	35	40	45
Density (kg/m^3)	600	620	640	630	640	640	630	590	590	590
Humidity (%)	21.7	21.6	22.1	23.2	23.5	22.6	23.3	27.3	27.6	29.0
Water absorption (g/cm^3)	370	380	380	380	400	400	390	430	430	450
Open porosity volume (cm^3)	235	249	249	248	257	255	255	298	300	313
Compressive strength (x 10^6 N/m^2)	6.1	5.0	5.2	5.0	5.7	5.0	5.3	5.2	5.1	4.4
Flexural strength (x 10^6 N/m^2)	2.61	2.69	2.71	2.69	2.43	2.66	2.71	2.80	2.89	1.73

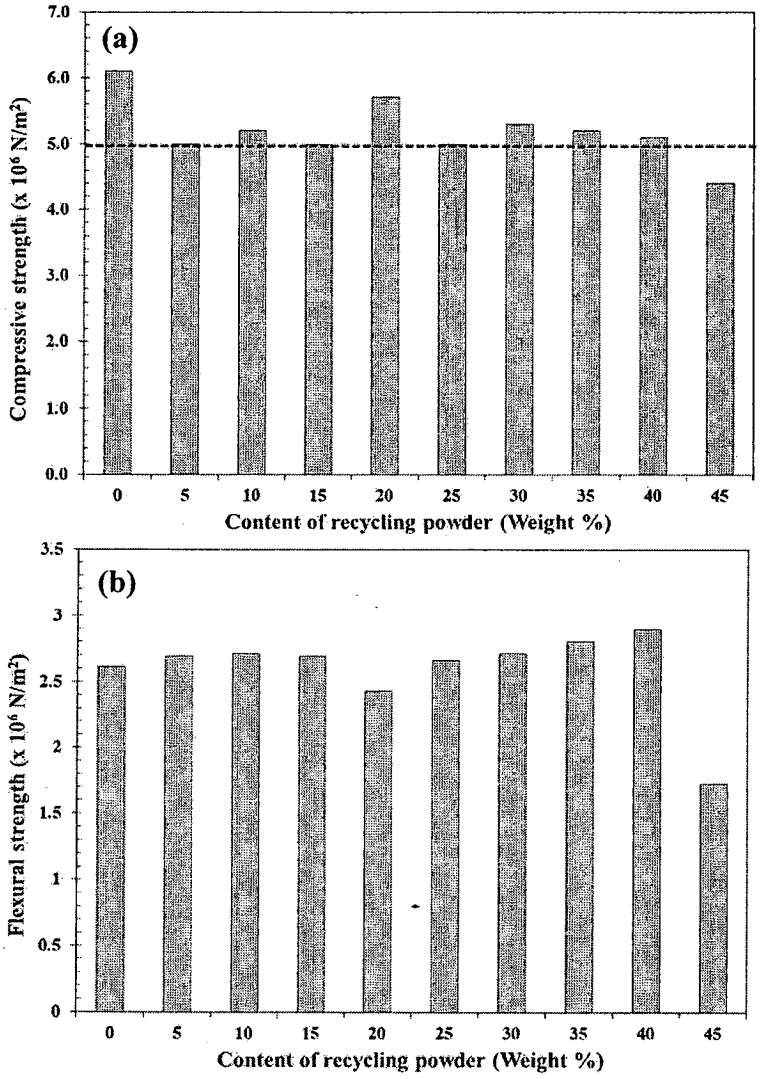

Figure 36 (a) The compressive strength and (b) the flexural strength of AAC-SSR with different contents of fine recycling powder.

Analysis result of phase change material (PCM)

Hydrated salt based Phase Change Material (PCM) generally appeared temperature range of various melting points that related to the outstanding working temperature range of PCM in heat storage capacity. This melting point of PCM therefore is important for suitable application. From a manufacturer data, there are several hydrated salt based PCM types such as S7, S8, S10, S13, S17, S19, S21, S23, S27, S30, S32, S44, S50, S58, S71, S72, S83, S89 and S117 which exhibited the

melting point at around 7 °C, 8 °C, 10 °C, 13 °C, 17 °C, 19 °C, 21 °C, 23 °C, 27 °C, 30 °C, 32 °C, 44 °C, 50 °C, 58 °C, 71 °C, 72 °C, 83 °C, 89 °C and 117 °C, respectively.

To apply to the wall temperatures of most buildings in Thailand in the range of 40-60 °C, S32 and S44 were selected for testing the thermal effectiveness of materials. Further, the temperature range of the melting point in Phase Change Material (PCM) type of S32 and S44 was investigated using DSC measurement, as shown in Figure 37 (a) and (b). The PCM type of S32 obviously exhibited 2 endothermic peaks as shown in Figure 37 (a). The first small endothermic peak was observed at ~30 °C as a result of the starting point of the PCM (S32) melting with a related enthalpy of 6,050 J/kg. Next, the effect of an increase in temperature to 60 °C resulted in the appearance of a second broadening endothermic peak at ~38 °C. This peak was due to the process of the molten PCM (S32) and continued with the first endothermic peak that was the result of the heat absorption of PCM (S32) with a related enthalpy of 137,670 J/kg. For the PCM type of S44, it only illustrated an endothermic peak as shown in Figure 37 (b). The broadening endothermic peak was observed at ~40.5 °C. This peak was due to the process of the molten phase change material that was the result of the heat absorption with a related enthalpy of 58,980 J/kg. These results indicated that the temperature range of melting point and the capacity of thermal storage of salt hydrated phase change material type of S32 were more efficient than that of S44. The salt hydrated phase change material could be thereby considered for coating on the outside surface of AAC when used for construction in Thailand, as the temperature ranges emulated Thai temperature conditions, and was therefore used to construct one of the test houses.

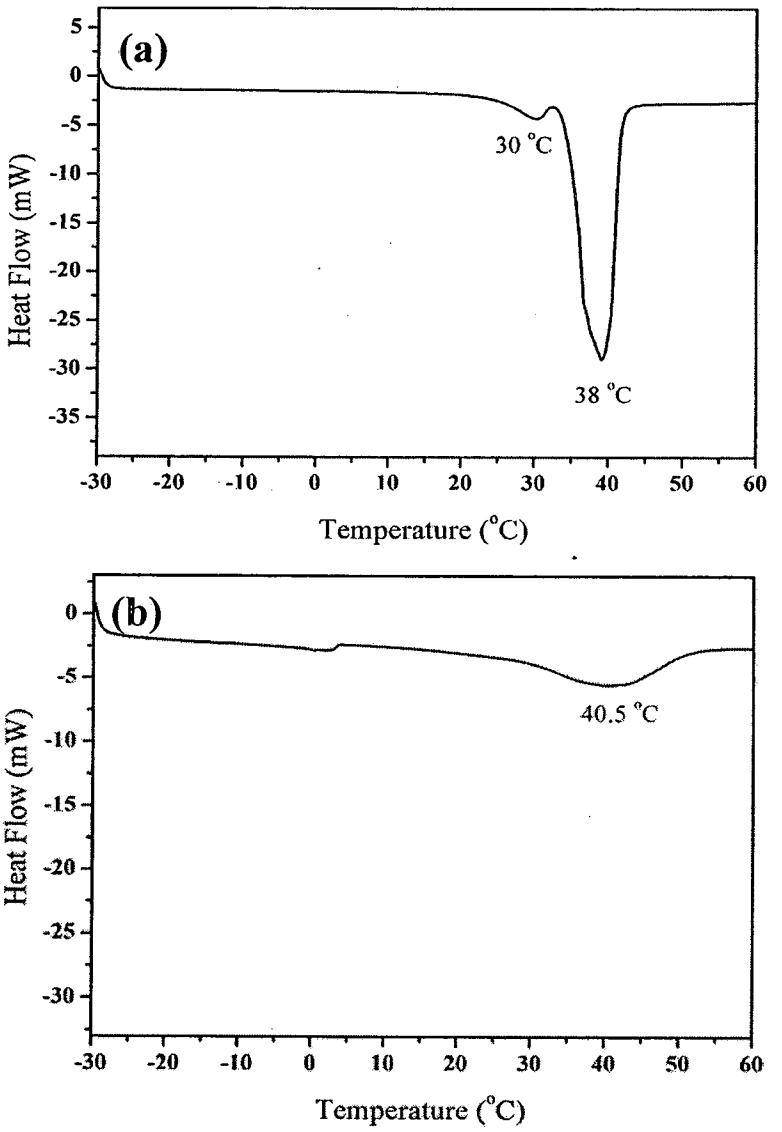

Figure 37 DSC plots showing the melting point of PCM: (a) S32 and (b) S44.

Phase formation analysis result of autoclaved aerated concrete by X-ray diffraction

A survey of the literature has found that previous works only reported that the presence of tobermorite structure in AAC had affected higher strength [42, 86, 87]. Further, the higher crystallinity of tobermorite phases in AAC samples resulted in superior strength as has been reported by Yang, et al. [85] and Ungkoon, et al. [88]. Notwithstanding, an increased quantity of the tobermorite phase proportion, which appeared in the autoclaved aerated concrete, has not been clearly reported in the previous works [20, 21, 22, 23, 24, 25, 26, 27, 28, 29, 30, 31, 32, 85, 88].

To investigate and confirm that the increase of the tobermorite crystalline proportion had an influence on the increased strength in the autoclaved aerated concrete, the optimum composition in each process was considered in the study which compared the phase formation of AAC. This study was carried out by X-ray diffraction (XRD) to demonstrate the proportion of tobermorite crystalline in AAC-S0, AAC-S30, AAC-L7.5, AAC-SSR0 and AAC-SSR20. The X-ray diffraction patterns of AAC-S0, AAC-S30, AAC-L7.5, AAC-SSR0 and AAC-SSR20 are illustrated in Figure 38. The phases of calcite, quartz and tobermorite were detected in the AAC-S0, AAC-S30, AAC-L7.5, AAC-SSR0 and AAC-SSR20. Three phases of AAC-S0, AAC-S30, AAC-L7.5, AAC-SSR0 and AAC-SSR20 were indexed on the basis of the rhombohedral, hexagonal and orthorhombic structure which matched with JCPDS file number 02-0629, 05-0490 and 06-0359, respectively. To study the ratio of the phases in each sample, the percentage of three phases ratio was calculated with the equation (4.1), (4.2) and (4.3) which are the well-known equations widely employed in connection with the preparation of complex structure materials [89]. Here $I_{calcite}$, I_{quartz} and $I_{tobermorite}$ referred to the intensities of the highest calcite, quartz and tobermorite peaks, respectively.

$$\% \text{ ratio of the calcite phase} = \left(\frac{I_{Calcite}}{I_{Quartz} + I_{Tobermorite} + I_{Calcite}} \right) \times 100 \quad (4.1)$$

$$\% \text{ ratio of the quartz phase} = \left(\frac{I_{Quartz}}{I_{Quartz} + I_{Tobermorite} + I_{Calcite}} \right) \times 100 \quad (4.2)$$

$$\% \text{ ratio of the tobermorite phase} = \left(\frac{I_{Tobermarite}}{I_{Quartz} + I_{Tobermorite} + I_{Calcite}} \right) \times 100 \quad (4.3)$$

The percentage of the phase ratio of the calcite, quartz and tobermorite in AAC-S0, AAC-S30, AAC-L7.5, AAC-SSR0 and AAC-SSR20 was computed and are listed in Table 12. For the first, second and third process, AAC-S30, AAC-L7.5, AAC-SSR0 and AAC-SSR20 showed the high compressive strength. These compositions were analyzed and compared to the tobermorite phase proportion with AAC-S0

(without adding the sugar sediment). It was found that the maximum ratio of calcite, quartz and tobermorite phases was appeared from the samples of AAC-SSR0, AAC-S0 and AAC-SSR0 had values of approximately 37.4, 75.7 and 28.9%, respectively. The higher ratio of tobermorite and calcite phases and the lower ratio of quartz phase corresponded to the higher compressive strength were obviously evident as illustrated in Table 12. This shows that the traditional raw materials sand and lime were replaced by the sugar sediment waste influenced the change of the phase ratio in AAC. This result confirms that the increasing of the tobermorite phase improved the mechanical properties of AAC. Importantly, this result is in a good agreement with previous works [85, 88].

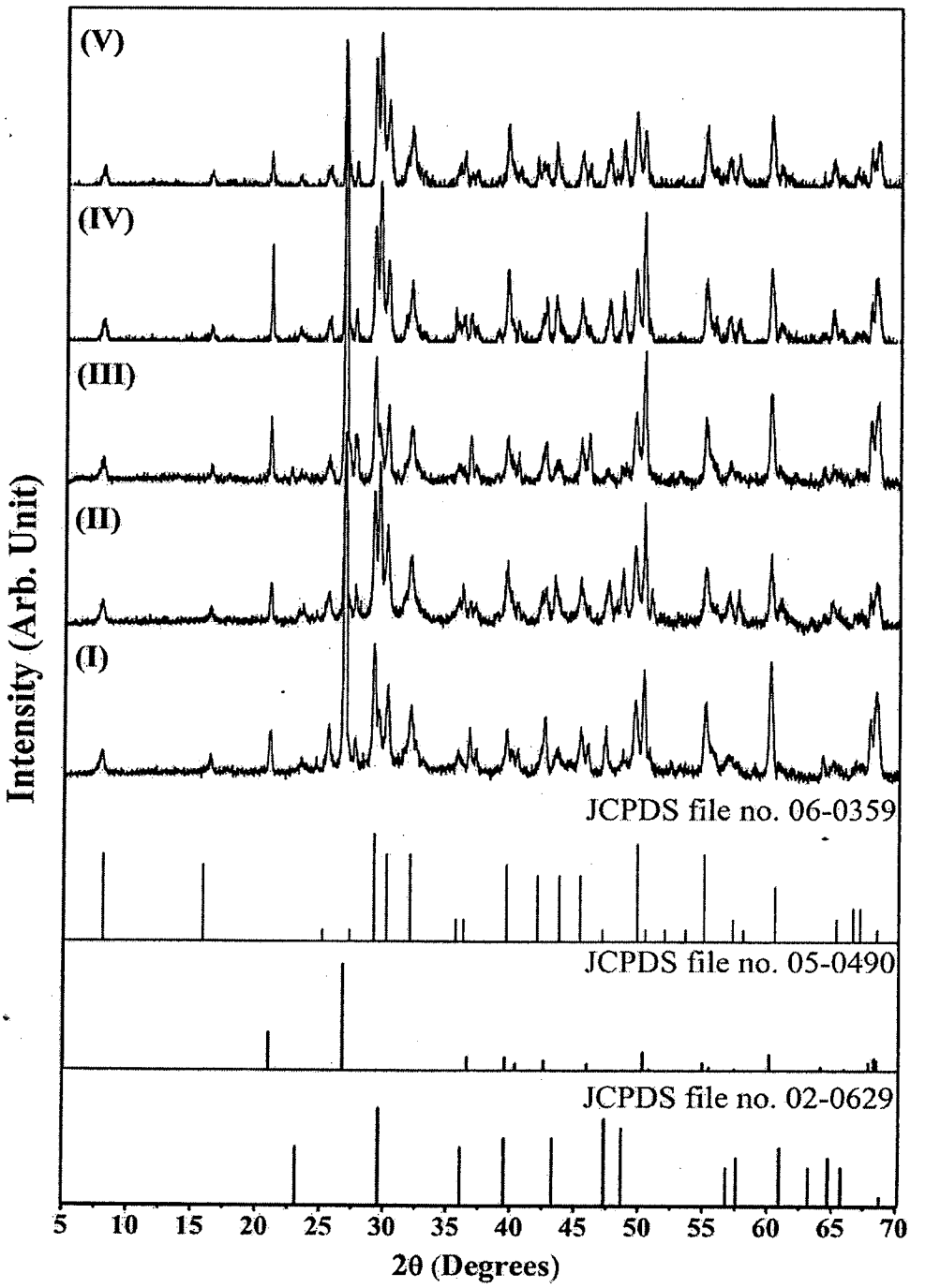

Figure 38 X-ray diffraction patterns of AAC with different compositions in the 2θ range of 5° to 70°: (I) AAC-S0, (II) AAC-S30, (III) AAC-L7.5, (IV) AAC-SSR0 and (V) AAC-SSR20.

Table 12 The ratio of phase formation of AAC with different compositions.

Composition	Ratio of phase formation (%)		
	Calcite	Quart	Tobermorite
AAC-S0	8.2	75.7	16.1
AAC-S30	32.4	40.1	27.5
AAC-L7.5	9.8	67.2	22.9
AAC-SSR0	37.4	33.7	28.9
AAC-SSR20	28.9	48.2	22.9

Microstructure analysis result by the scanning electron microscopy

To exhibit the microstructure of the traditional composition of AAC (AAC-S0) and the improved composition of AAC (AAC-S30, AAC-L7.5, AAC-SSR0 and AAC-SSR20), Figure 39 (a) - (e) illustrate the morphological AAC-S0 surface, AAC-S30 surface, AAC-L7.5 surface, AAC-SSR0 surface and AAC-SSR20 surface. The features of the AAC-S0, AAC-S30, AAC-L7.5, AAC-SSR0 and AAC-SSR20 microstructure surface were the finer needle-like crystalline structures and all had a porous combined form. The sub-micron needle crystal of AAC-S0, AAC-S30, AAC-L7.5, AAC-SSR0 and AAC-SSR20 overlapped each other forming a firm skeleton and emptied the cavities between the layers. This implied that the microstructure of all samples shows a high compressive strength. While, the integration of spherical morphology into sub-micron needle crystal was appeared in the sample of AAC-SSR20 as shown in Figure 39 (e). This may be caused from the recycling powder was incorporated into the raw material mix for the production of autoclaved aerated concrete. The formation of the needle-like crystalline structure of AAC-SSR0 clearly had the largest crystalline size in all samples (AAC-S0, AAC-S30, AAC-L7.5, AAC-SSR0 and AAC-SSR20). The crystallized tobermorite size of AAC-S0 was between 55-160 nm in width and 1.1-3.2 μm in length. The crystallized tobermorite size of AAC-S30 was between 83-180 nm in width and 1.25-4.5 μm in length. The crystallized tobermorite size of AAC-L7.5 was between 40-160 nm in width and 1.1-3.5 μm in length. The crystallized tobermorite size of AAC-SSR0 was between 83-204 nm in width and 1.25-6 μm in length. The crystallized tobermorite size of

AAC-SSR20 was between 76-194nm in width and 1.3-4.5 μm in length. The larger crystalline size of AAC-SSR0 appears to correspond to the higher compressive strength and the increase of tobermorite phase.

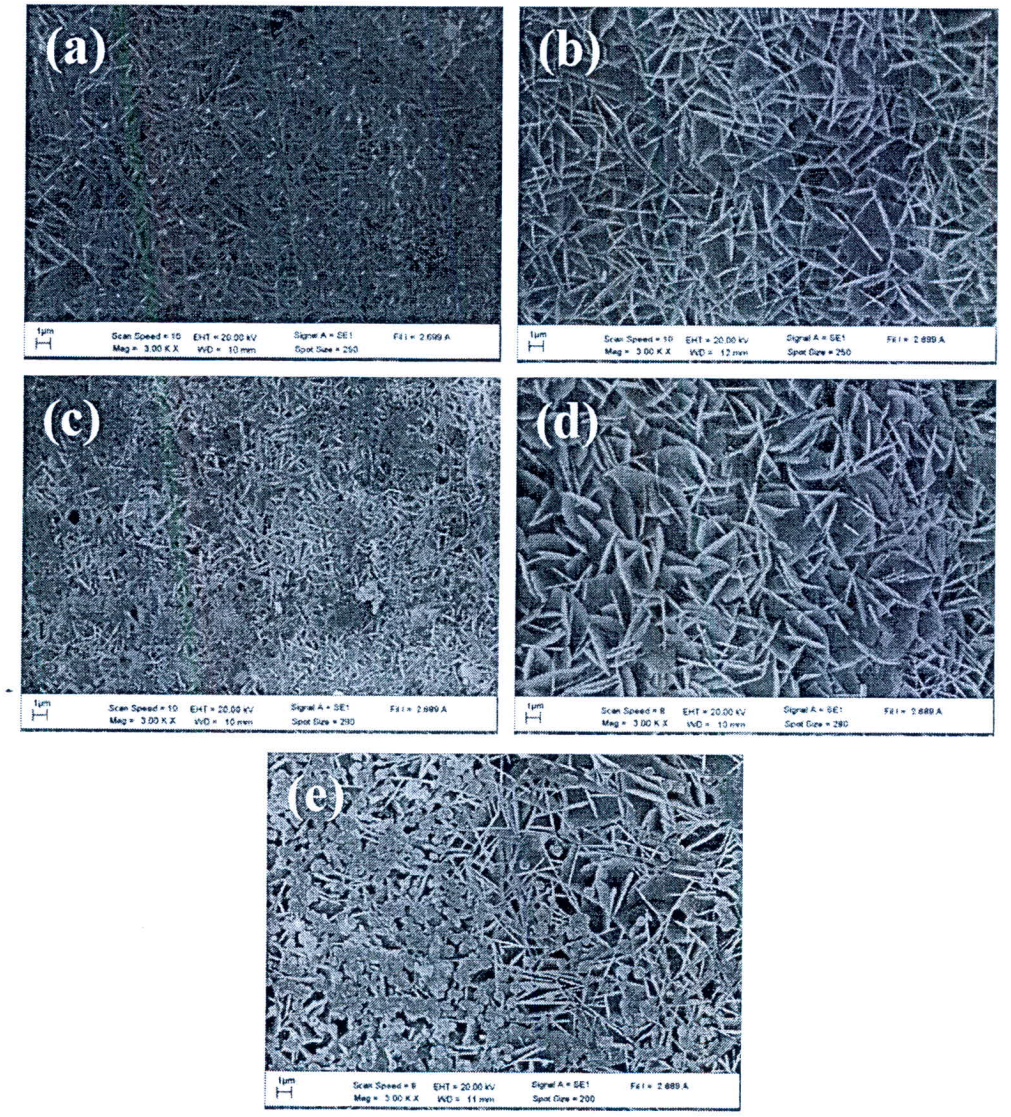

Figure 39 SEM photographs of AAC surface at different systems: (a) AAC, (b) AAC-SS30, (c) AAC-L7.5, (d) AAC-SSR0 and (e) AAC-SSR20

Thermal test results of optimal proportion of autoclaved aerated concrete with different contents of phase change material

The wall temperature (T_w), and the room temperature (T_{room}) of the test brick wall with cement coating are illustrated in Figure 40-Figure 42 and Table 13. The wall temperature of brick in each temperature condition as a function of the different thicknesses is shown in Figure 40-Figure 42 and Table 13. The wall temperature of brick in each temperature condition decreased when there was an increase of thickness from 0 to 80 mm. Total thermal resistances of brick is also shown in Table 13.

Time lag and decrement factor of the brick wall

The time lag (Φ) and the decrement factor (λ) [90, 91] are the parameters used to assess the thermal performance of the wall. The time lag is the time taken by the heat wave to propagate from the outer surface to the inner surface. The decrement factor is the decreasing ratio of its temperature amplitude [90, 91]. Therefore, the heat flux time lag and decrement factor are defined by the following equations (4.4) and (4.5).

$$\Phi = \tau_{qi,max} - \tau_{qe,max} \tag{4.4}$$

$$\lambda = \frac{A_i}{A_e} = \frac{q_{i,max} - q_{i,min}}{q_{e,max} - q_{e,min}} \tag{4.5}$$

Where $\tau_{qi,max}$, $\tau_{qe,max}$ are the times that the interior surface heat flux and the exterior surface heat flux of the wall are at a maximum, respectively. A_i and A_e are the amplitudes of the wave in the inner and in the outer surfaces of the wall respectively. $q_{i,max}$, $q_{i,min}$, $q_{e,max}$, $q_{e,min}$ are the maximum and the minimum heat flux of the interior and the exterior surface of the wall, respectively.

When the thermal source was controlled at the temperature of 40 °C, it was found that the time lag of brick wall increased from 32 to 38 min while the decrement factor decreased from 0.412 to 0.342 when the thickness of brick wall increased from 0 to 80 mm. When the thermal source was controlled at temperatures of 50 and 60 °C, the time lag and decrement factor at these 2 temperatures were similar to that of the temperature of 40 °C with the increase of brick wall thickness, as shown in Table 13.

This result shows that time lag and decrement factor are related to the thickness of the AAC wall. A closer reading of Table 13 will show that time lag was positively proportionate to the thickness of the wall while the decrement factor increased inversely to its thickness. This indicated that an increase of wall thickness will result in lower heat flow.

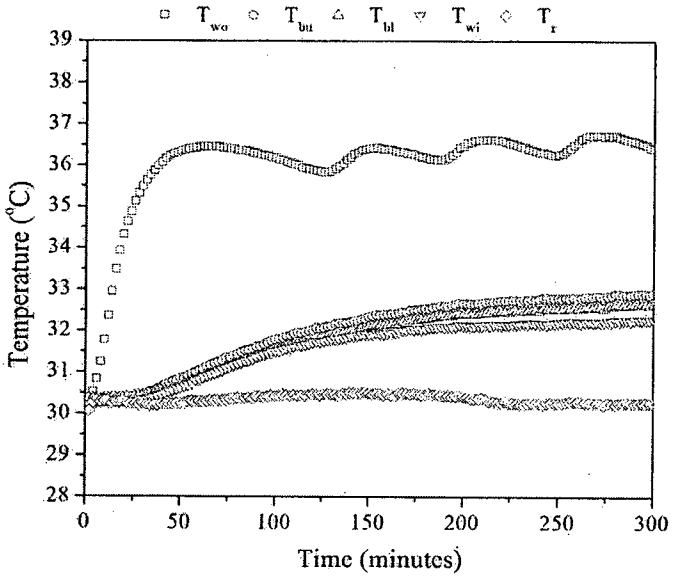

Figure 40 Temperature revolution of brick wall at the test temperature of 40 °C.

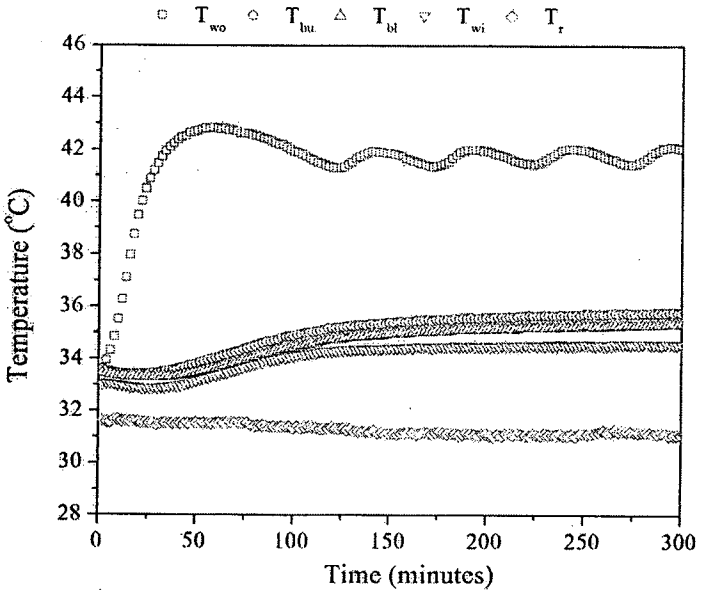

Figure 41 Temperature revolution of brick wall at the test temperature of 50 °C.

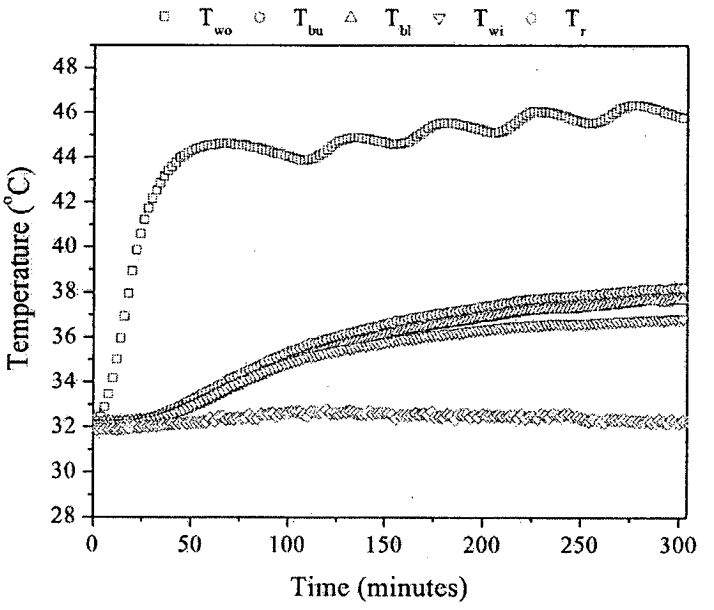

Figure 42 Temperature revolution of brick wall at the test temperature of 60 °C.

Table 13 The total thermal resistance (R), the heat conduction (Q), wall temperature (T_w), and the room temperature (T_{room}), the time lag (τ), and decrement factor (λ) of brick.

R (m^2·K/W)	Q (W)	Temperature	x(mm)	T_w (°C)	τ (min)	λ	T_{room}
0.1697	25.34	40	0	36.5			30.3
			30	32.6	32	0.412	
			45	32.5	34	0.377	
			80	32.2	38	0.342	
	45.37	50	0	41.8			31.2
			30	35.7	28	0.718	
			45	35.2	32	0.690	
			80	34.5	34	0.662	
	54.21	60	0	45.8			32.4
			30	37.8	28	0.865	
			45	37.3	30	0.750	
			80	36.9	32	0.711	

The thermal resistance, wall temperature (T_w), and room temperature (T_{room}) of the original AAC without sugar sediment (AAC-S0), AAC with 0.050 kg of PCM-coated external surface (AAC-S0-50), AAC with 0.10 kg of PCM-coated external surface (AAC-S0-100), AAC with 0.050 kg of PCM-coated external surface and cement-coated surface in both sides (AAC-S0-50C) and AAC with 0.10 kg of PCM-coated external surface and coated cement surface in both sides (AAC-S0-100C) walls are illustrated in Figure 43-Figure 57 and Table 14. The wall temperature of the AAC-S0, AAC-S0-50, AAC-S0-100, AAC-S0-50C and AAC-S0-100C walls in each temperature condition as a function of the different thicknesses is shown in Figure 43-Figure 57 and Table 14. The wall temperature of the AAC-S0, AAC-S0-50, AAC-S0-100, AAC-S0-50C and AAC-S0-100C walls in each temperature condition decreased when there was an increase of thickness from 0 to 75 mm as shown in Figure 43-Figure 57 and Table 14.

Time lag and decrement factor of AAC at different conditions

The time lag (Φ) and decrement factor (λ) of the AAC-S0, AAC-S0-50, AAC-S0-100, AAC-S0-50C and AAC-S0-100C walls are illustrated in Table 14. When the thermal source was controlled at the temperature of 40 °C, it was found that the time lag of the AAC-S0 wall increased from 18 to 68 min while the decrement factor decreased from 0.418 to 0.032 when the thickness of the AAC-S0 wall increased from 0 to 75 mm. When the thermal source was controlled at temperatures of 50 and 60 °C, the time lag and decrement factor at these 2 temperatures were similar to that of the temperature of 40 °C with the increase of the AAC-S0 wall thickness, as shown in Table 14. For the cases of AAC-S0-50, AAC-S0-100, AAC-S0-50C and AAC-S0-100C, the time lag also increased from 30 to 80 min, 26 to 56 min, 26 to 50 min and 20 to 46 min while the decrement factor decreased from 0.224 to 0.032, 0.269 to 0.177, 0.207 to 0.0024 and 0.280 to 0.072 when the thickness of the wall increased from 0 to 75 mm, as listed in Table 14. This result shows that time lag and decrement factor are related to the thickness of the AAC wall. A closer reading of Table 14 will show that time lag was positively proportionate to the thickness of the wall while the decrement factor increased inversely to its thickness. This indicated that an increase of wall thickness will result in lower heat flow.

With comparing the time lag and decrement factor between AAC-S0, AAC-S0-50 and AAC-S0-100 in each condition, the time lag of AAC-S0 and AAC-S0-100 were slightly less than that of AAC-S0-50. As well, the decrement factor of AAC-S0 and AAC-S0-100 was slightly higher than that of AAC-S0-50. This demonstrates that the optimal composition of AAC-S0-50 can slightly extend the time of the heat wave to propagate from the outer wall to the inner wall and obviously decrease the ratio of its amplitude during this process when compared to the composition of AAC-S0 and AAC-S0-100. This result shows that the room temperature of AAC-S0-50 was approximately 1-3 °C lower than that of the AAC-S0 and AAC-S0-100, the longer time lag does have an effect, as exhibited in Table 14.

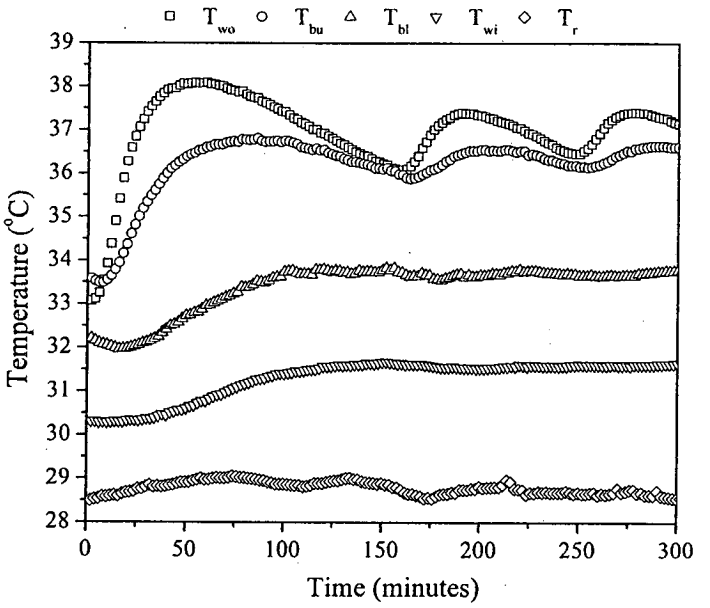

Figure 43 Temperature revolution of AAC at the test temperature of 40 °C.

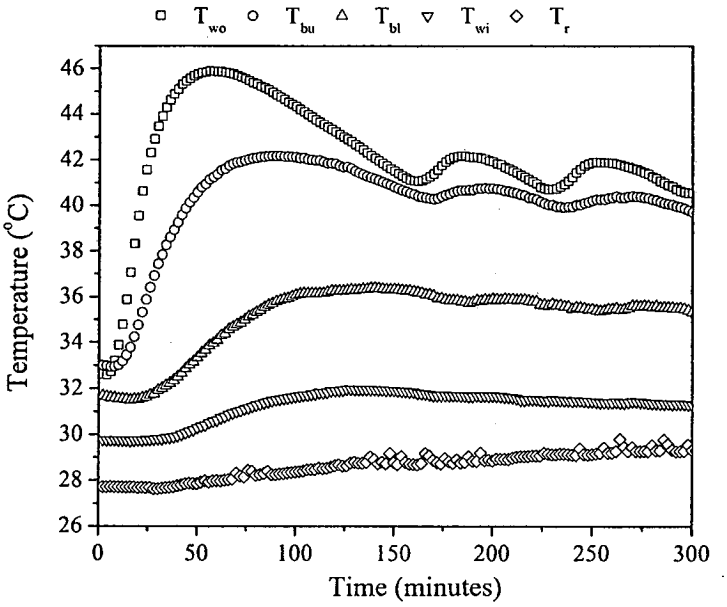

Figure 44 Temperature revolution of AAC at the test temperature of 50 °C.

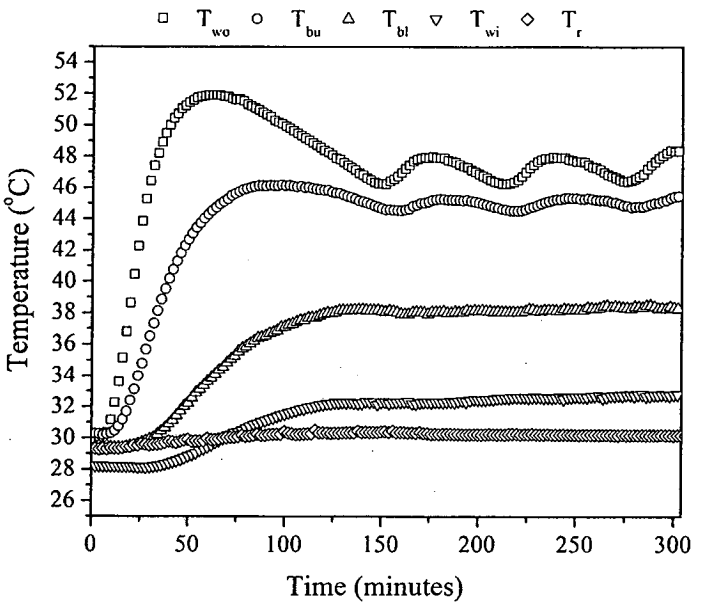

Figure 45 Temperature revolution of AAC at the test temperature of 60 °C.

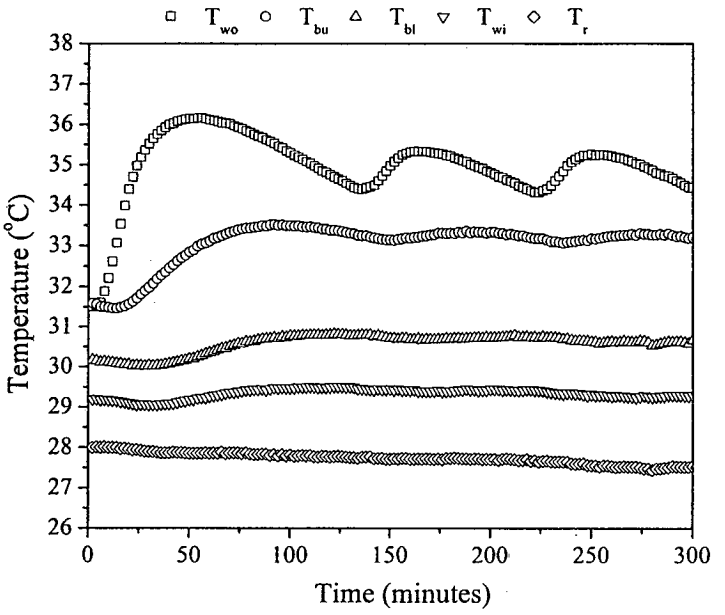

Figure 46 Temperature revolution of PCM-coated AAC wall (0.050 kg or ~0.417 kg/m^2) at the test temperature of 40 °C.

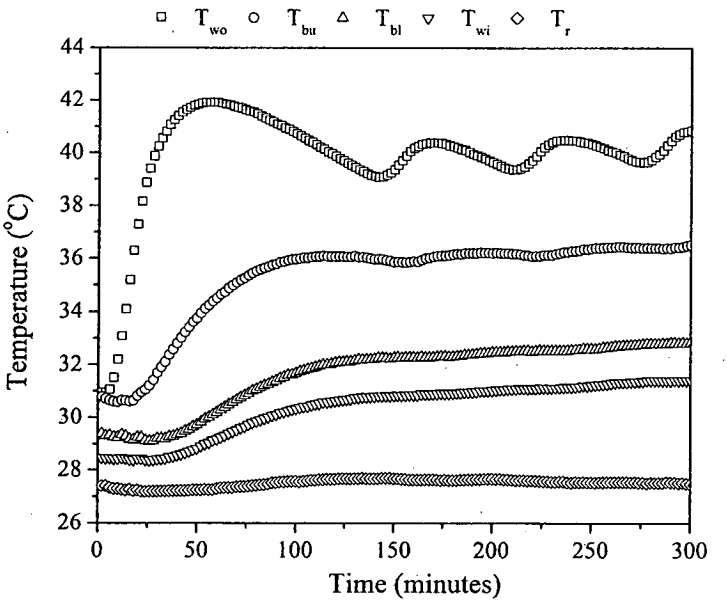

Figure 47 Temperature revolution of PCM-coated AAC wall (0.050 kg or ~0.417 kg/m^2) at the test temperature of 50 °C.

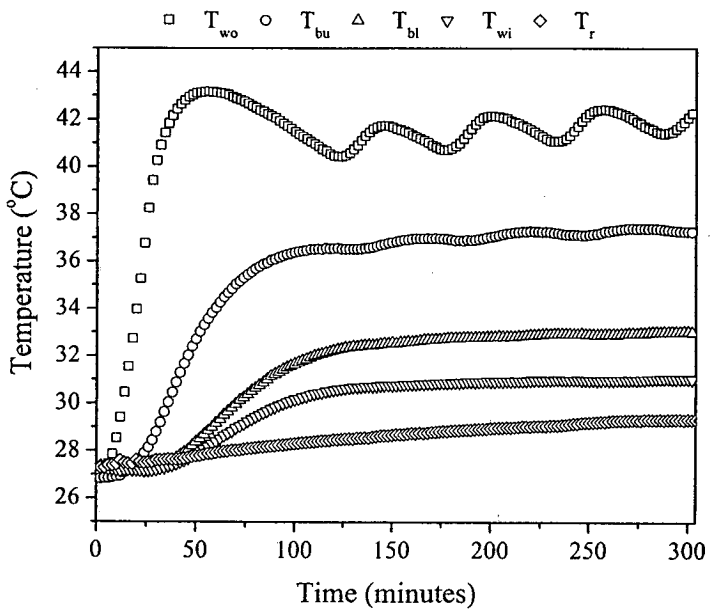

Figure 48 Temperature revolution of PCM-coated AAC wall (0.050 kg or ~0.417 kg/m^2) at the test temperature of 60 °C.

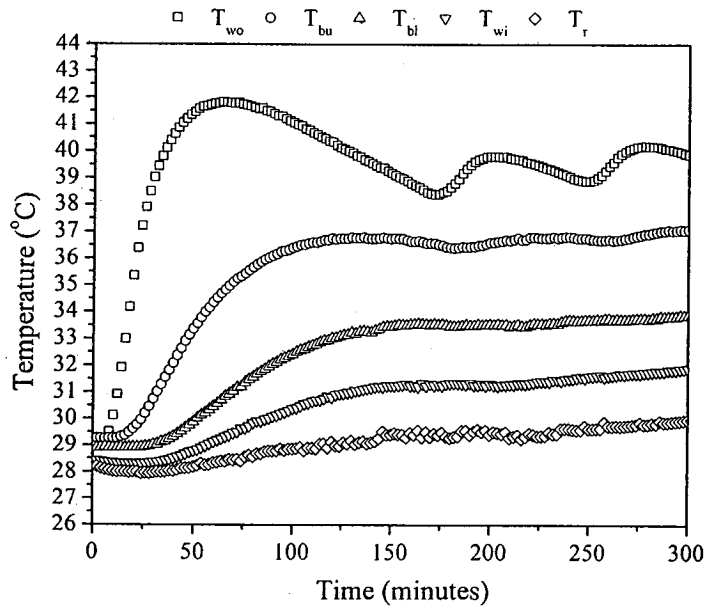

Figure 49 Temperature revolution of PCM-coated AAC wall (0.10 kg or ~0.833 kg/m^2) at the test temperature of 40 °C.

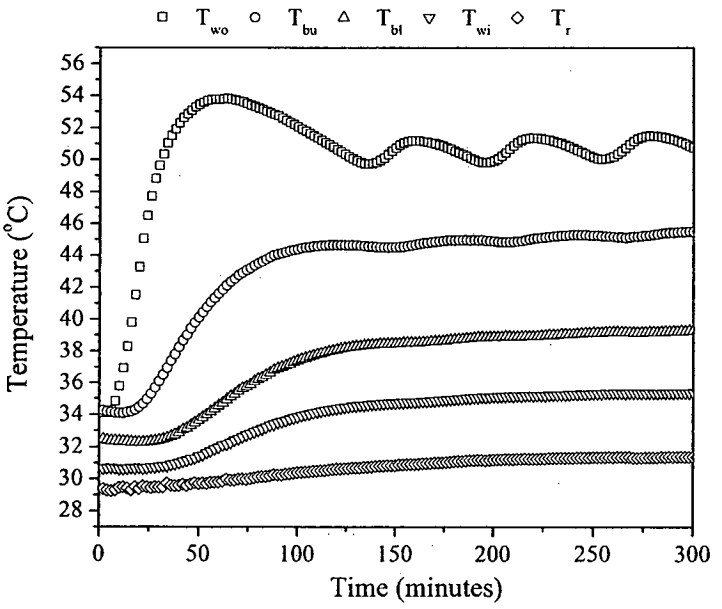

Figure 50 Temperature revolution of PCM-coated AAC wall (0.10 kg or ~0.833 kg/m^2) at the test temperature of 50 °C.

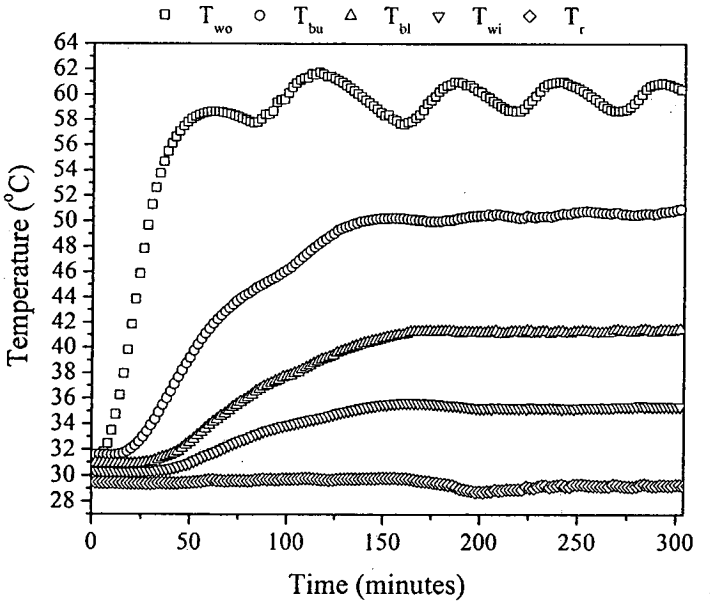

Figure 51 Temperature revolution of PCM-coated AAC wall (0.10 kg or ~0.833 kg/m^2) at the test temperature of 60 °C.

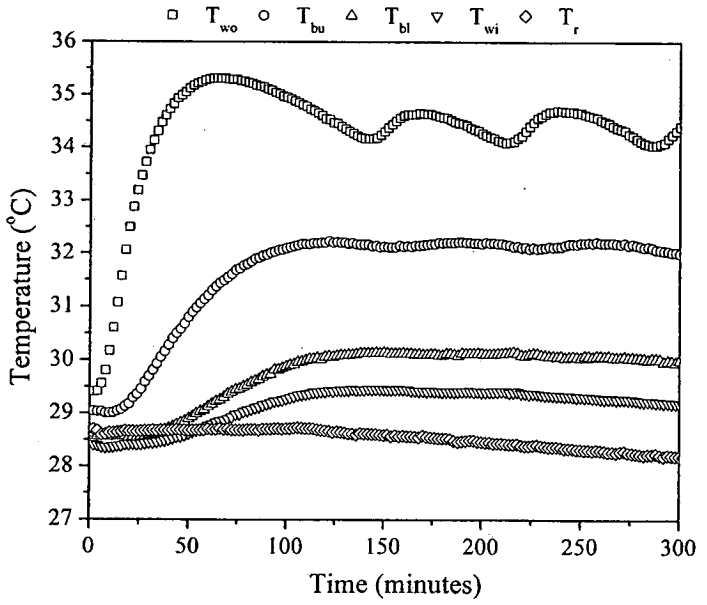

Figure 52 Temperature revolution of PCM-coated AAC wall (0.050 kg or ~0.417 kg/m^2) with cement coating in both sides at the test temperature of 40 °C.

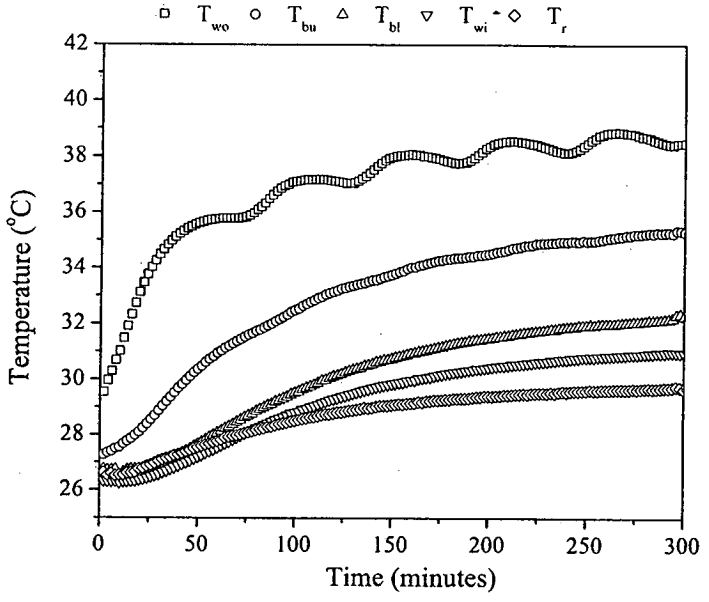

Figure 53 Temperature revolution of PCM-coated AAC wall (0.050 kg or ~0.417 kg/m^2) with cement coating in both sides at the test temperature of 50 °C.

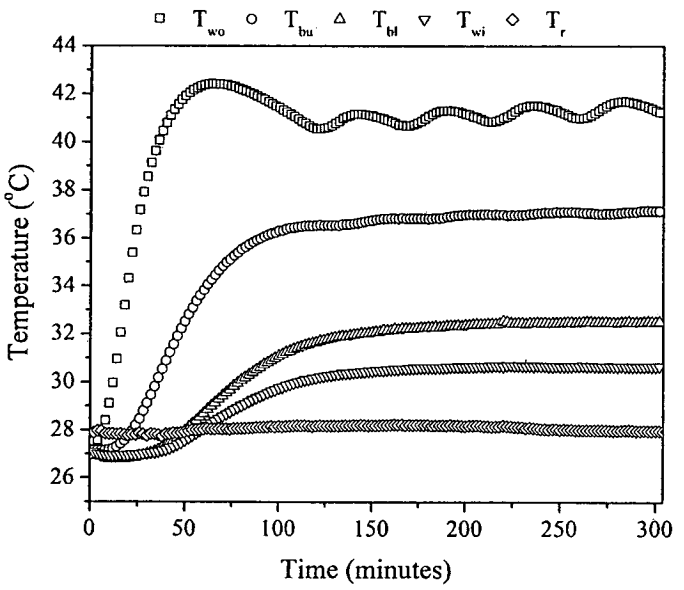

Figure 54 Temperature revolution of PCM-coated AAC wall (0.050 kg or ~0.417 kg/m^2) with cement coating in both sides at the test temperature of 60 °C.

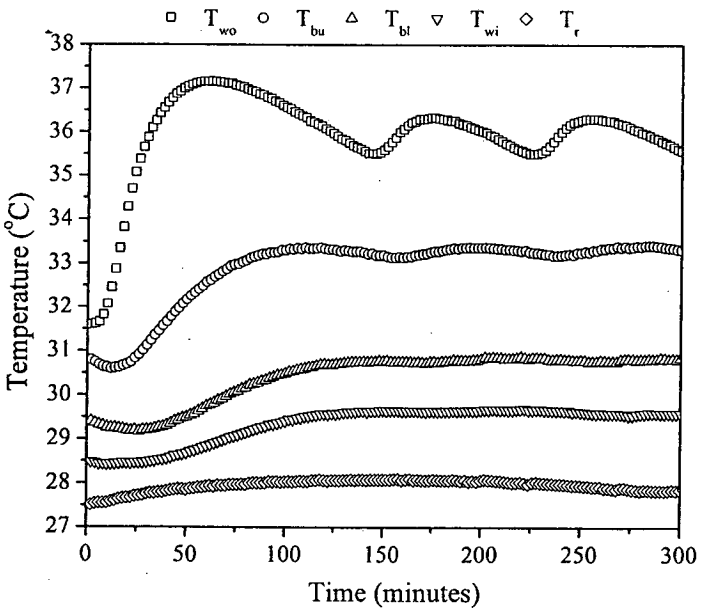

Figure 55 Temperature revolution of PCM-coated AAC wall (0.10 kg or ~0.833 kg/m^2) with cement coating in both sides at the test temperature of 40 °C.

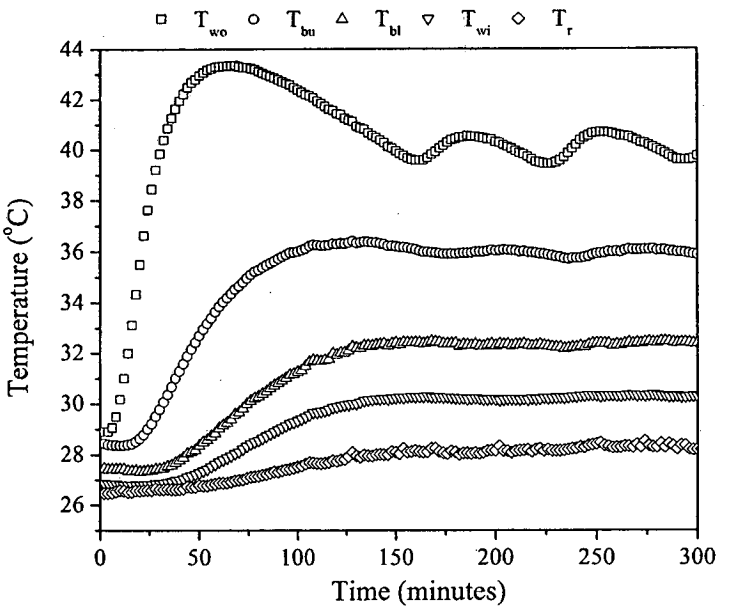

Figure 56 Temperature revolution of PCM-coated AAC wall (0.10 kg or ~0.833 kg/m^2) with cement coating in both sides at the test temperature of 50 °C.

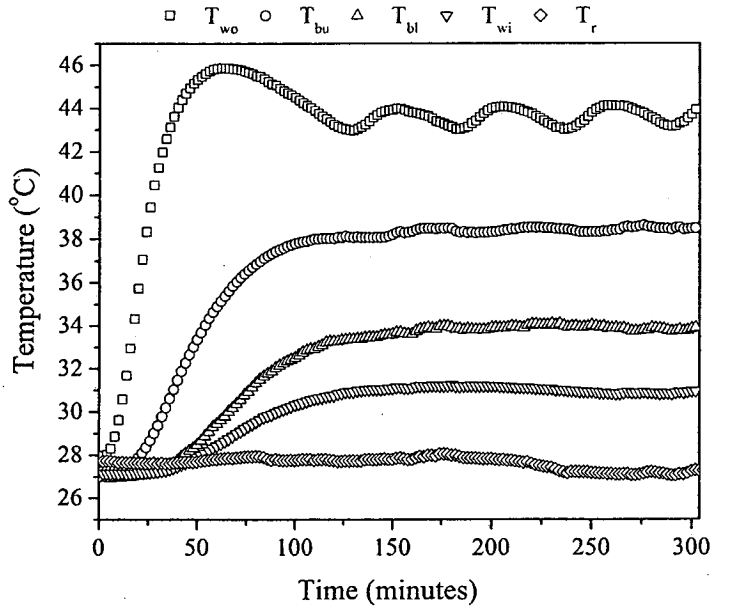

Figure 57 Temperature revolution of PCM-coated AAC wall (0.10 kg or ~0.833 kg/m^2) with cement coating in both sides at the test temperature of 60 °C.

Table 14 The total thermal resistance (R), the heat conduction (Q), wall temperature (T_w), and the room temperature (T_{room}), the time lag (τ), and decrement factor (λ).

The type of AAC	R ($m^2 \cdot K/W$)	Q (W)	Temperature	x(mm)	T_w (°C)	τ (min)	λ	T_{room}
AAC-S0	0.5769	3.42	40	0	37.1	-	-	28.7
				25	36.4	18	0.418	
				50	33.7	32	0.172	
				75	31.6	68	0.032	
		6.20	50	0	41.4			29.2
				25	40.3	10	0.403	
				50	35.6	20	0.177	
				75	31.5	50	0.089	
		9.15	60	0	47.2			30.2
				25	45.1	6	0.428	
				50	38.2	18	0.246	
				75	32.6	46	0.201	
AAC-S0-50	0.5775	3.42	40	0	34.8			27.4
				25	33.3	30	0.224	
				50	30.7	50	0.117	
				75	29.4	80	0.032	
		5.51	50	0	40.1			27.9
				25	36.3	22	0.283	
				50	32.6	44	0.153	
				75	31.2	54	0.085	
		6.73	60	0	41.8			28.1
				25	37.3	20	0.280	
				50	32.9	36	0.098	
				75	31.2	46	0.046	

Table 14 (cont.)

The type of AAC	R ($m^2 \cdot K/W$)	Q (W)	Temperature	x(mm)	T_w (°C)	τ (min)	λ	T_{room}
AAC-S0-100	0.5780	5.03	40	0	39.6			29.1
				25	36.8	26	0.269	
				50	33.6	42	0.219	
				75	31.5	56	0.177	
		9.64	50	0	50.8			29.6
				25	45.2	20	0.328	
				50	39.1	32	0.249	
				75	35.3	46	0.197	
		15.34	60	0	60.0			31.3
				25	50.6	16	0.139	
				50	41.3	28	0.070	
				75	35.3	42	0.032	
AAC-S0-50C	0.5832	3.12	40	0	34.4			27.9
				25	32.2	26	0.207	
				50	30.1	44	0.083	
				75	29.3	50	0.0024	
		4.77	50	0	38.4			28.2
				25	34.9	22	0.644	
				50	31.8	38	0.525	
				75	30.7	44	0.408	
		6.54	60	0	41.3			27.4
				25	37.1	18	0.278	
				50	32.5	36	0.124	
				75	30.7	44	0.051	

Table 14 (cont.)

The type of AAC	R (m^2·K/W)	Q (W)	Temperature	x(mm)	T_w (°C)	τ (min)	λ	T_{room}
AAC-S0-100C	0.5838	3.90	40	0	36.0			28.3
				25	33.3	20	0.280	
				50	30.8	38	0.122	
				75	29.6	46	0.072	
		6.08	50	0	40.1			28.1
				25	36.0	20	0.380	
				50	32.3	38	0.232	
				75	30.3	46	0.193	
		7.79	60	0	43.6			29.5
				25	38.4	16	0.247	
				50	33.9	32	0.216	
				75	31.0	38	0.049	

The thermal resistance, wall temperature (T_w), and room temperature (T_{room}) of the improved AAC with containing sugar sediment (AAC-SSR), improved AAC with 0.050 kg of PCM-coated external surface (AAC-SSR-50), improved AAC with 0.10 kg of PCM-coated external surface (AAC-SSR-100), improved AAC with 0.050 kg of PCM-coated external surface and cement-coated surface in both sides (AAC-SSR-50C) and improved AAC with 0.10 kg of PCM-coated external surface and coated cement surface in both sides (AAC-SSR-100C) walls are illustrated in Figure 58-Figure 72 and Table 15. The wall temperature of the AAC-SSR, AAC-SSR-50, AAC-SSR-100, AAC-SSR-50C and AAC-SSR-100C walls in each temperature condition as a function of the different thicknesses is shown in Figure 58-Figure 72 and Table 15. The wall temperature of the AAC-SSR, AAC-SSR-50, AAC-SSR-100, AAC-SSR-50C and AAC-SSR-100C walls in each temperature condition decreased when there was an increase of thickness from 0 to 75 mm as shown in Figure 58-Figure 72 and Table 15.

Time lag and decrement factor of AAC with containing sugar sediment at different conditions

The time lag (Φ) and decrement factor (λ) of the AAC-SSR, AAC-SSR-50, AAC-SSR-100, AAC-SSR-50C and AAC-SSR-100C walls are illustrated in Table 15. When the thermal source was controlled at the temperature of 40 °C, it was found that the time lag of the AAC-SSR wall increased from 20 to 68 min while the decrement factor decreased from 0.403 to 0.104 when the thickness of the AAC-SSR wall increased from 0 to 75 mm. When the thermal source was controlled at temperatures of 50 and 60 °C, the time lag and decrement factor at these 2 temperatures were similar to that of the temperature of 40 °C with the increase of the AAC-SSR wall thickness, as shown in Table 15. For the cases of AAC-SSR-50, AAC-SSR-100, AAC-SSR-50C and AAC-SSR-100C, the time lag also increased from 26 to 94 min, 18 to 54 min, 22 to 66 min and 16 to 46 min while the decrement factor decreased from 0.413 to 0.004, 0.452 to 0.197, 0.400 to 0.009 and 0.393 to 0.035 when the thickness of the wall increased from 0 to 75 mm, as listed in Table 15. This result shows that time lag and decrement factor are related to the thickness of the AAC-SSR wall. A closer reading of Table 15 will show that time lag was positively proportionate to the thickness of the wall while the decrement factor increased inversely to its thickness. This indicated that an increase of wall thickness will result in lower heat flow.

With comparing the time lag and decrement factor between AAC-SSR, AAC-SSR-50 and AAC-SSR-100 in each condition, the time lag of AAC-SSR and AAC-SSR-100 were less than that of AAC-SSR-50. As well, the decrement factor of AAC-SSR and AAC-SSR-100 was slightly higher than that of AAC-SSR-50. This demonstrates that the optimal composition of AAC-SSR-50 can slightly extend the time of the heat wave to propagate from the outer wall to the inner wall and obviously decrease the ratio of its amplitude during this process when compared to the composition of AAC-SSR and AAC-SSR-100. This result shows that the room temperature of AAC-SSR-50 was only 1 °C lower than that of the AAC-SSR and AAC-SSR-100, the longer time lag does have an effect, albeit a minor effect as exhibited in Table 15.

With comparing the time lag and decrement factor between Brick, AAC-S0-50 and AAC-SSR-50 in each condition, the time lag of brick and AAC-S0-50 were

less than that of AAC-SSR-50. As well, the decrement factor of brick and AAC-S0-50 was slightly higher than that of AAC-SSR-50. This shows that the optimal composition of AAC-SSR-50 can slightly extend the time of the heat wave to propagate from the outer wall to the inner wall and obviously reduce the ratio of its amplitude during this process when compared to the composition of brick and AAC-S0-50. This result exhibits that the room temperature of AAC-SSR-50 was around 2-3 °C lower than that of the brick, while was nearly the same that of AAC-S0-50, the longer time lag does have an effect as exhibited in Table 13-15.

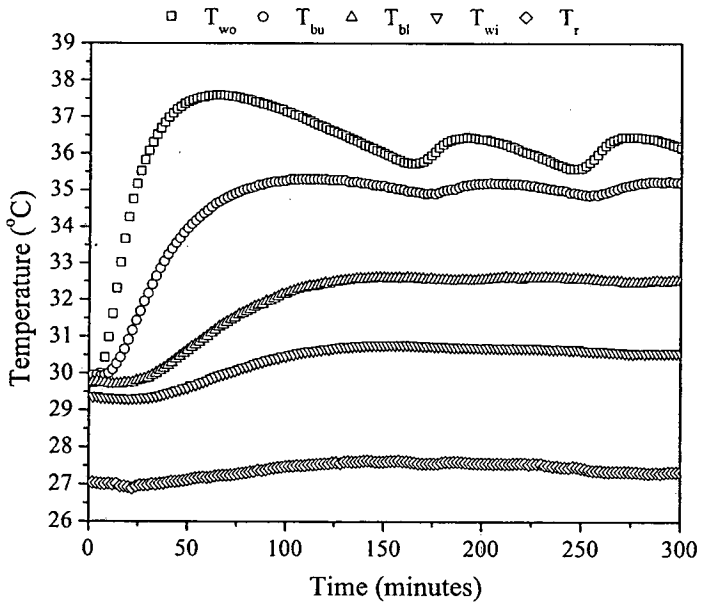

Figure 58 Temperature revolution of AAC-SSR wall at the test temperature of 40 °C.

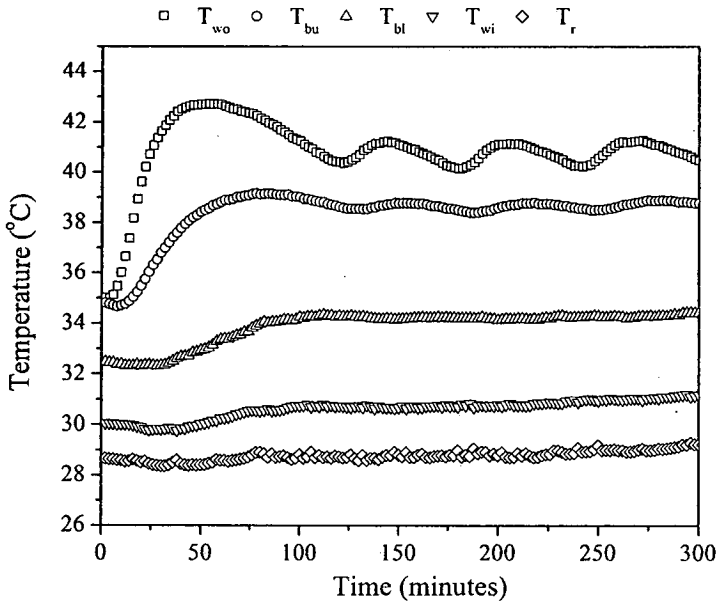

Figure 59 Temperature revolution of AAC-SSR wall at the test temperature of 50 °C.

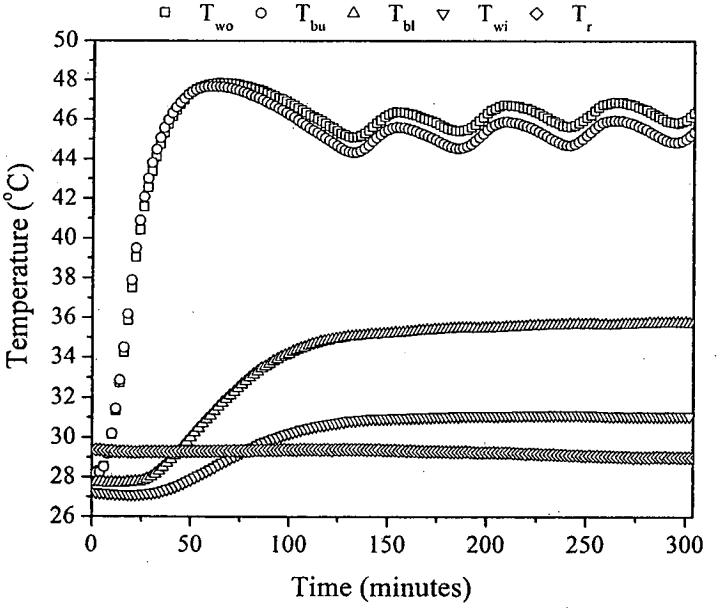

Figure 60 Temperature revolution of AAC-SSR wall at the test temperature of 60 °C.

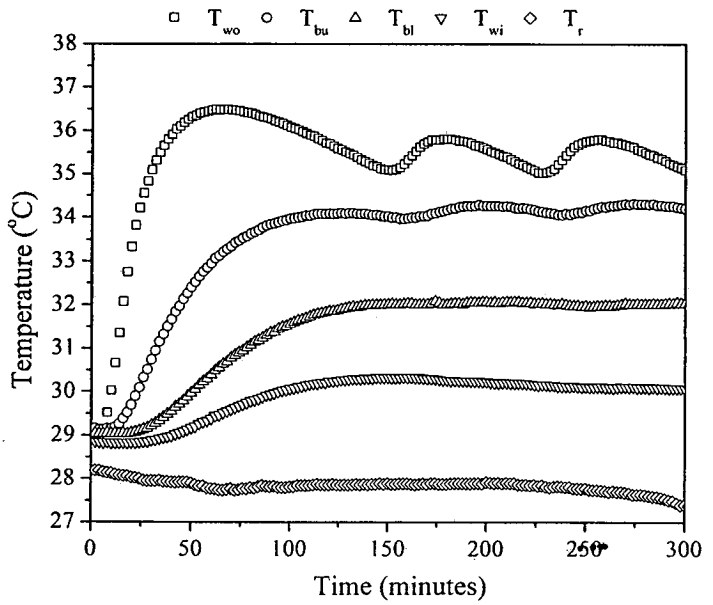

Figure 61 Temperature revolution of PCM-coated AAC-SSR wall (0.050 kg or ~0.417 kg/m^2) at the test temperature of 40 °C.

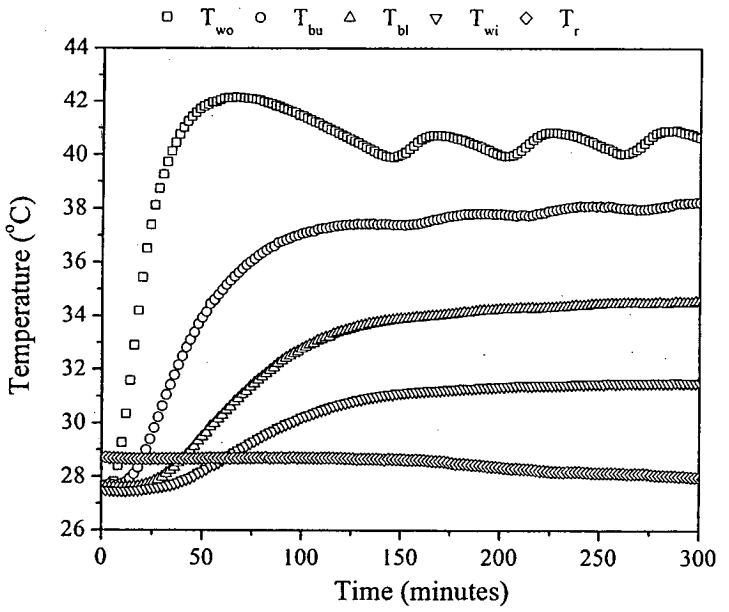

Figure 62 Temperature revolution of PCM-coated AAC-SSR wall (0.050 kg or ~0.417 kg/m^2) at the test temperature of 50 °C.

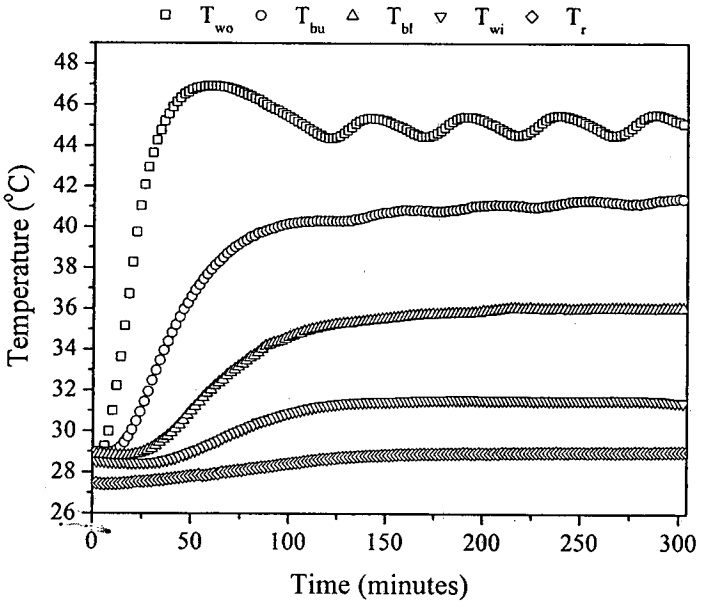

Figure 63 Temperature revolution of PCM-coated AAC-SSR wall (0.050 kg or ~0.417 kg/m^2) at the test temperature of 60 °C.

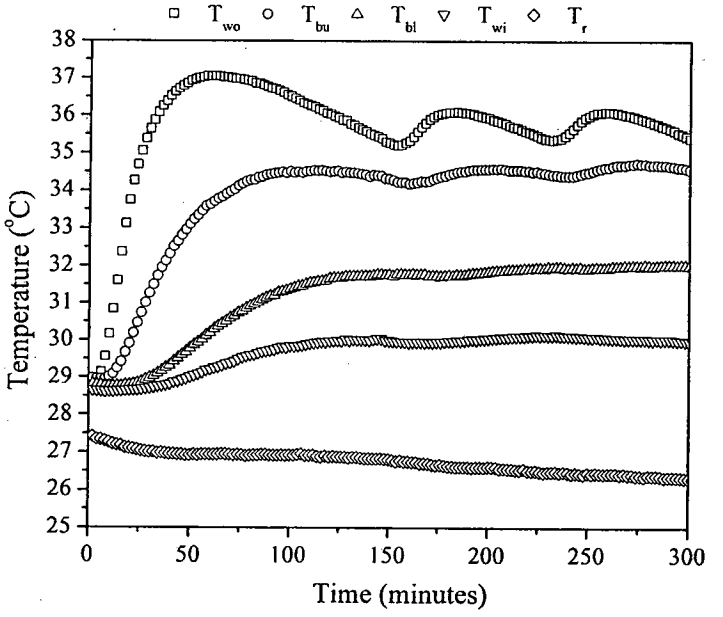

Figure 64 Temperature revolution of PCM-coated AAC-SSR wall (0.10 kg or ~0.833 kg/m^2) at the test temperature of 40 °C.

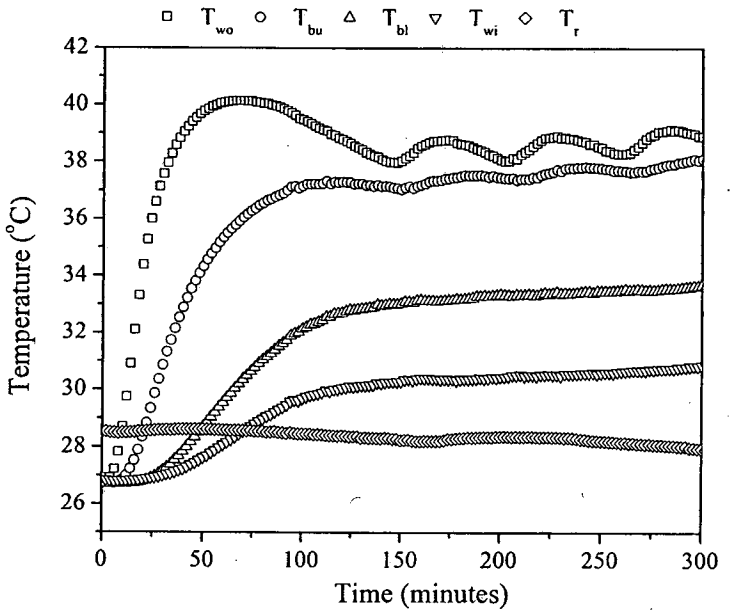

Figure 65 Temperature revolution of PCM-coated AAC-SSR wall (0.10 kg or ~0.833 kg/m^2) at the test temperature of 50 °C.

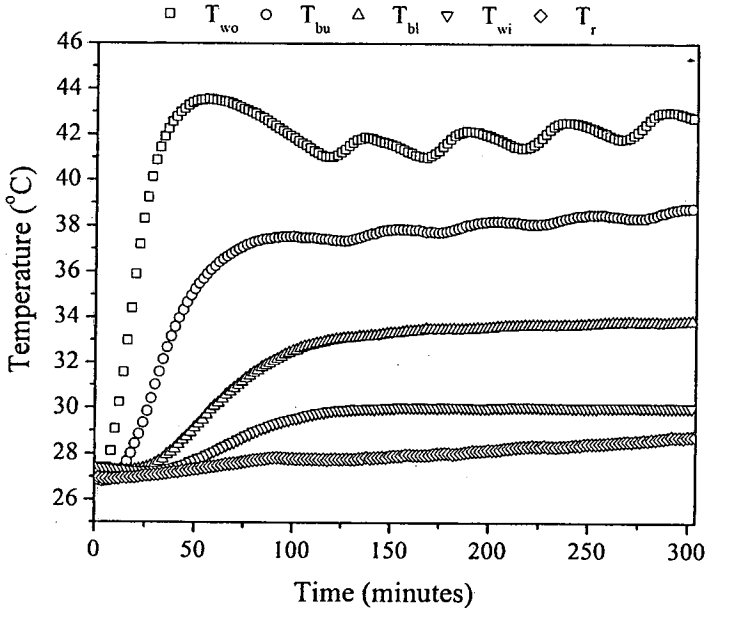

Figure 66 Temperature revolution of PCM-coated AAC-SSR wall (0.10 kg or ~0.833 kg/m^2) at the test temperature of 60 °C.

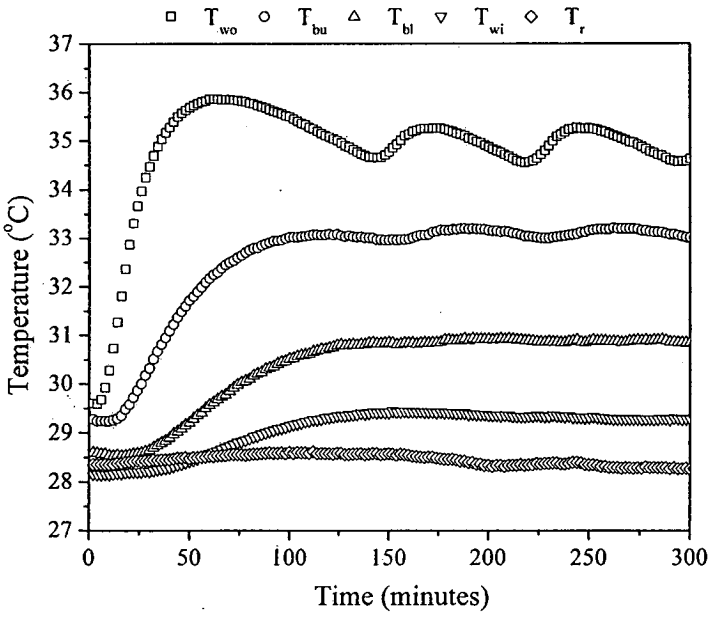

Figure 67 Temperature revolution of PCM-coated AAC-SSR wall (0.050 kg or ~0.417 kg/m^2) with cement coating in both sides at the test temperature of 40 °C.

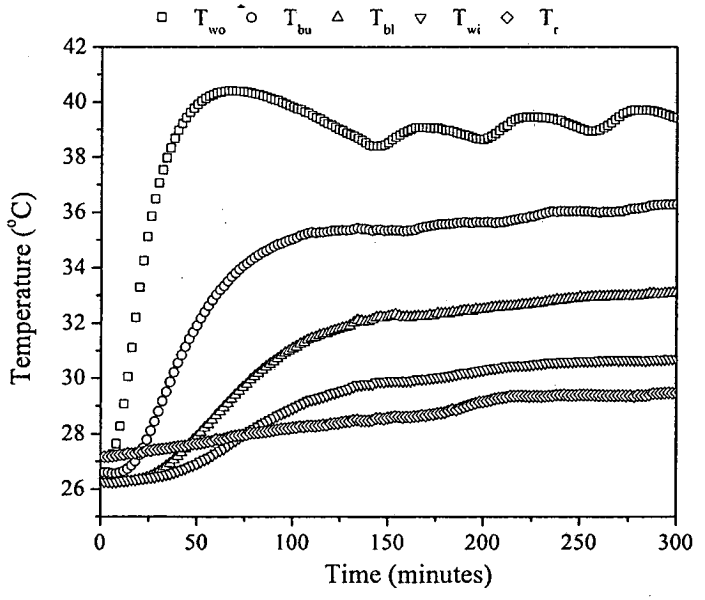

Figure 68 Temperature revolution of PCM-coated AAC-SSR wall (0.050 kg or ~0.417 kg/m^2) with cement coating in both sides at the test temperature of 50 °C.

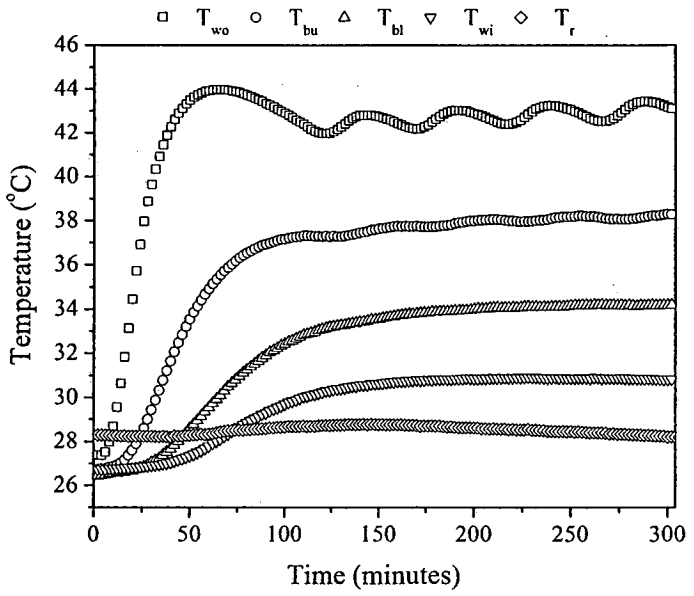

Figure 69 Temperature revolution of PCM-coated AAC-SSR wall (0.050 kg or ~0.417 kg/m^2) with cement coating in both sides at the test temperature of 60 °C.

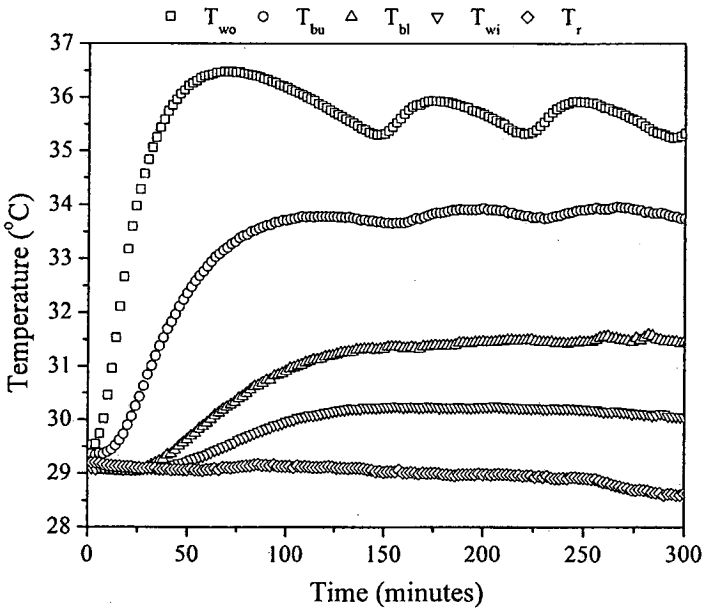

Figure 70 Temperature revolution of PCM-coated AAC-SSR wall (0.10 kg or ~0.833 kg/m^2) with cement coating in both sides at the test temperature of 40 °C.

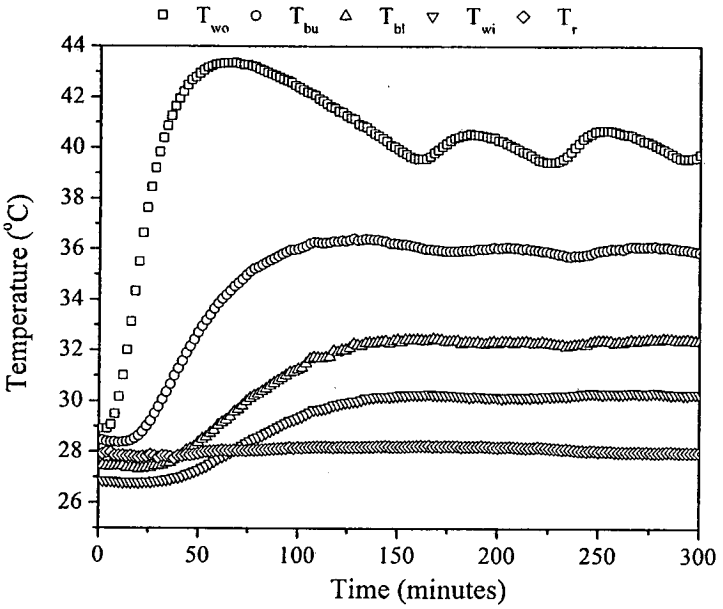

Figure 71 Temperature revolution of PCM-coated AAC-SSR wall (0.10 kg or ~0.833 kg/m^2) with cement coating in both sides at the test temperature of 50 °C.

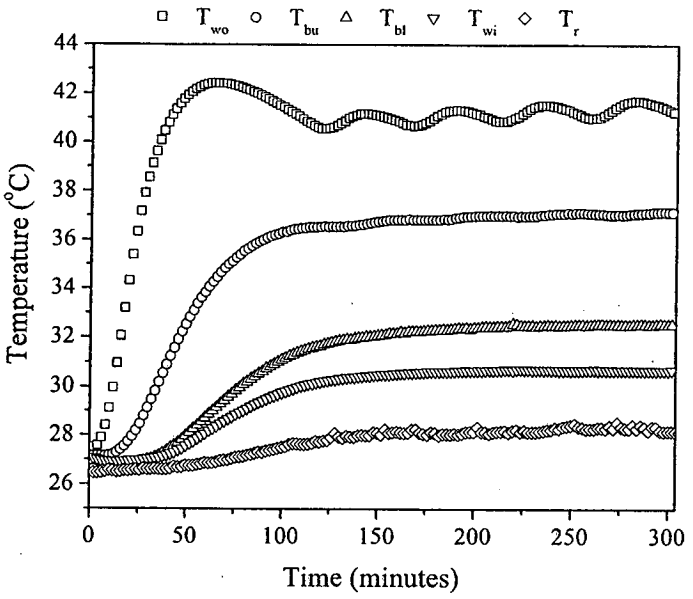

Figure 72 Temperature revolution of PCM-coated AAC-SSR wall (0.10 kg or ~0.833 kg/m^2) with cement coating in both sides at the test temperature of 60 °C.

Table 15 The total thermal resistance (R), the heat conduction (Q), wall temperature (T_w), and the room temperature (T_{room}), the time lag (τ), and decrement factor (λ).

The type of AAC	R ($m^2 \cdot K/W$)	Q (W)	Temperature	x(mm)	T_w (°C)	τ (min)	λ	T_{room}
AAC-SSR	0.7653	2.59	40	0	36.2			27.5
				25	35.1	20	0.403	
				50	32.6	38	0.125	
				75	30.7	68	0.104	
		4.66	50	0	40.8			29.0
				25	38.7	12	0.277	
				50	34.3	36	0.084	
				75	30.9	54	0.010	
		7.10	60	0	46.2			29.1
				25	45.3	6	0.977	
				50	35.6	32	0.188	
				75	31.1	54	0.070	
AAC-SSR-50	0.7659	2.54	40	0	35.5			27.7
				25	34.2	26	0.413	
				50	32.0	50	0.083	
				75	30.1	94	0.004	
		4.28	50	0	40.5			28.2
				25	38.0	26	0.532	
				50	34.4	40	0.334	
				75	31.4	60	0.186	
		6.39	60	0	45.1			29.0
				25	41.2	20	0.263	
				50	36.0	36	0.105	
				75	31.5	54	0.021	

Table 15 (cont.)

The type of AAC	R ($m^2 \cdot K/W$)	Q (W)	Temperature	x(mm)	T_w (°C)	τ (min)	λ	T_{room}
AAC-SSR-100	0.7664	2.68	40	0	35.8			28.2
				25	34.6	18	0.452	
				50	31.9	44	0.248	
				75	30.1	54	0.197	
		5.17	50	0	41.6			28.4
				25	37.7	16	0.556	
				50	33.4	30	0.349	
				75	30.6	44	0.258	
		7.56	60	0	46.2			29.5
				25	38.3	14	0.402	
				50	33.7	30	0.140	
				75	30.1	42	0.032	
AAC-SSR-50C	0.7702	2.43	40	0	34.5			28.3
				25	33.1	22	0.400	
				50	30.9	48	0.183	
				75	29.3	66	0.009	
		4.07	50	0	39.2			29.3
				25	35.9	20	0.490	
				50	32.8	38	0.401	
				75	30.5	60	0.356	
		5.61	60	0	42.9			28.5
				25	38.1	16	0.389	
				50	34.1	30	0.212	
				75	30.9	40	0.076	

Table 15 (cont.)

The type of AAC	R (m^2·K/W)	Q (W)	Temperature	x(mm)	T_w (°C)	τ (min)	λ	T_{room}
AAC-SSR-100C	0.7707	2.52	40	0	35.6			28.9
				25	33.9	16	0.393	
				50	31.5	34	0.157	
				75	30.2	46	0.035	
		4.11	50	0	40.4			30.0
				25	37.2	16	0.515	
				50	33.6	34	0.349	
				75	31.6	44	0.156	
		5.93	60	0	44.6			29.2
				25	39.3	14	0.430	
				50	34.7	30	0.352	
				75	31.9	40	0.234	

Test results of houses with different house walls in actual condition of use

The thermal effectiveness performance of the four small houses was tested. These houses were built using the three different wall materials; brick, cement block and AAC, with one house using AAC with coated PCM). Data collection was investigated on June 29, July 2 and July 4, 2013 for testing in the summer and July 5, July 7 and July 9, 2013 for testing in the simulated rainy season.

The rainy season was simulated using water spray onto the four houses and the surrounding in day time during 6 am to 6 pm (12 h). The simulated rainfall level in this study was considered from mean annual rainfall in Thailand in last 10 year period (2004-2013).All data were recorded at 5 min intervals using a data logger. Data was recorded continuously over 24 h in real ambient condition.

Test results in the summer

The fluctuations in solar radiation, ambient temperatures and percentage of relative humidity are shown in Figure 73-Figure 75. These tests were done and results observed from 6am of day to 6am of the following day, giving a 24 h test cycle (on June 29, July 2 and July 4, 2013).

The fluctuating nature of solar radiation in the tropics occurs because of periodical cloud cover which is typical between sunrise (6.00 am) and sunset (7.00 pm) with the highest values of up to around 1.1 kW/m^2 around midday. Wind velocity at the test site was between 0.25 and 3.54 m/s. The ambient temperature depended upon weather conditions and fluctuated between approximately 26 °C in the morning between 5-6am and up the maximum value of about 36 °C at around 5pm. The percentage of relative humidity depended also upon weather conditions and fluctuated between approximately 55% at around 5pm and up the maximum value of approximately 90% in the morning between 5-6am.

With considering the relation of fluctuations in solar radiation, ambient temperatures and percentage of relative humidity, it was found that fluctuations in solar radiation was positively proportionate to the ambient temperatures as exhibited in Figure 73. While the fluctuations in solar radiation and ambient temperatures increased inversely to percentage of relative humidity as shown in Figure 74-75.

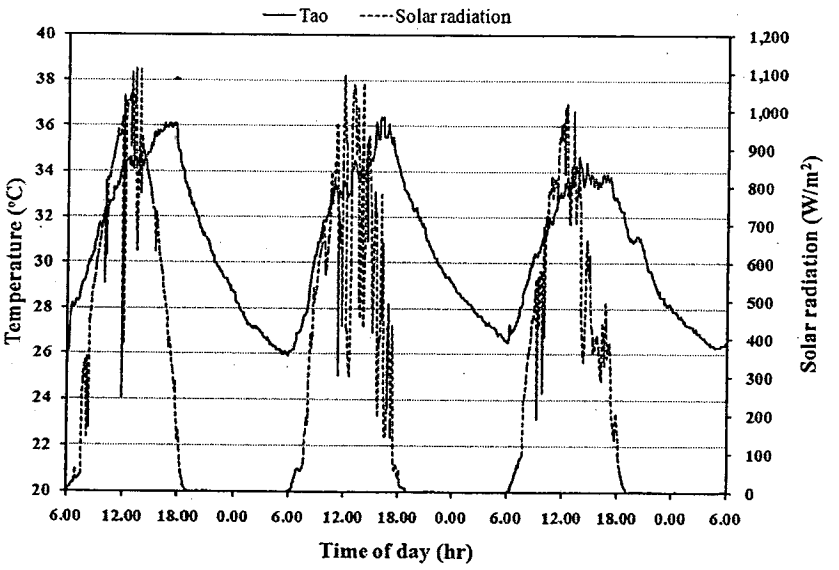

Figure 73 Variation of temperature and solar radiation.

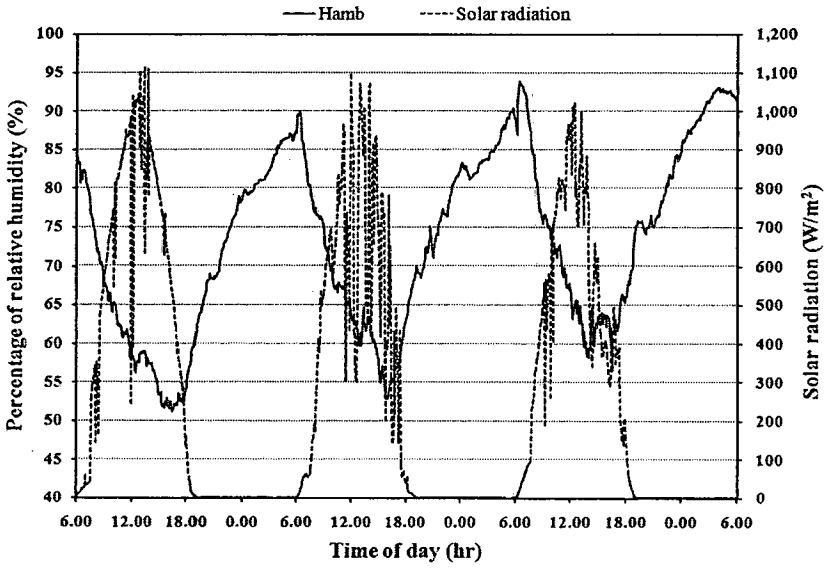

Figure 74 Variation of relative humidity and solar radiation.

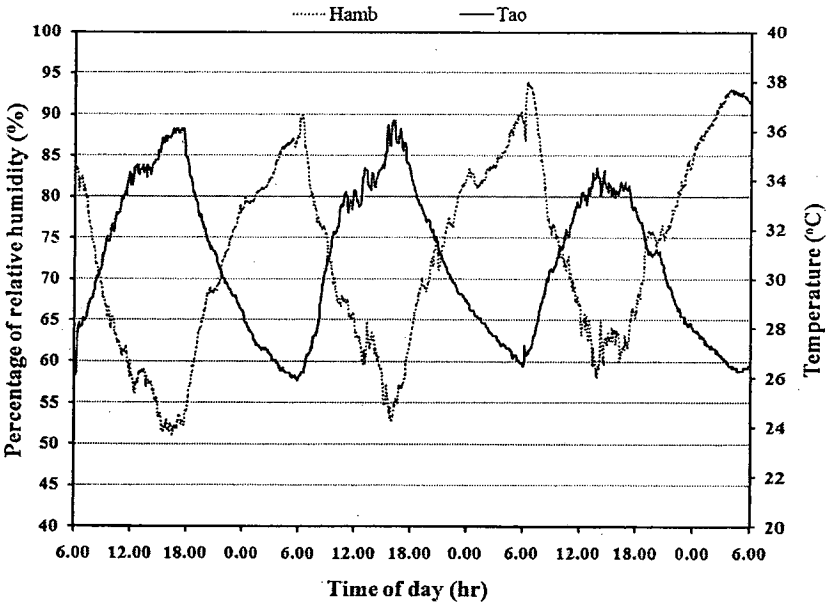

Figure 75 Variation of relative humidity and temperature.

Figure 76-111 show the results from the test houses each with different wall types that measured concurrently. The exterior and interior surface temperature evolution, heat flux and room temperature of the four houses with no air conditioning

were investigated and compared, and subsequent tests were done with the air conditioning operative.

The autoclaved aerated concrete wall with phase change material coating

External wall surfaces

The temperature evolution of the exterior surface temperature of the PCM coated AAC house wall in all sides is shown in Figure 76. The maximum exterior wall temperature of the north, south, east and west surfaces reached as high as approximately 37 °C, 46.7 °C, 50 °C and 48 °C at around 3.30pm, 4.30pm, 8.30-9.00am and 4.30-5 pm respectively and then dropped in value over time passed after each those times. The average exterior surface temperature in all of the north, south, east and west surfaces was at approximately 33 °C, 36 °C, 40.5 °C and 36.5 °C was observed in midday time from 6am to 6pm, giving a 12 h in each day. In midnight time from 6pm to 6am, that was at approximately 30 °C, 31 °C, 32 °C and 31 °C, respectively.

Internal wall surfaces

The temperature evolution of the interior surface temperature of the PCM coated AAC house wall in all sides is shown in Figure 77. The maximum exterior wall temperature of the north, south, east and west surfaces peaked as high as 36 °C, 37.3 °C, 37.7 °C and 37.0 °C, at around the same time, 5.30-6pm and then dropped in value over time passed after each those times. The average interior surface temperature in all of the north, south, east and west surfaces was at approximately 31.3 °C, 31.7 °C, 33.5 °C and 32.2 °C was observed in midday time from 6am to 6pm, giving a 12 h in each day. In midnight time from 6pm to 6am, that was while at approximately 30.9 °C, 31.2 °C, 31.5 °C and 31.2 °C, respectively.

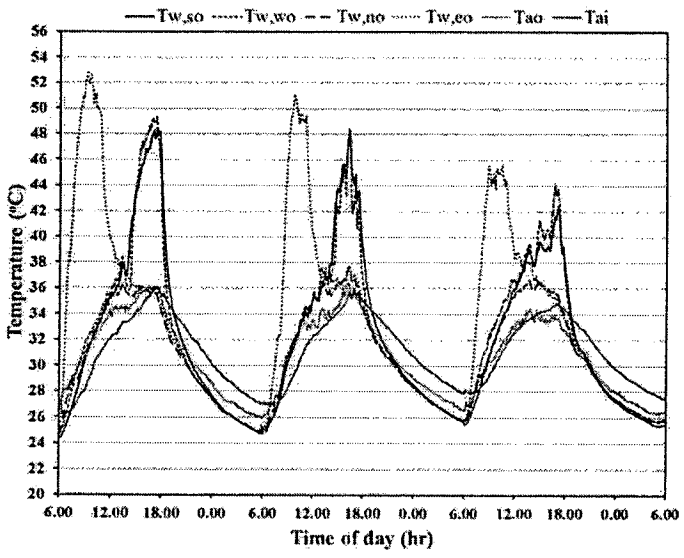

Figure 76 The temperature variation of exterior improved autoclaved aerated concrete wall surfaces.

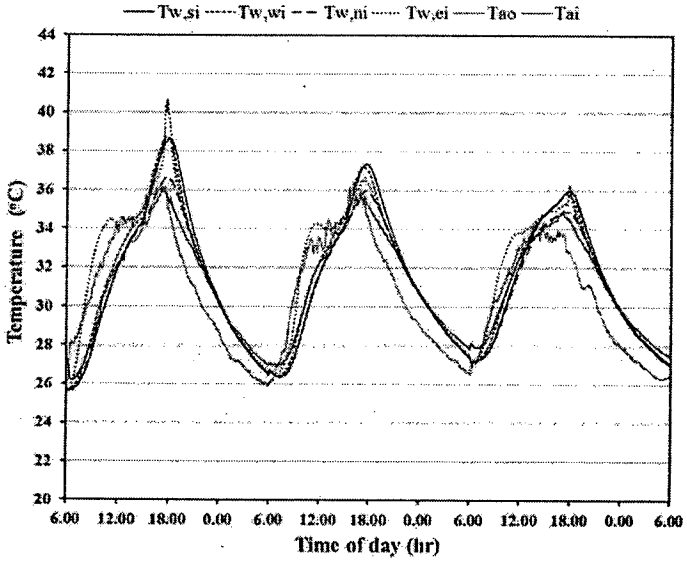

Figure 77 The temperature variation of interior improved autoclaved aerated concrete wall surfaces.

Northerly aspect wall surfaces

The temperature fluctuation of Northerly aspect interior and exterior surface temperature of the PCM coated AAC house is shown in Figure 78. The maximum

value of ambient temperature (Tao) was observed at about 35.4 °C at the day time around 4.30pm. The exterior wall temperature of the Northerly aspect rapidly heated to as high as approximately 37 °C at around 3.30pm while peak temperatures of the interior surface reached its maximum value of approximately 36 °C at around 5.30-6pm. The maximum room temperature (Tai) as approximately 35.5 °C was found at the day time around 5.30pm.

Southerly aspect wall surfaces

The temperature fluctuation of Southerly aspect interior and exterior surface temperature of the PCM coated AAC house is shown in Figure 79. The maximum value of ambient temperature (Tao) was observed at about 35.4 °C at the day time around 4.30pm. The exterior wall temperature of the Southerly aspect rapidly heated to as high as approximately 46.7 °C at around 4.30pm while peak temperatures of the interior surface reached its maximum value of approximately 37.3 °C at around 5.30-6pm. The maximum room temperature (Tai) as approximately 35.5 °C was found at the day time around 5.30pm.

Easterly aspect wall surfaces

The temperature variation of Easterly aspect interior and exterior surface temperature of the PCM coated AAC house is shown in Figure 80. The maximum value of ambient temperature (Tao) was observed at about 35.4 °C at the day time around 4.30pm. The exterior wall temperature of the Easterly aspect rapidly heated to as high as approximately 50 °C at around 8.30-9.00am while peak temperatures of the interior surface reached its maximum value of approximately 37.7 °C at around 5.30-6pm. The maximum room temperature (Tai) as approximately 35.5 °C was found at the day time around 5.30pm.

Westerly aspect wall surfaces

The temperature fluctuation of Westerly aspect interior and exterior surface temperature of the PCM coated AAC house is shown in Figure 81. The maximum value of ambient temperature (Tao) was observed at about 35.4 °C at the day time around 4.30pm. The exterior wall temperature of the Westerly aspect rapidly heated to as high as approximately 48 °C at around 4.30-5 pm while peak temperatures of the interior surface reached its maximum value of approximately 37.0 °C at around 5.30-

6pm. The maximum room temperature (Tai) as approximately 35.5 °C was found at the day time around 5.30pm.

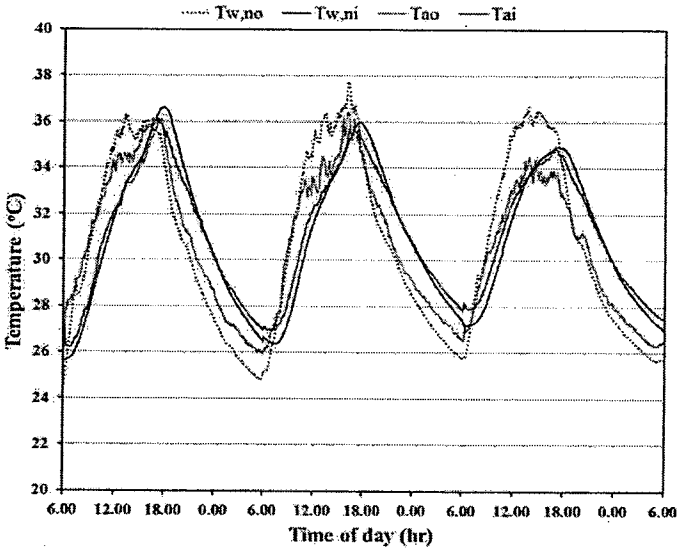

Figure 78 The temperature change of northerly aspect exterior and interior improved autoclaved aerated concrete wall surfaces.

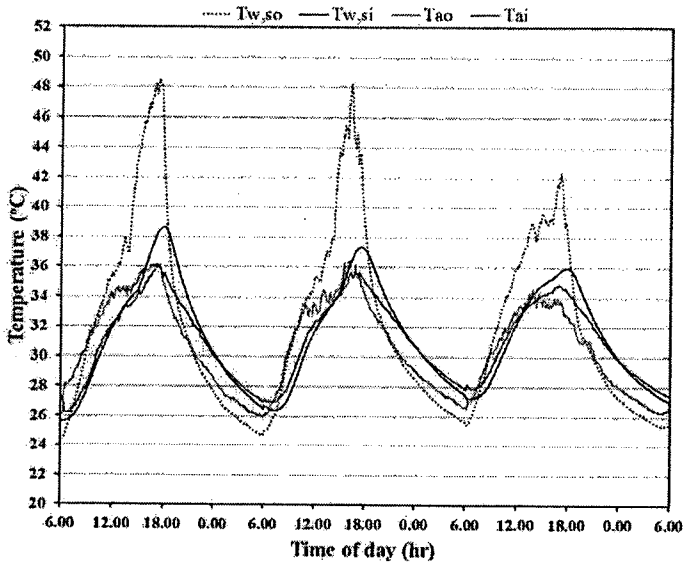

Figure 79 The temperature change of southerly aspect exterior and interior improved autoclaved aerated concrete wall surfaces.

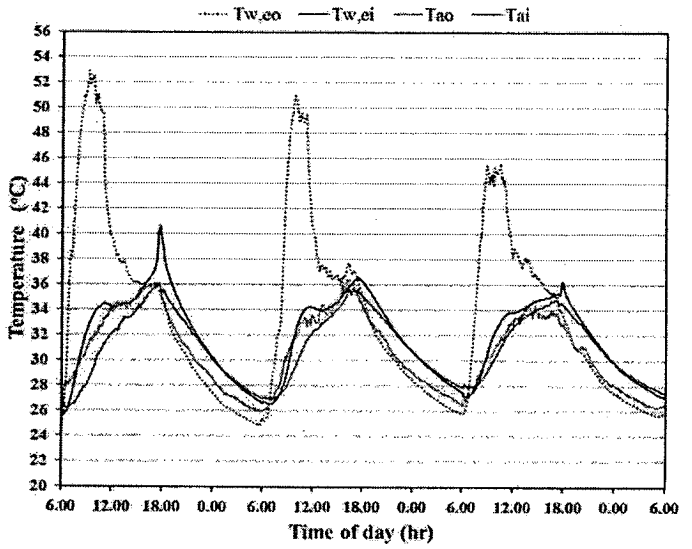

Figure 80 The temperature change of easterly aspect exterior and interior improved autoclaved aerated concrete wall surfaces.

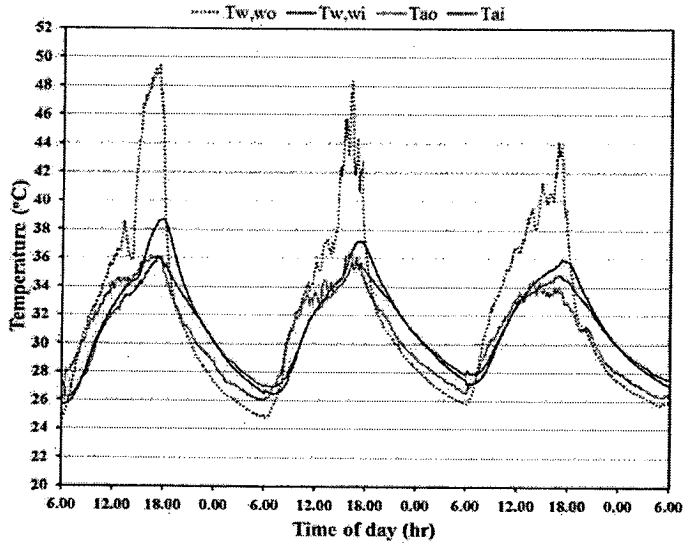

Figure 81 The temperature change of westerly aspect exterior and interior improved autoclaved aerated concrete wall surfaces.

The cement block wall

External wall surfaces

The temperature evolution of the exterior surface temperature of the cement block house wall in all sides is shown in Figure 82. The maximum exterior wall temperature of the north, south, east and west surfaces reached as high as 36.5 °C, 43.2 °C, 44.5 °C and 42.5 °C at around 4.30-5pm, 5.30-6pm, 10.30-11am and 4.30-5pm respectively and then dropped in value over time passed after each those times. The average exterior surface temperature in all of the north, south, east and west surfaces was at approximately 32 °C, 35.5 °C, 37.3 °C and 34 °C was observed in midday time from 6am to 6pm, giving a 12 h in each day. In midnight time from 6pm to 6am, that was at approximately 29.5 °C, 31.7 °C, 30 °C and 30.5 °C, respectively.

Internal wall surfaces

The temperature evolution of the interior surface temperature of the cement block house wall in all sides is shown in Figure 83. The maximum interior wall temperature of the north, south, east and west surfaces peaked as high as 37.3 °C, 42.2 °C, 38.2 °C and 40 °C at the same time, around 5.30-6pm and then dropped in value over time passed after each those times. The average exterior surface temperature in all of the north, south, east and west surfaces was at approximately 32 °C, 33.5 °C, 35 °C and 32.7 °C respectively was observed in midday time from 6am to 6pm, giving a 12 h in each day. In midnight time from 6pm to 6am, that was while at approximately 31 °C, 33 °C, 31.5 °C and 32 °C, respectively.

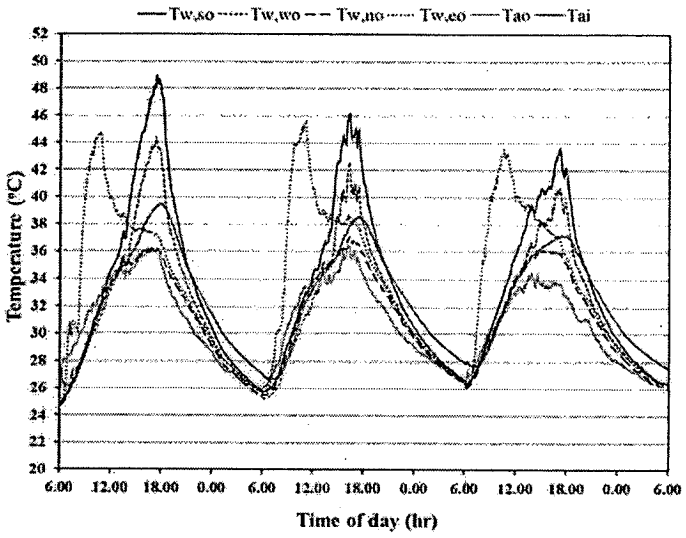

Figure 82 The temperature variation of exterior cement block wall surfaces.

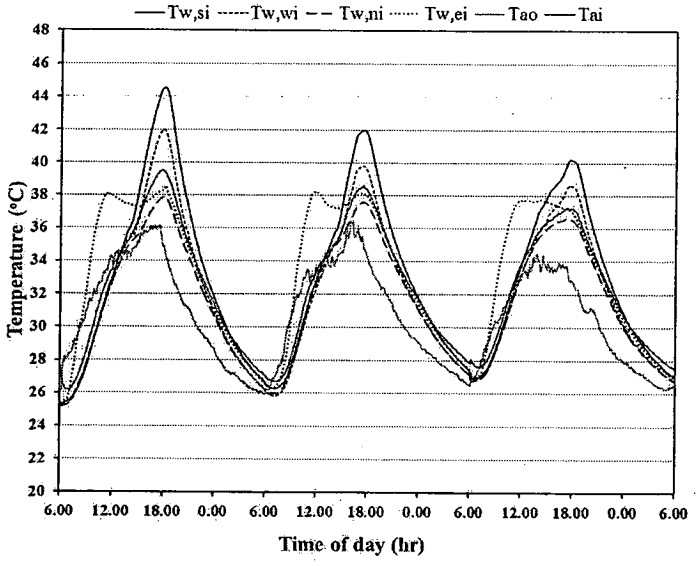

Figure 83 The temperature variation of interior cement block wall surfaces.

Northerly aspect wall surfaces

The temperature fluctuation of Northerly aspect interior and exterior surface temperature of the cement block house is shown in Figure 84. The maximum value of ambient temperature (Tao) was observed at about 35.4 °C at the day time around 4.30pm. The exterior wall temperature of the Northerly aspect rapidly heated to as

high as approximately 36.5 °C at around 4.30-5pm while peak temperatures of the interior surface reached its maximum value of approximately 37.3 °C at around 5.30-6pm. The maximum room temperature (Tai) as approximately 38.4 °C was found at the day time around 5.30pm.

Southerly aspect wall surfaces

The temperature fluctuation of Southerly aspect interior and exterior surface temperature of the cement block house is shown in Figure 85. The maximum value of ambient temperature (Tao) was observed at about 35.4 °C at the day time around 4.30pm. The exterior wall temperature of the Southerly aspect rapidly heated to as high as approximately 43.2 °C at around 5.30-6pm while peak temperatures of the interior surface reached its maximum value of approximately 42.2 °C at around 5.30-6pm. The maximum room temperature (Tai) as approximately 38.4 °C was found at the day time around 5.30pm.

Easterly aspect wall surfaces

The temperature variation of Easterly aspect interior and exterior surface temperature of the cement block house is shown in Figure 86. The maximum value of ambient temperature (Tao) was observed at about 35.4 °C at the day time around 4.30pm. The exterior wall temperature of the Easterly aspect rapidly heated to as high as approximately 44.5 °C at around 10.30-11am while peak temperatures of the interior surface reached its maximum value of approximately 38.2 °C at around 5.30-6pm. The maximum room temperature (Tai) as approximately 38.4 °C was found at the day time around 5.30pm.

Westerly aspect wall surfaces

The temperature fluctuation of Westerly aspect interior and exterior surface temperature of the cement block house is shown in Figure 87. The maximum value of ambient temperature (Tao) was observed at about 35.4 °C at the day time around 4.30pm. The exterior wall temperature of the Westerly aspect rapidly heated to as high as approximately 42.5 °C at around 4.30-5pm while peak temperatures of the interior surface reached its maximum value of approximately 40 °C at around 5.30-6pm. The maximum room temperature (Tai) as approximately 38.4 °C was found at the day time around 5.30pm.

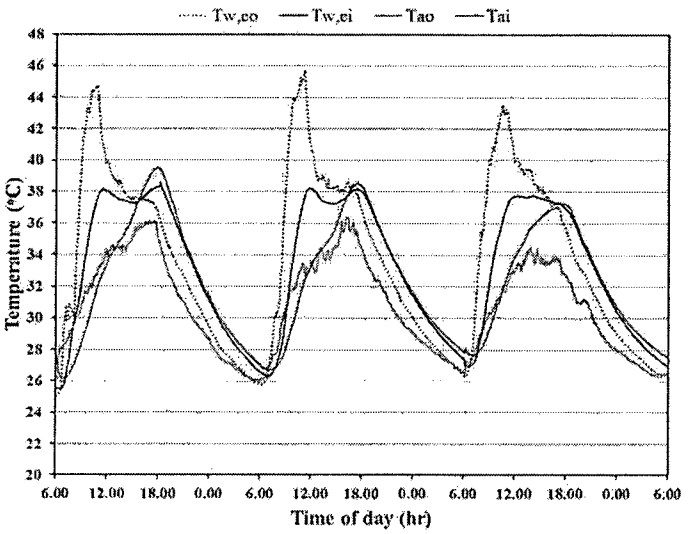

Figure 86 The temperature change of easterly aspect exterior and interior cement block wall surfaces.

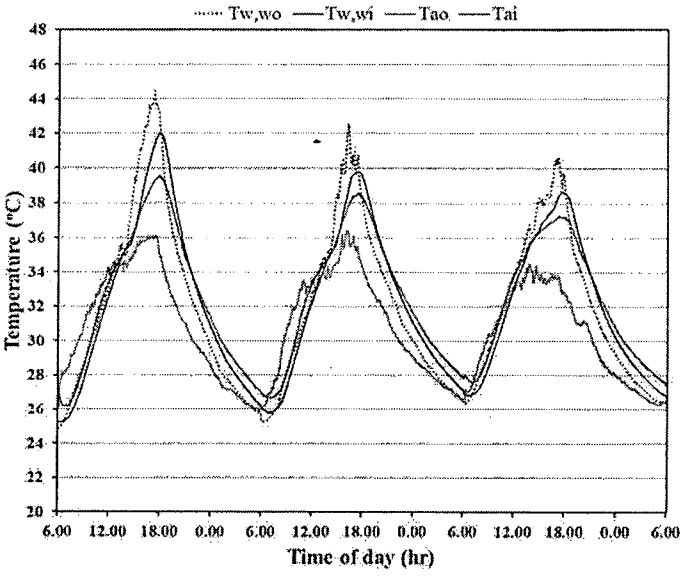

Figure 87 The temperature change of westerly aspect exterior and interior cement block wall surfaces.

The commercial autoclaved aerated concrete wall

External wall surfaces

The temperature evolution of the exterior surface temperature of the commercial autoclaved aerated concrete house wall in all sides is shown in Figure 88. The maximum exterior wall temperature of the north, south, east and west surfaces reached as high as 36.5 °C, 46 °C, 49.4 °C and 47.5 °C at around 3.30-4pm, 4.30-5pm, 9.30am and 4.30-5pm respectively and then dropped in value over time passed after each those times. The average exterior surface temperature in all of the north, south, east and west surfaces was at approximately 32.5 °C, 36 °C, 40.2 °C and 36.5 °C respectively was observed in midday time from 6am to 6pm, giving a 12 h in each day. In midnight time from 6pm to 6am, that was at approximately 28.2 °C, 29.5 °C, 28.5 °C and 29.0 °C, respectively.

Internal wall surfaces

The temperature evolution of the interior surface temperature of the PCM coated AAC house wall in all sides is shown in Figure 89. The maximum exterior wall temperature of the north, south, east and west surfaces peaked as high as 36.5 °C, 38.2 °C, 39 °C and 38.5 °C at the same time, around 5.30-6pm and then dropped in value over time passed after each those times. The average interior surface temperature in all of the north, south, east and west surfaces was at approximately 31.5 °C, 32 °C, 34.3 °C and 32.3 °C was observed in midday time from 6am to 6pm, giving a 12 h in each day. In midnight time from 6pm to 6am, that was while at approximately 30.7 °C, 31.5 °C, 31 °C and 31.2 °C, respectively.

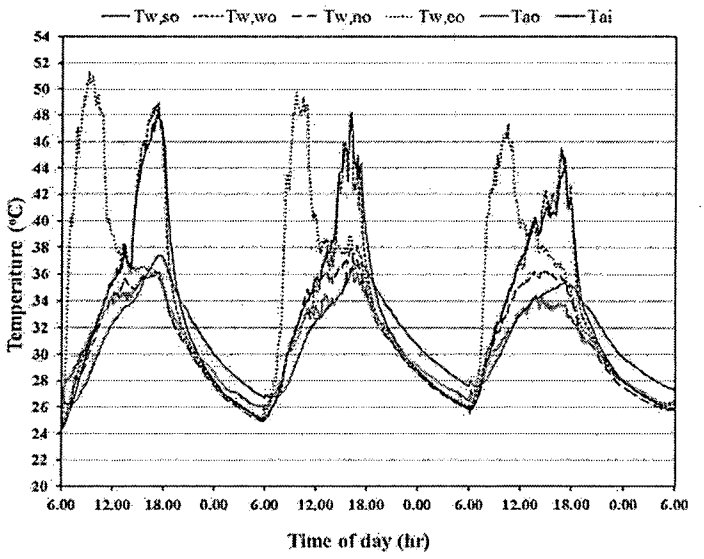

Figure 88 The temperature variation of exterior autoclaved aerated concrete wall surfaces.

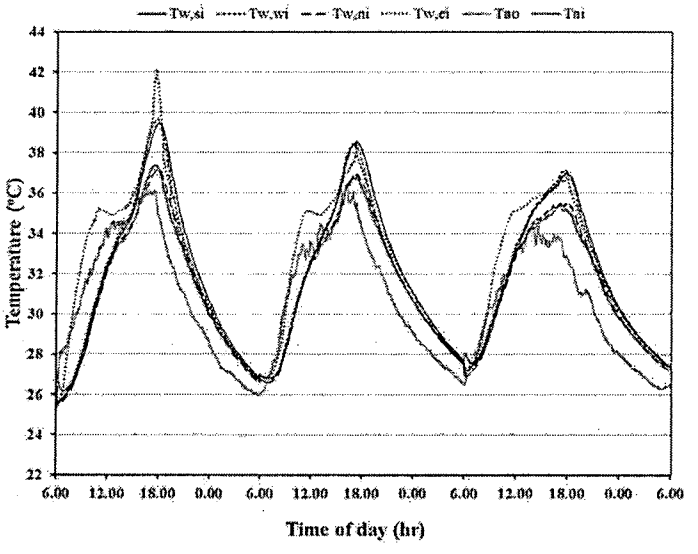

Figure 89 The temperature variation of interior autoclaved aerated concrete wall surfaces.

Northerly aspect wall surfaces

The temperature fluctuation of Northerly aspect interior and exterior surface temperature of the commercial autoclaved aerated concrete house is shown in Figure

90. The maximum value of ambient temperature (Tao) was observed at about 35.4 °C at the day time around 4.30pm. The exterior wall temperature of the Northerly aspect rapidly heated to as high as approximately 36.5 °C at around 3.30-4pm while peak temperatures of the interior surface reached its maximum value of approximately 36.5 °C at around 5.30-6pm. The maximum room temperature (Tai) as approximately 36.5 °C was found at the day time around 5.30pm.

Southerly aspect wall surfaces

The temperature fluctuation of Southerly aspect interior and exterior surface temperature of the commercial autoclaved aerated concrete house is shown in Figure 91. The maximum value of ambient temperature (Tao) was observed at about 35.4 °C at the day time around 4.30pm. The exterior wall temperature of the Southerly aspect rapidly heated to as high as approximately 46 °C at around 4.30-5pm while peak temperatures of the interior surface reached its maximum value of approximately 38.2 °C at around 5.30-6pm. The maximum room temperature (Tai) as approximately 36.5 °C was found at the day time around 5.30pm.

Easterly aspect wall surfaces

The temperature variation of Easterly aspect interior and exterior surface temperature of the commercial autoclaved aerated concrete house is shown in Figure 92. The maximum value of ambient temperature (Tao) was observed at about 35.4 °C at the day time around 4.30pm. The exterior wall temperature of the Easterly aspect rapidly heated to as high as approximately 49.4 °C at around 9.30am while peak temperatures of the interior surface reached its maximum value of approximately 39 °C at around 5.30-6pm. The maximum room temperature (Tai) as approximately 36.5 °C was found at the day time around 5.30pm.

Westerly aspect wall surfaces

The temperature fluctuation of Westerly aspect interior and exterior surface temperature of the commercial autoclaved aerated concrete house is shown in Figure 93. The maximum value of ambient temperature (Tao) was observed at about 35.4 °C at the day time around 4.30pm. The exterior wall temperature of the Westerly aspect rapidly heated to as high as approximately 47.5 °C at around 4.30-5pm while peak temperatures of the interior surface reached its maximum value of approximately

38.5 °C at around 5.30-6pm. The maximum room temperature (Tai) as approximately 36.5 °C was found at the day time around 5.30pm.

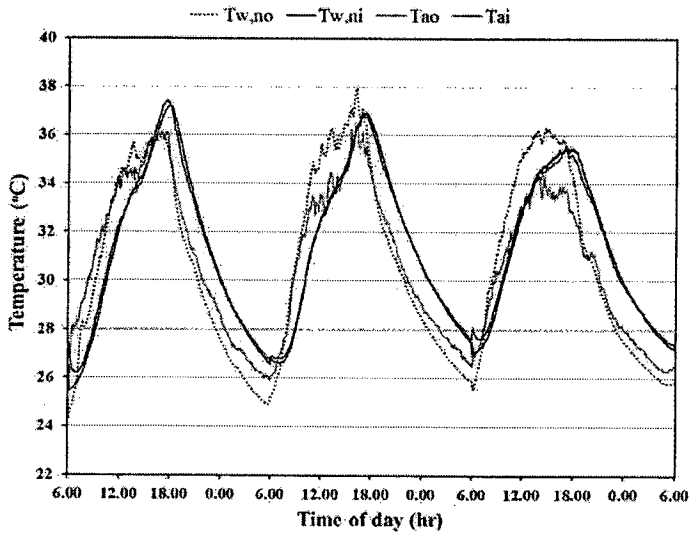

Figure 90 The temperature change of northerly aspect exterior and interior autoclaved aerated concrete wall surfaces.

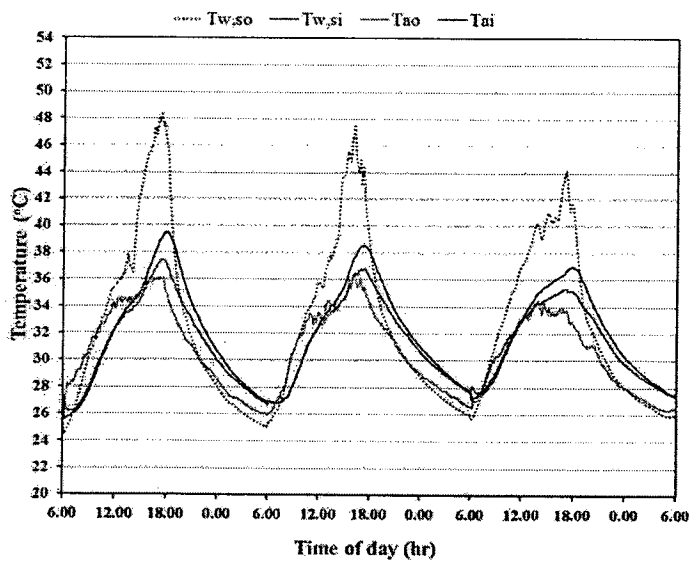

Figure 91 The temperature change of southerly aspect exterior and interior autoclaved aerated concrete wall surfaces.

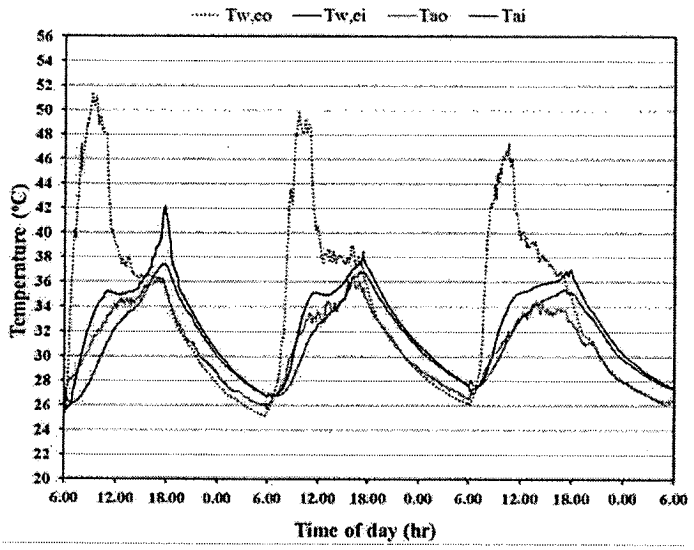

Figure 92 The temperature change of easterly aspect exterior and interior autoclaved aerated concrete wall surfaces.

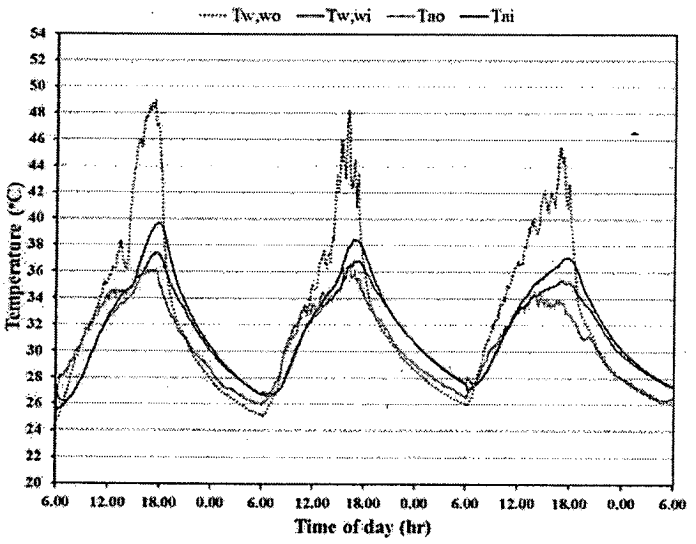

Figure 93 The temperature change of westerly aspect exterior and interior autoclaved aerated concrete wall surfaces.

The brick wall

External wall surfaces

The temperature evolution of the exterior surface temperature of the brick house wall in all sides is shown in Figure 94. The maximum exterior wall temperature of the north, south, east and west surfaces reached as high as 37.5 °C, 45.5 °C, 44.5 °C and 45.0 °C at around 4.30-5pm, 4.30-5pm, 10.30-11am and 4.30-5pm respectively and then dropped in value over time passed after each those times. The average exterior surface temperature in all of the north, south, east and west surfaces was at approximately 32.8 °C, 35.4 °C, 38 °C and 35.0 °C was observed in midday time from 6am to 6pm, giving a 12 h in each day. In midnight time from 6pm to 6am, that was at approximately 30.3 °C, 32 °C, 30.4 °C and 31.0 °C, respectively.

Internal wall surfaces

The temperature evolution of the interior surface temperature of the brick house wall in all sides is shown in Figure 95. The maximum interior wall temperature of the north, south, east and west surfaces peaked as high as 38.5 °C, 41.7 °C, 39.2 °C and 41.4 °C at the same time, around 5.30-6pm and then dropped in value over time passed after each those times. The average exterior surface temperature in all of the north, south, east and west surfaces was at approximately 32.3 °C, 33.3 °C, 35.3 °C and 33.5 °C was observed in midday time from 6am to 6pm, giving a 12 h in each day. In midnight time from 6pm to 6am, that was while at approximately 31.9 °C, 33.3 °C, 31.8 °C and 32.5 °C, respectively.

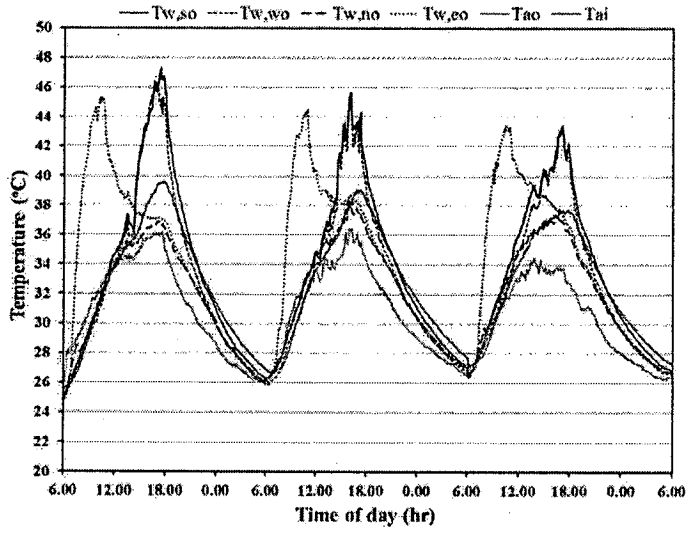

Figure 94 The temperature variation of exterior brick house wall surfaces.

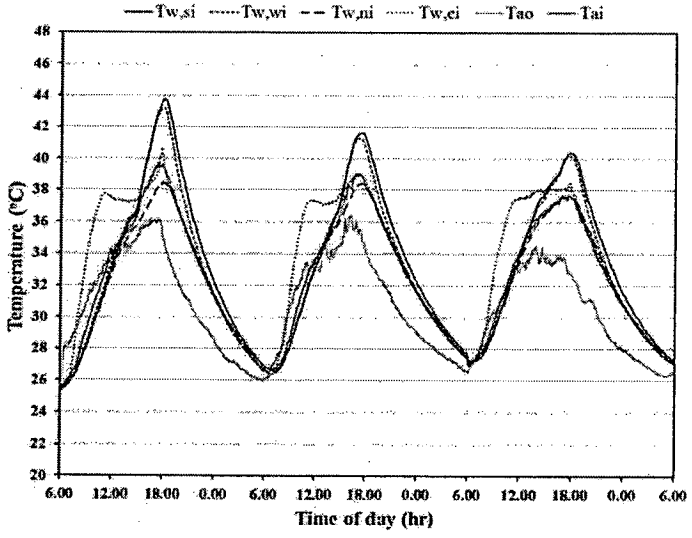

Figure 95 The temperature variation of interior surface of brick house wall.

Northerly aspect wall surfaces

The temperature fluctuation of Northerly aspect interior and exterior surface temperature of the brick house is shown in Figure 96. The maximum value of ambient temperature (Tao) was observed at about 35.4 °C at the day time around 4.30pm. The exterior wall temperature of the Northerly aspect rapidly heated to as high as

approximately 37.5 °C at around 4.30-5pm while peak temperatures of the interior surface reached its maximum value of approximately 38.5 °C at around 5.30-6pm. The maximum room temperature (Tai) as approximately 38.7 °C was found at the day time around 5.30pm.

Southerly aspect wall surfaces

The temperature fluctuation of Southerly aspect interior and exterior surface temperature of the brick house is shown in Figure 97. The maximum value of ambient temperature (Tao) was observed at about 35.4 °C at the day time around 4.30pm. The exterior wall temperature of the Southerly aspect rapidly heated to as high as approximately 45.5 °C at around 4.30-5pm while peak temperatures of the interior surface reached its maximum value of approximately 41.7 °C at around 5.30-6pm. The maximum room temperature (Tai) as approximately 38.7 °C was found at the day time around 5.30pm.

Easterly aspect wall surfaces

The temperature variation of Easterly aspect interior and exterior surface temperature of the brick house is shown in Figure 98. The maximum value of ambient temperature (Tao) was observed at about 35.4 °C at the day time around 4.30pm. The exterior wall temperature of the Easterly aspect rapidly heated to as high as approximately 44.5 °C at around 10.30-11am while peak temperatures of the interior surface reached its maximum value of approximately 39.2 °C at around 5.30-6pm. The maximum room temperature (Tai) as approximately 38.7 °C was found at the day time around 5.30pm.

Westerly aspect wall surfaces

The temperature fluctuation of Westerly aspect interior and exterior surface temperature of the brick house is shown in Figure 99. The maximum value of ambient temperature (Tao) was observed at about 35.4 °C at the day time around 4.30pm. The exterior wall temperature of the Westerly aspect rapidly heated to as high as approximately 45.0 °C at around 4.30-5pm while peak temperatures of the interior surface reached its maximum value of approximately 41.4 °C at around 5.30-6pm. The maximum room temperature (Tai) as approximately 38.7 °C was found at the day time around 5.30pm.

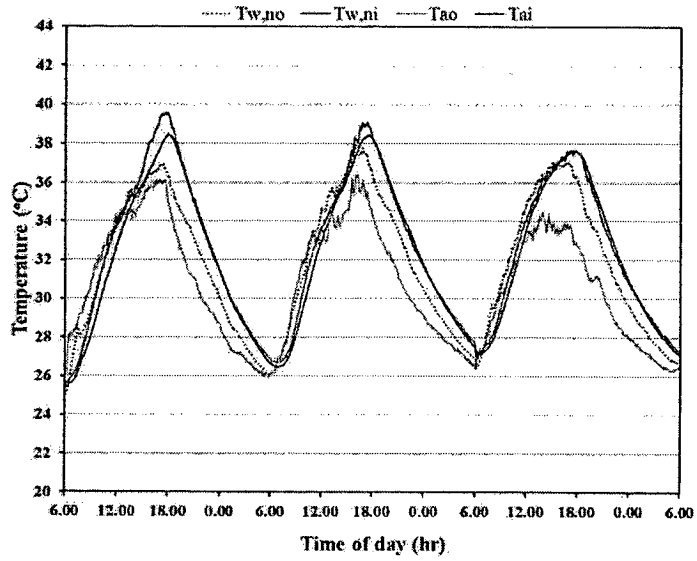

Figure 96 The temperature change of northerly aspect exterior and interior brick wall surfaces.

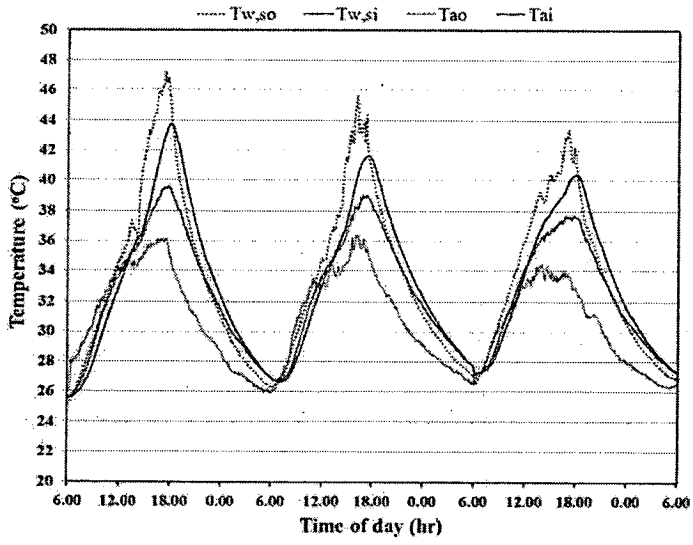

Figure 97 The temperature change of southerly aspect exterior and interior brick wall surfaces.

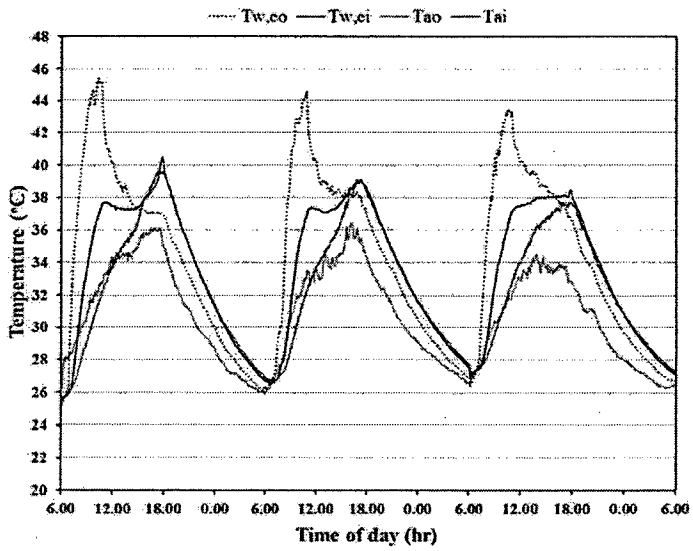

Figure 98 The temperature change of easterly aspect exterior and interior brick wall surfaces.

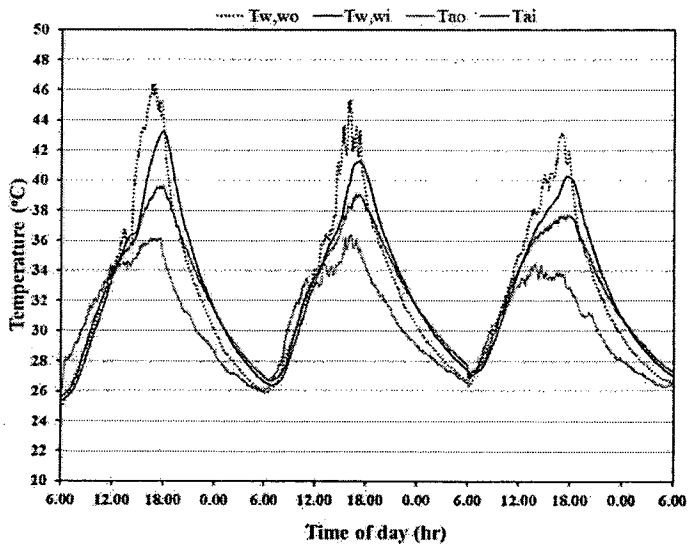

Figure 99 The temperature change of westerly aspect exterior and interior brick wall surfaces.

Comparison of exterior and interior surface temperature, room temperature and relative humidity and heat flux revolution

Northerly aspect external wall surfaces

Figure 100 illustrates the northerly aspect exterior surfaces temperature of the four houses. The maximum exterior wall temperature of the houses with cement block, brick, AAC and PCM-coated AAC reached as high as 36.5, 37.5, 36.5 and 37 °C respectively at the same time around 3.30-5pm. This result shows that the maximum exterior wall temperature of north facing wall surfaces of each house was not different in value. Throughout the period of midnight to early morning, about 6am, the exterior surface temperature of the AAC house had a temperature lower than the ambient temperature, presumably due to the higher insulative property of the AAC material. The PCM-coated AAC house had an even lower temperature than the ambient temperature because of the heat emission property of the PCM coating. On the other hand the temperatures of the cement block and brick houses were approximately 1 °C higher than ambient temperature.

Northerly aspect internal wall surfaces

Figure 101 shows the north interior surface temperature of the four houses. The maximum interior wall temperature of cement block, brick, AAC and PCM coated AAC reached as high as 37.3 °C, 38.5 °C, 36.5 °C and 36 °C repectively for each material at the same time, around 5.30-6pm.

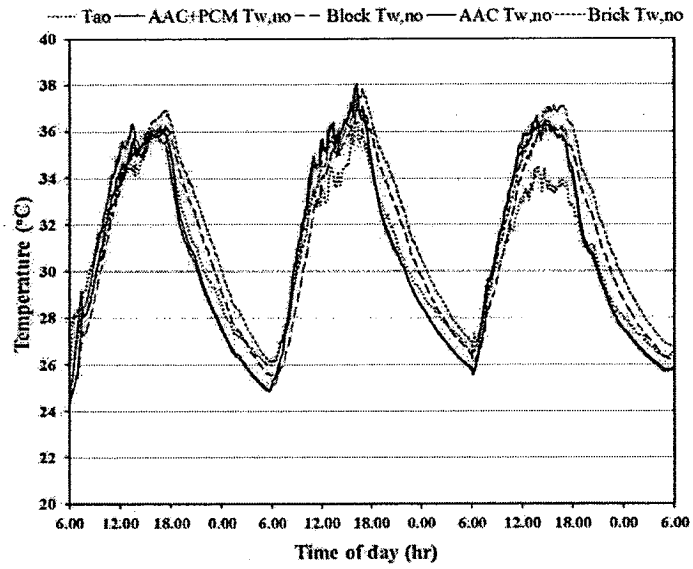

Figure 100 Comparison of northerly aspect exterior wall surface temperature of the 4 houses.

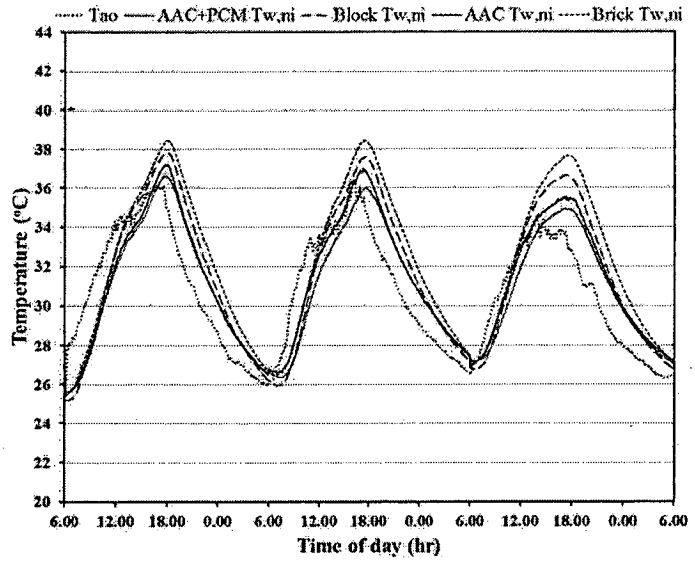

Figure 101 Comparison of northerly aspect interior wall temperature surface of the 4 houses.

Southerly aspect external wall surfaces

Figure 102 illustrates the southerly aspect exterior surfaces temperature of the four houses. The south exterior surface temperature of each house was approximately

equal throughout the morning and afternoon. The maximum temperature of all of the test houses reached a temperature of ~46 °C at around 4pm. Then, between 6pm and 5am the following morning, the exterior surface temperature of the AAC and PCM coated AAC houses cooled to around 2-3 °C lower than the walls of the cement block and brick houses in the same period.

Southerly aspect internal wall surfaces

Figure 103 exhibits the south interior surface temperature of the four houses. The maximum interior wall temperature of cement block wall peaked as high as 42.2 °C at around 5.30-6pm while that of brick, AAC and PCM coated AAC was at approximately 41.7 °C, 38.2 °C and 37.3 °C at around the same time of 5.30-6pm.

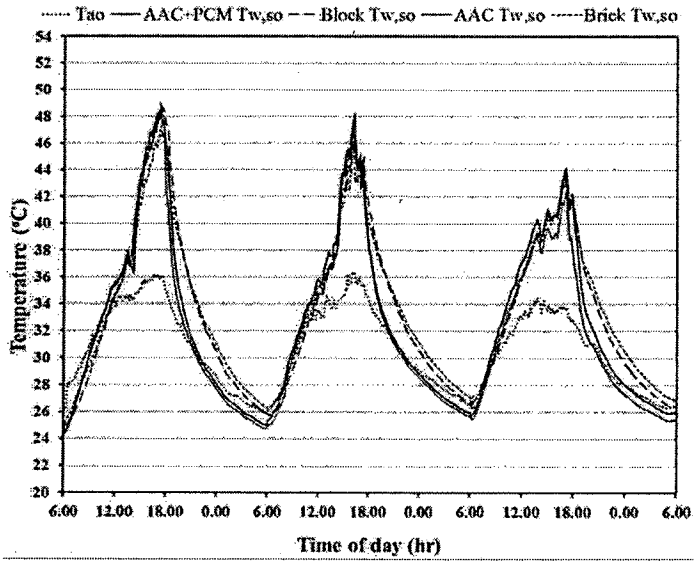

Figure 102 Comparison of southerly aspect exterior wall surface temperature of the 4 houses.

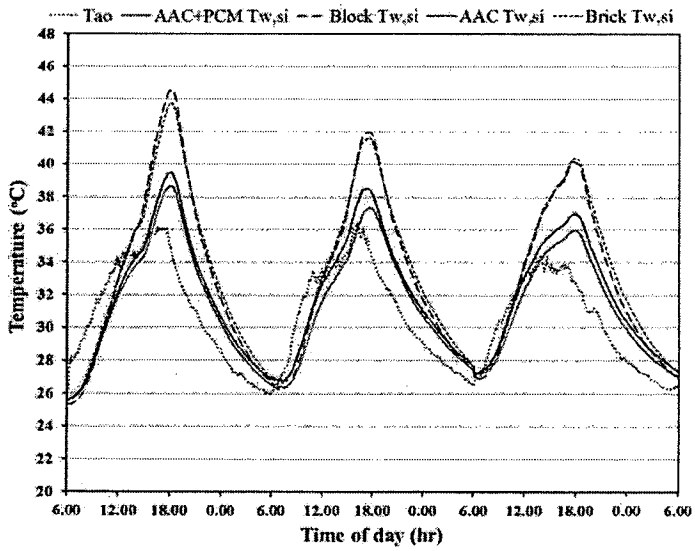

Figure 103 Comparison of southerly aspect interior wall surface temperature of the 4 houses.

Easterly aspect external wall surfaces

Figure 104 shows the east exterior surface temperature of the four houses. The exterior wall temperature of the PCM coated AAC house rapidly heated to as high as 50 °C at around 9.00am while peak temperatures of the untreated AAC, cement block and brick walls were approximately 49.5 °C at ~ 9.30am, 45 °C at ~ 10.30am and 44.5 °C at 11am, respectively, showing different rates of temperature rise over time. So the maximum exterior wall temperature of the PCM coated AAC house was about 0.5 °C – 5.5 °C higher and rose more quickly than that of the uncoated wall materials. This may be due to the higher insulative property of the AAC material not allowing the temperature to be transferred to the interior wall, or thermal energy being stored at the outer surface due to coating PCM, and not radiated into the ambient environment. Throughout the period from around 5pm to early morning the next day, the exterior surface temperature of both the AAC and PCM coated AAC walls fell more quickly and fell to between 0.5 °C and 2.5 °C lower than that of the cement block and brick.

Easterly aspect internal wall surfaces

Figure 105 exhibits the east interior surface temperature of the four houses. The maximum interior wall temperature of the cement block wall house rapidly peaked as high as 38.2 °C at around 5.30-6pm while that of brick, AAC and PCM

coated AAC houses were approximately 39.2 °C, 39 °C and 37.7 °C respectively, at around the same time, 5.30-6pm.

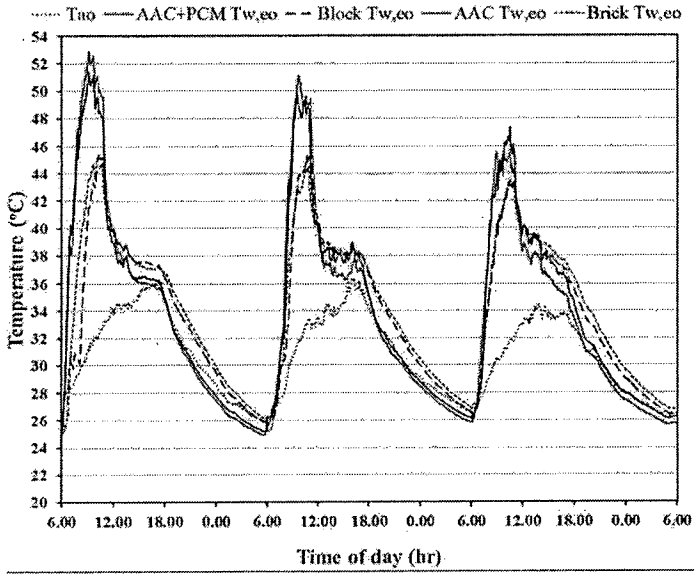

Figure 104 Comparison of easterly aspect exterior wall surface temperature of the 4 houses.

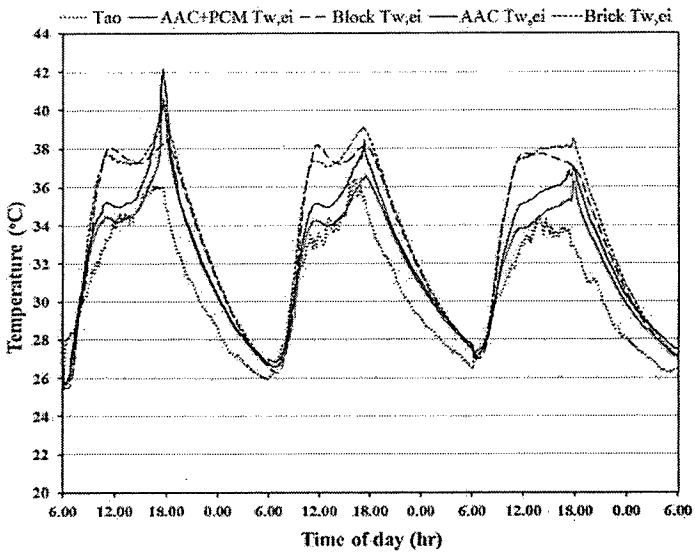

Figure 105 Comparison of easterly aspect interior wall surface temperature of the 4 houses.

Westerly aspect external wall surfaces

Figure 106 illustrates the west exterior surface temperature of the four houses. The maximum exterior wall temperature of cement block peaked as high as 42.5 °C at around 4.30-5pm while that of the brick, AAC and PCM coated AAC were at approximately 45 °C, 47.5 °C and 48 °C respectively at around 4.30-5pm. It is noteworthy that the maximum exterior wall temperature of the PCM coated AAC only 0.5 °C was higher than that of the untreated AAC, while being about 3-5.5 °C higher than that of the cement brick and block materials (also uncoated) at 4.30-5pm. The exterior surface temperature of both the AAC and PCM coated AAC fell faster and to between 1 °C and 4 °C lower than that of cement block and brick during the period of 6pm to 6am. Again, this is presumed to be due to the more effective heat transfer characteristics of the AAC material.

Westerly aspect internal wall surfaces

Figure 107exhibits the west interior surface temperature of the four houses. The maximum interior wall temperature of cement block peaked as high as 40 °C at around 5.30-6pm while that of brick, AAC and PCM coated AAC was at approximately 41.5 °C, 38.5 °C and 37 °C respectively, also at around 5.30-6pm.

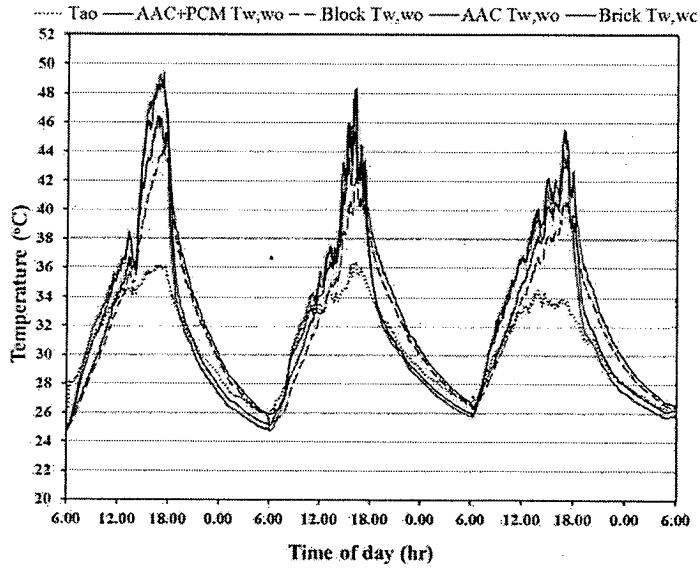

Figure 106 Comparison of westerly aspect exterior wall surface temperature of the 4 houses.

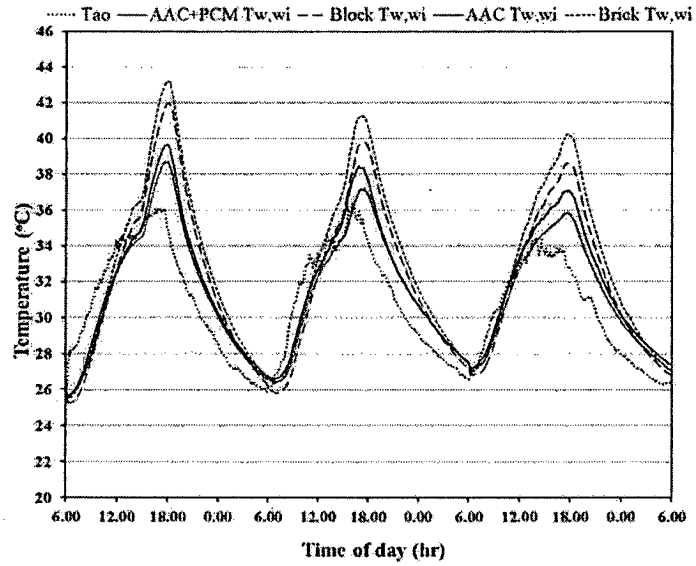

Figure 107 Comparison of westerly aspect interior wall surface temperature of the 4 houses.

Comparison of flux evolution and room temperature

Heat fluxes on both the interior and exterior surfaces of the easterly and westerly aspects walls of the four houses were investigated, as illustrated in Figure 108-Figure 109. Heat flux on the wall surface is positive when the heat wave propagates from the outer surface to the inner surface (That is, when the exterior surface temperature is higher than the interior surface temperature) while heat flux on the wall surface is negative when heat wave propagates from the inside surface to the outside surface (exterior surface temperature is less than interior surface temperature).

With the cement block house, positive heat fluxes in all of the east and west surfaces were first increased and reached its maximum value of approximately 73 and 27 W/m^2 at around 9.30am and 4 pm the east and west surfaces respectively and then dropped in value over time passed after each those times. It was found that the negative heat fluxes of the east and west surfaces began at around 5pm and 5.30pm, respectively. The highest value of the heat fluxes were about 13 and 14 W/m^2 at around 7pm and 6.30pm for the east and west surfaces respectively, then dropped for day time below these values.

For the heat fluxes of the brick house walls, the maximum positive value for the east and west surfaces was observed at about 54 and 35 W/m^2 at around 9.30am and 3pm, respectively. While, the maximum negative value in the part of the east and west surfaces was observed at about 11 and 12.5 W/m^2 at around 7 pm and 6.30pm, respectively.

For the heat fluxes of the AAC house wall, the maximum positive value for each of the east and west surfaces was observed at about 34 and 20 W/m^2 at around 9.30 am and 4pm, respectively. The maximum negative values were observed at about 4.5 and 5 W/m^2 at around 7.30pm and 7.30pm, respectively.

For the heat fluxes of AAC with PCM house wall, the maximum positive value in the part of the east and west surfaces was observed at about 31 and 18 W/m^2 at around 9.30am and 4pm, respectively. The maximum negative value for each of the east and west surfaces was observed at about 4.5 and 4.5 W/m^2 at around 7pm and 7.30pm, respectively.

This shows that the maximum positive heat flux of the PCM coated AAC house wall in the east and west sides had the least positive heat flux value, while that of cement block house wall in all sides had the maximum value. The maximum positive heat flux of the PCM coated AAC wall on each of the east and west surfaces was less than that of the uncoated AAC wall of around 3 and 2 W/m^2, that of brick wall of around 23 and 17 W/m^2 and that of cement block wall of around 42 and 9 W/m^2.

The average positive heat flux values of the PCM coated AAC house on the east and west wall surfaces were around 10.5 and 6.7 W/m^2, respectively. The average positive heat flux values of the uncoated AAC wall surfaces were around 11.9 and 7.0 W/m^2, respectively. For the cement block house walls the values were around 24.7 and 6.7 W/m^2, respectively, and for the brick house walls were around 21.9 and 8.7 W/m^2, respectively. These average positive heat flux values corresponded to the Overall Thermal Transfer Value (OTTV). OTTV is a measure of heat gain into the building through the building envelope, which can be controlled as a means of enhancing the energy efficiency of buildings [92]. OTTV in Thailand is stated in building codes as to not exceed a statutory limit by 45 W/m^2 [93]. In the comparison of OTTV of the 4 houses, it was found that the PCM coated AAC house walls had the lowest OTTV, on

the east and west sides, of all the test houses and did not exceed the statutory limit in any case. This demonstrates that the utilization of PCM on the exterior surfaces of a building using Autoclaved Aerated Concrete (AAC) can reduce the heat transfer through the building envelop and lead to an improvement in the insulative efficiency of buildings.

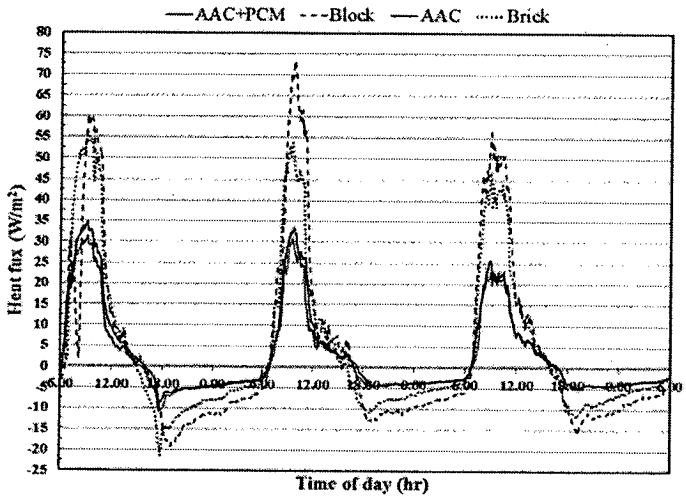

Figure 108 Heat flux comparison of easterly aspect wall surface of the 4 houses.

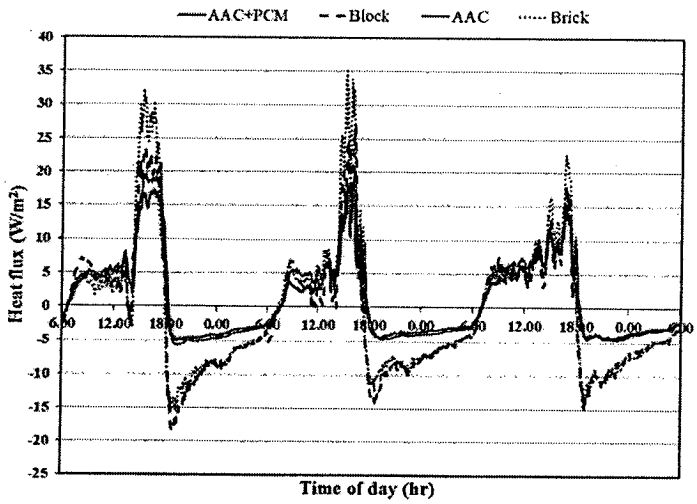

Figure 109 Heat flux comparison of westerly aspect wall surface of the 4 houses.

Room temperatures in the four houses between 6am and 6pm are shown in Figure 110. The effect of the fluctuating nature of solar radiation, ambient temperature, heat flux transfer and exterior and interior surface temperature evolution of the house walls on each side on the room temperature of each house varied over the course of the day. It can be seen that the room temperatures of the four houses was approximately equal between the times of 6am and 10.30am. After that time, different peak temperatures were reached in each test house at different times. By 11am the PCM coated AAC building room temperature was between 1 °C and 4.5 °C lower than the other 3 houses. After 11am the temperature readings diverged. The room temperature of the cement block house rose more rapidly, and achieved the highest peak value of all the houses; 39.5 °C at about 6pm. The room temperature of the brick house peaked at 39 °C at about 5pm. The AAC houses had the slowest temperature rise. The uncoated AAC house reached a peak temperature of 36.5 °C at 5pm, and the PCM coated AAC house had the lowest peak temperature, 35.5 °C, reached at 5pm.

These readings indicate that the utilization of AAC with PCM coating significantly attenuates the daily room temperature fluctuation of partitions. The daily room temperature swing was reduced from 12.5 °C (cement block house), 12 °C (brick house) and 9.5 °C (uncoated AAC house) to only 8.5 °C in the PCM coated house.

The relative humidity in the four houses was measured from 6am of day to 6am of the following day are shown in Figure 111. The fluctuating nature of relative humidity in the tropics occurs because of the evolution of solar radiation, ambient temperature, heat flux transfer and exterior and interior surface temperature evolution of the house walls on each side on the relative humidity of each house varied over the course of the day. It can be seen that the relative humidity of the four houses was nearly the same level during the daily period of 6am to 6am

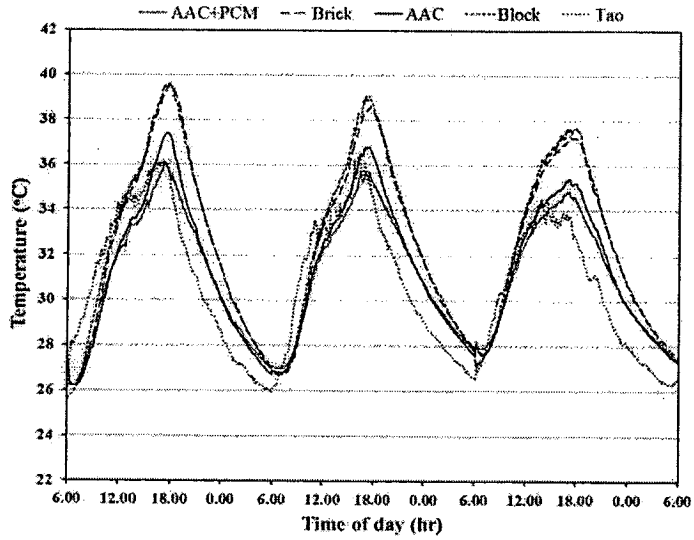

Figure 111 Comparison of room temperature of the 4 houses.

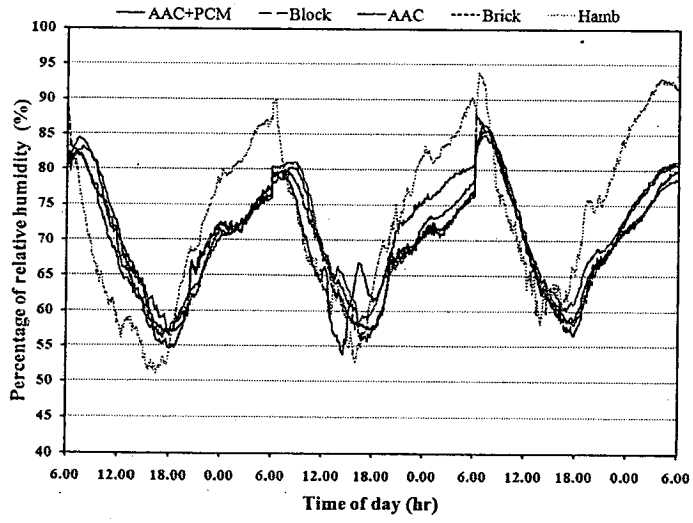

Figure 102 Comparison of interior relative humidity of the 4 houses.

Test results in the simulated rainy season

The fluctuations in solar radiation, ambient temperatures and percentage of relative humidity in the simulated rainy season are illustrated in Figure 112-114. These tests were done and results observed from 6am of day to 6am of the following day, giving a 24 h test cycle (on July 5, July 7 and July 9, 2013). The simulated rainfall

level in this study was considered from mean annual rainfall in Thailand in last 10 year period (2004-2013).

The fluctuating nature of solar radiation in the tropics occurs because of periodical cloud cover which is typical between sunrise (6.00 am) and sunset (7.00 pm) with the highest values of up to approximately 1.13 kW/m^2 around midday. Wind velocity at the test site was between 0.30 and 3.60 m/s. The ambient temperature depended upon weather conditions and fluctuated between approximately 26-28 °C in the morning between 5-6am and up the maximum value of about 35 °C at around 4pm. The percentage of relative humidity depended also upon weather conditions and fluctuated between approximately 60% at around 2-3pm and up the maximum value of approximately 95% in the morning between 5-7am.

With considering the relation of fluctuations in solar radiation, ambient temperatures and percentage of relative humidity, it was observed that fluctuations in solar radiation was positively proportionate to the ambient temperatures as exhibited in Figure 112. While the fluctuations in solar radiation and ambient temperatures increased inversely to percentage of relative humidity as shown in Figure 113-114.

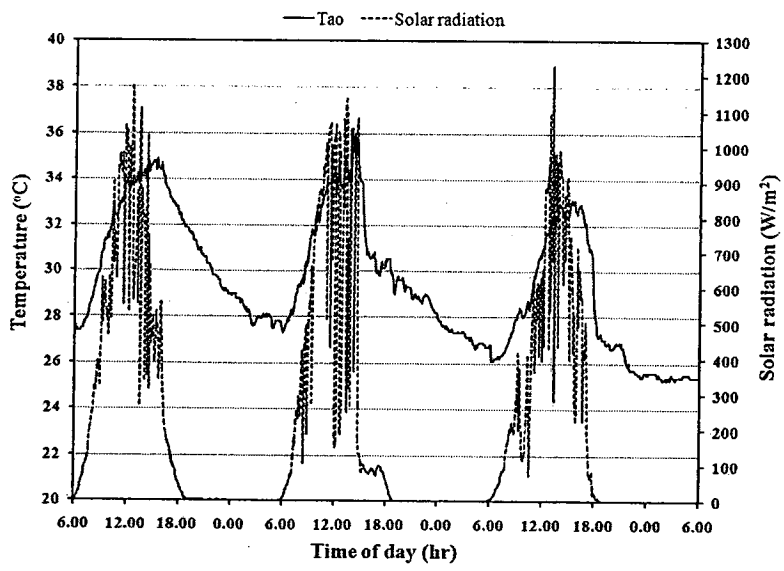

Figure 112 Variation of temperature and solar radiation.

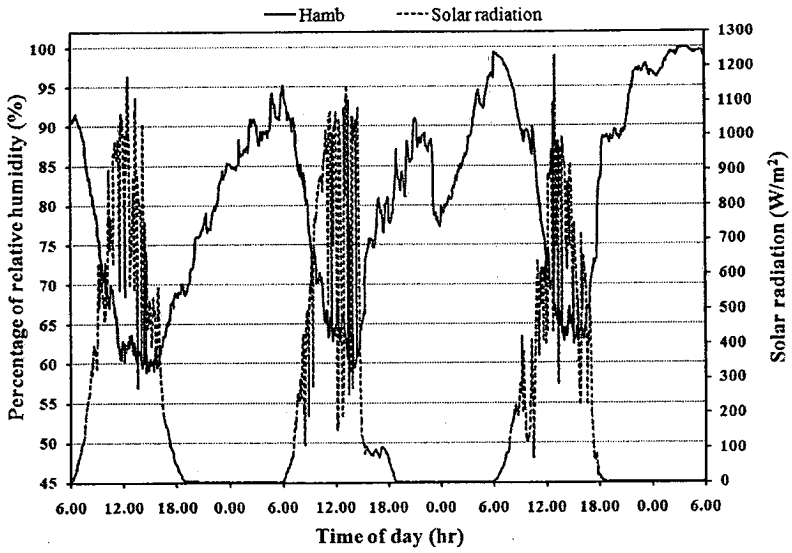

Figure 113 Variation of relative humidity and solar radiation.

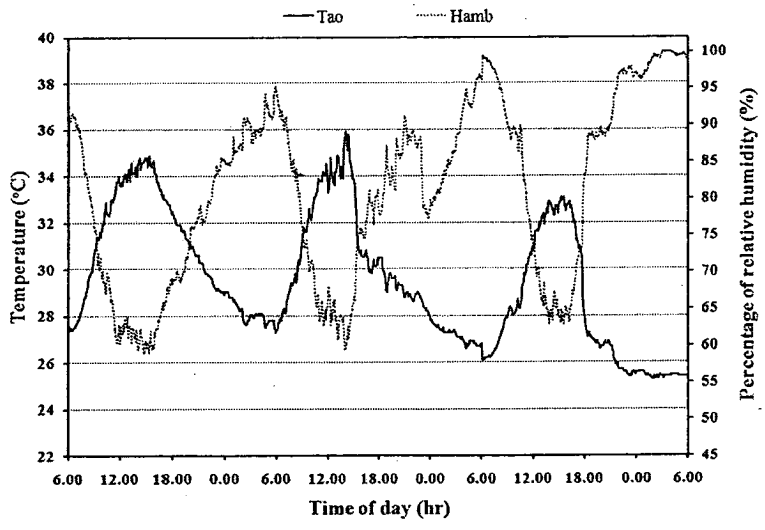

Figure 114 Variation of relative humidity and temperature.

The autoclaved aerated concrete wall with phase change material coating

External wall surfaces

The temperature evolution of the exterior surface temperature of the PCM coated AAC house wall in all sides is shown in Figure 115. The maximum exterior wall temperature of the north, south, east and west surfaces reached as high as approximately 31.3 °C, 38.5 °C, 42.3 °C and 38.5 °C at around 2.30pm, 2.30pm,

10.00am and 3-3.30 pm respectively and then dropped in value over time passed after each those times. The average exterior surface temperature in all of the north, south, east and west surfaces was at approximately 28.6 °C, 31.3°C, 36 °C and 32.3 °C was observed in midday time from 6am to 6pm, giving a 12 h in each day. In midnight time from 6pm to 6am, that was at approximately 27 °C, 27 °C, 27.7 °C and 27.6 °C, respectively.

Internal wall surfaces

The temperature evolution of the interior surface temperature of the PCM coated AAC house wall in all sides is shown in Figure 116. The maximum exterior wall temperature of the north, south, east and west surfaces peaked as high as 32.0 °C, 32.8 °C, 33.3 °C and 33.3 °C, at around the same time, 4.30-5.30pm and then dropped in value over time passed after each those times. The average interior surface temperature in all of the north, south, east and west surfaces was at approximately 30.3 °C, 30.6 °C, 31.7 °C and 31 °C was observed in midday time from 6am to 6pm, giving a 12 h in each day. In midnight time from 6pm to 6am, that was while at approximately 28.6 °C, 298 °C, 29 °C and 29 °C, respectively.

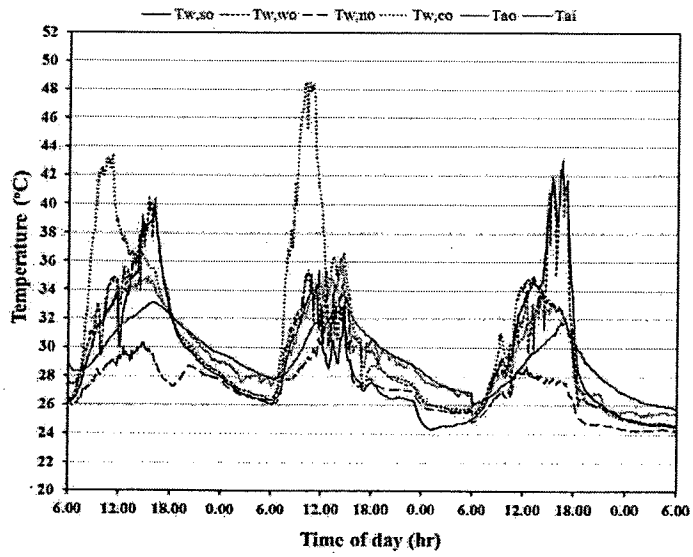

Figure 115 The temperature variation of exterior improved autoclaved aerated concrete wall surfaces.

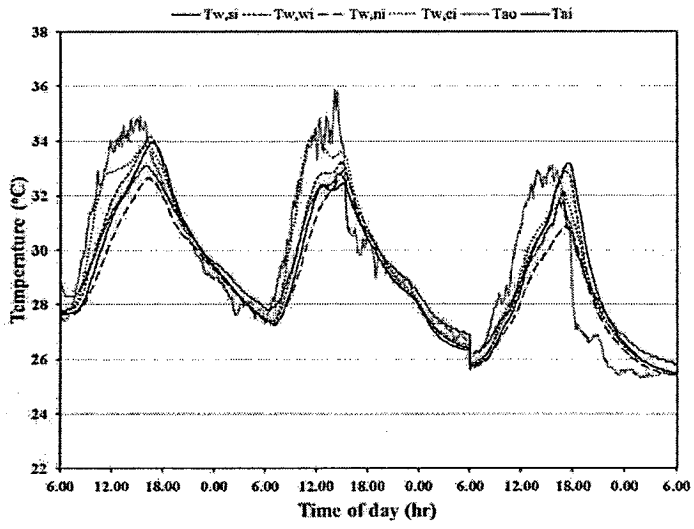

Figure 116 The temperature variation of interior improved autoclaved aerated concrete wall surfaces.

Northerly aspect wall surfaces

The temperature fluctuation of Northerly aspect interior and exterior surface temperature of the PCM coated AAC house is shown in Figure 117. The maximum value of ambient temperature (Tao) was observed at about 34.5 °C at the day time around 3-3.30pm. The exterior wall temperature of the Northerly aspect rapidly heated to as high as approximately 31.3 °C at around 2.30pm while peak temperatures of the interior surface reached its maximum value of approximately 32.0 °C at around 4-4.30pm. The maximum room temperature (Tai) as approximately 32.5 °C was found at the day time around 4-4.30pm.

Southerly aspect wall surfaces

The temperature fluctuation of Southerly aspect interior and exterior surface temperature of the PCM coated AAC house is shown in Figure 118. The maximum value of ambient temperature (Tao) was observed at about 34.5 °C at the day time around 3-3.30pm. The exterior wall temperature of the Southerly aspect rapidly heated to as high as approximately 38.5 °C at around 2.30pm while peak temperatures of the interior surface reached its maximum value of approximately 32.8 °C at around 5-5.30pm. The maximum room temperature (Tai) as approximately 32.5 °C was found at the day time around 4-4.30pm.

Easterly aspect wall surfaces

The temperature variation of Easterly aspect interior and exterior surface temperature of the PCM coated AAC house is shown in Figure 119. The maximum value of ambient temperature (Tao) was observed at about 34.5 °C at the day time around 3-3.30pm. The exterior wall temperature of the Easterly aspect rapidly heated to as high as approximately 42.3 °C at around 10.30am while peak temperatures of the interior surface reached its maximum value of approximately 33.3 °C at around 4pm. The maximum room temperature (Tai) as approximately 32.5 °C was found at the day time around 4-4.30pm.

Westerly aspect wall surfaces

The temperature fluctuation of Westerly aspect interior and exterior surface temperature of the PCM coated AAC house is shown in Figure 120. The maximum value of ambient temperature (Tao) was observed at about 34.5 °C at the day time around 3-3.30pm. The exterior wall temperature of the Westerly aspect rapidly heated to as high as approximately 38.5 °C at around 3-3.30 pm while peak temperatures of the interior surface reached its maximum value of approximately 33.3 °C at around 4.30-5pm. The maximum room temperature (Tai) as approximately 32.5 °C was found at the day time around 4-4.30pm.

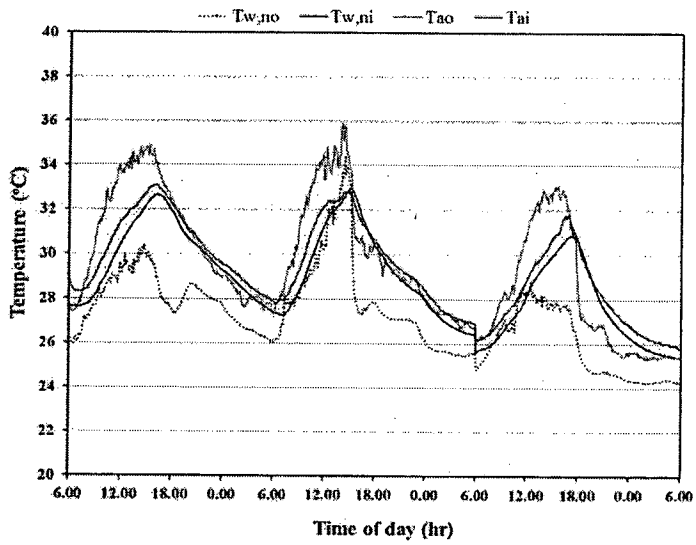

Figure 117 The temperature change of northerly aspect exterior and interior improved autoclaved aerated concrete wall surfaces.

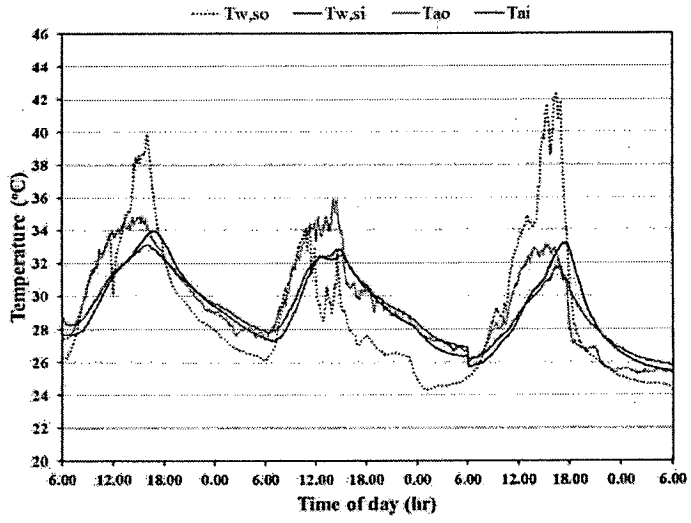

Figure 118 The temperature change of southerly aspect exterior and interior improved autoclaved aerated concrete wall surfaces.

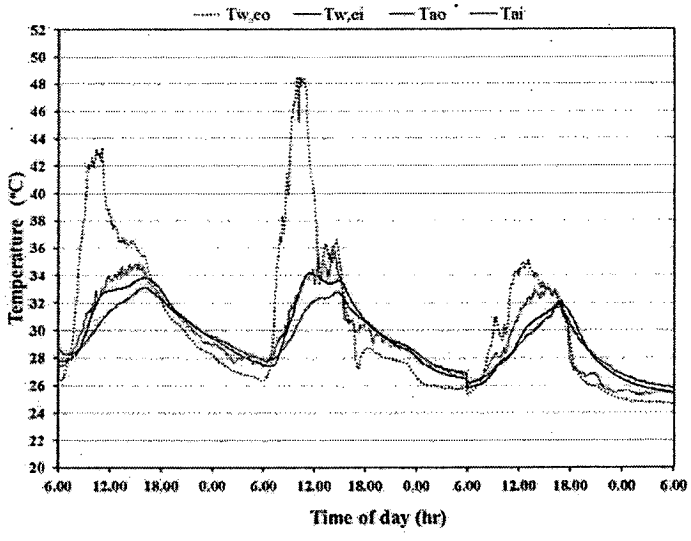

Figure 119 The temperature change of easterly aspect exterior and interior improved autoclaved aerated concrete wall surfaces.

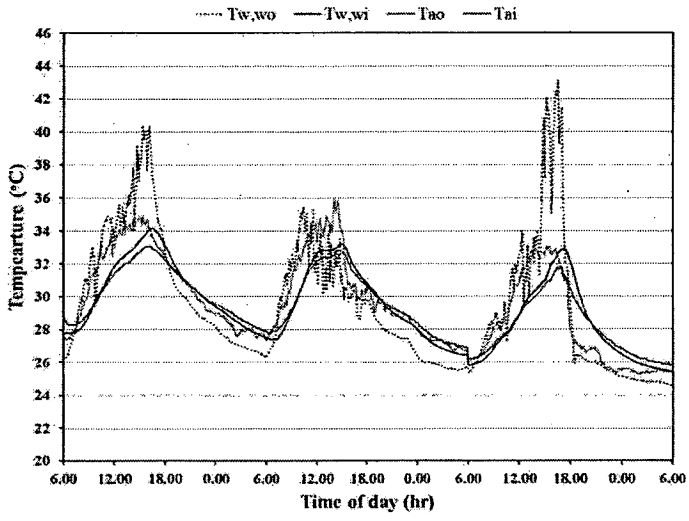

Figure 120 The temperature change of westerly aspect exterior and interior improved autoclaved aerated concrete wall surfaces.

The cement block wall

External wall surfaces

The temperature evolution of the exterior surface temperature of the cement block house wall in all sides is shown in Figure 121. The maximum exterior wall temperature of the north, south, east and west surfaces reached as high as 30.8 °C, 40.6 °C, 39.2 °C and 34.0 °C at around 3-3.30pm, 4-4.30pm, 11am and 3-3.30pm respectively and then dropped in value over time passed after each those times. The average exterior surface temperature in all of the north, south, east and west surfaces was at approximately 29 °C, 33.1 °C, 35.7 °C and 30.4 °C was observed in midday time from 6am to 6pm, giving a 12 h in each day. In midnight time from 6pm to 6am, that was at approximately 27.4 °C, 29 °C, 28.6 °C and 28.3 °C, respectively.

Internal wall surfaces

The temperature evolution of the interior surface temperature of the cement block house wall in all sides is shown in Figure 122. The maximum interior wall temperature of the north, south, east and west surfaces peaked as high as 32.5 °C, 36.8 °C, 34.6 °C and 33.8 °C at the same time, around 4.30-5pm and then dropped in value over time passed after each those times. The average exterior surface temperature in all of the north, south, east and west surfaces was at approximately 30.2 °C, 32.1 °C,

33.4 °C and 31.0 °C respectively was observed in midday time from 6am to 6pm, giving a 12 h in each day. In midnight time from 6pm to 6am, that was while at approximately 28.3 °C, 29.5 °C, 29.3 °C and 29 °C, respectively.

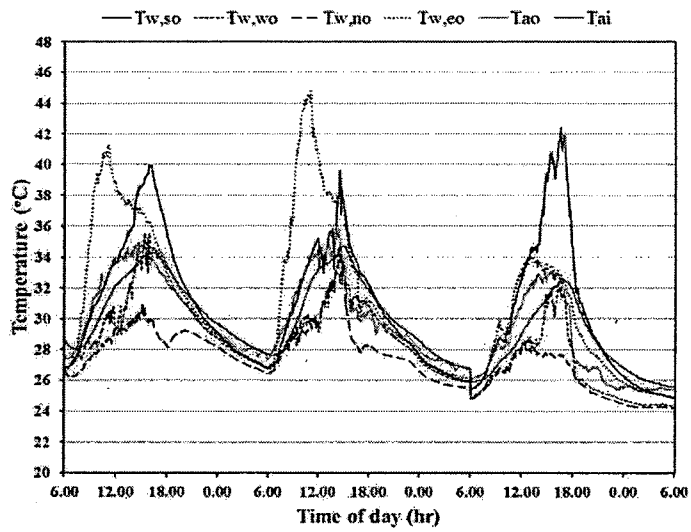

Figure 121 The temperature variation of exterior cement block wall surfaces.

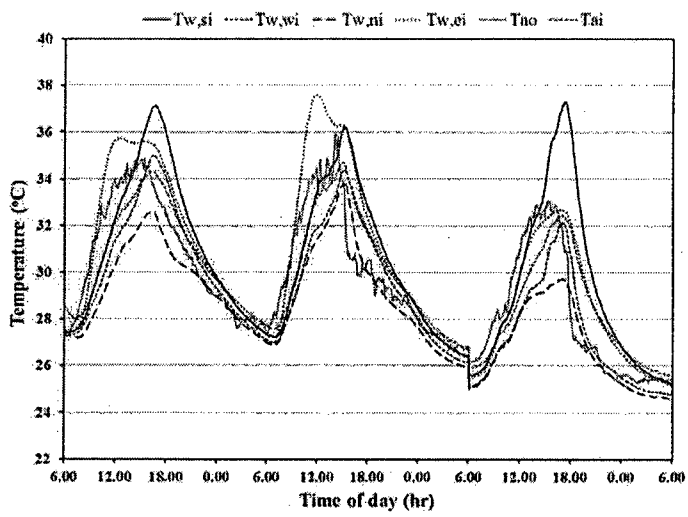

Figure 122 The temperature variation of interior cement block wall surfaces.

Northerly aspect wall surfaces

The temperature fluctuation of Northerly aspect interior and exterior surface temperature of the cement block house is shown in Figure 123. The maximum value of ambient temperature (Tao) was observed at about 34.5 °C at the day time around 3-3.30pm. The exterior wall temperature of the Northerly aspect rapidly heated to as high as approximately 30.8 °C at around 3-3.30pm while peak temperatures of the interior surface reached its maximum value of approximately 32.5 °C at around 4-4.30pm. The maximum room temperature (Tai) as approximately 35.0 °C was found at the day time around 4-4.30pm.

Southerly aspect wall surfaces

The temperature fluctuation of Southerly aspect interior and exterior surface temperature of the cement block house is shown in Figure 124. The maximum value of ambient temperature (Tao) was observed at about 34.5 °C at the day time around 3-3.30pm. The exterior wall temperature of the Southerly aspect rapidly heated to as high as approximately 40.6 °C at around 4-4.30pm while peak temperatures of the interior surface reached its maximum value of approximately 36.8 °C at around 4.30-5pm. The maximum room temperature (Tai) as approximately 35.0 °C was found at the day time around 4-4.30pm.

Easterly aspect wall surfaces

The temperature variation of Easterly aspect interior and exterior surface temperature of the cement block house is shown in Figure 125. The maximum value of ambient temperature (Tao) was observed at about 34.5 °C at the day time around 3-3.30pm. The exterior wall temperature of the Easterly aspect rapidly heated to as high as approximately 39.2 °C at around 11am while peak temperatures of the interior surface reached its maximum value of approximately 34.6 °C at around 4.30-5pm. The maximum room temperature (Tai) as approximately 35.0 °C was found at the day time around 4-4.30pm.

Westerly aspect wall surfaces

The temperature fluctuation of Westerly aspect interior and exterior surface temperature of the cement block house is shown in Figure 126. The maximum value of ambient temperature (Tao) was observed at about 34.5 °C at the day time around 3-3.30pm. The exterior wall temperature of the Westerly aspect rapidly heated to as

high as approximately 34.0 °C at around 3-3.30pm while peak temperatures of the interior surface reached its maximum value of approximately 33.8 °C at around 4.30-5pm. The maximum room temperature (Tai) as approximately 35.0 °C was found at the day time around 4-4.30pm.

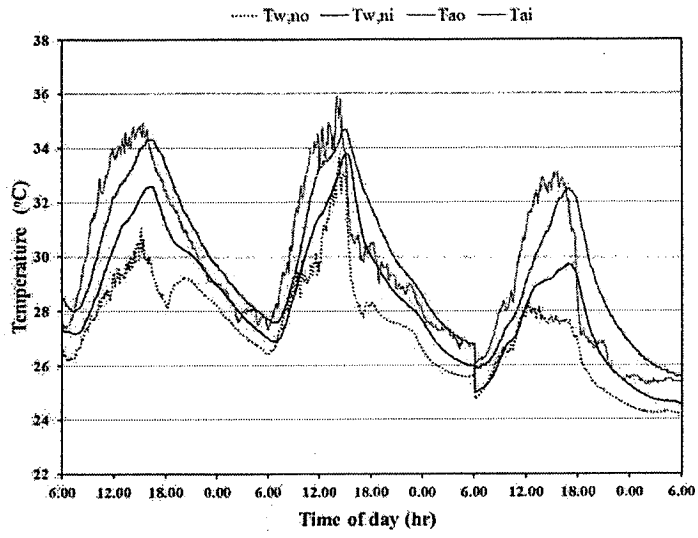

Figure 123 The temperature change of northerly aspect exterior and interior cement block wall surfaces.

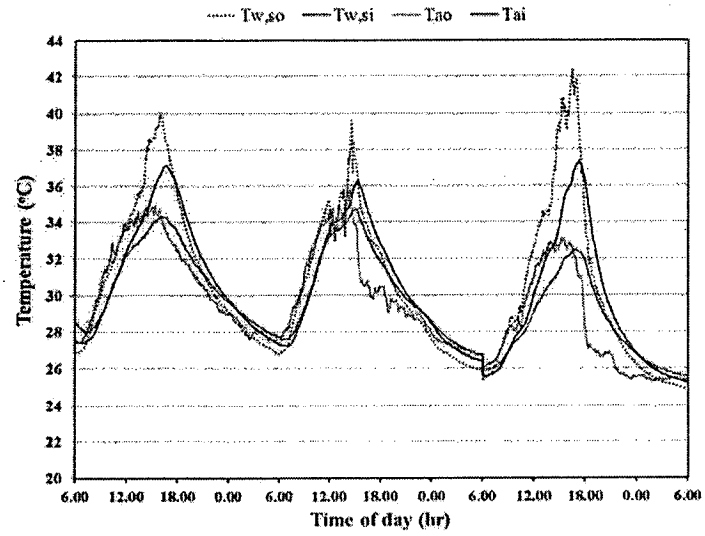

Figure 124 The temperature change of southerly aspect exterior and interior cement block wall surfaces.

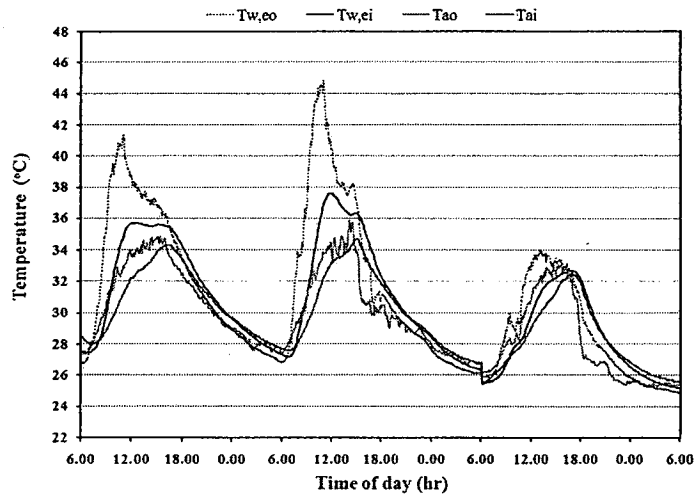

Figure 125 The temperature change of easterly aspect exterior and interior cement block wall surfaces.

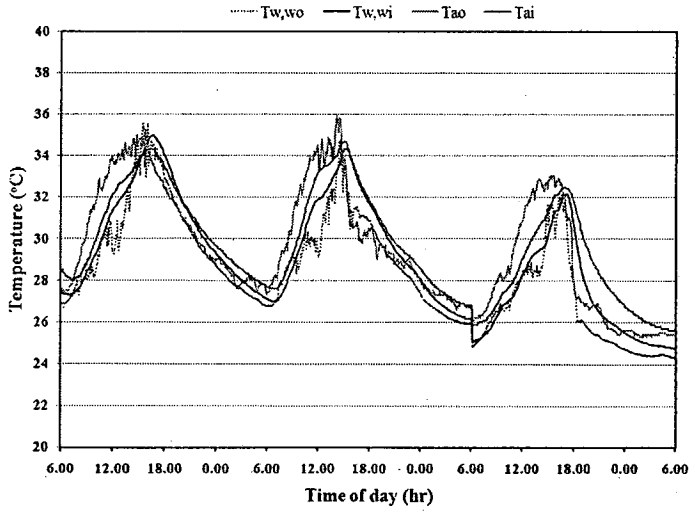

Figure 126 The temperature change of westerly aspect exterior and interior cement block wall surfaces.

The autoclaved aerated concrete wall

External wall surfaces

The temperature evolution of the exterior surface temperature of the commercial autoclaved aerated concrete house wall in all sides is shown in Figure 127. The maximum exterior wall temperature of the north, south, east and west surfaces

reached as high as 31.5 °C, 41 °C, 43 °C and 41.5 °C at around 3pm, 4-4.30pm, 10.30-11am and 3-4.30pm respectively and then dropped in value over time passed after each those times. The average exterior surface temperature in all of the north, south, east and west surfaces was at approximately 29.5 °C, 33.1 °C, 36.4 °C and 33.3 °C respectively was observed in midday time from 6am to 6pm, giving a 12 h in each day. In midnight time from 6pm to 6am, that was at approximately 27 °C, 28 °C, 28.1 °C and 28.1 °C, respectively.

Internal wall surfaces

The temperature evolution of the interior surface temperature of the PCM coated AAC house wall in all sides is shown in Figure 128. The maximum exterior wall temperature of the north, south, east and west surfaces peaked as high as 33.1 °C, 34.4 °C, 34.2 °C and 35 °C at the same time, around 4-5pm and then dropped in value over time passed after each those times. The average interior surface temperature in all of the north, south, east and west surfaces was at approximately 31.0 °C, 31.7 °C, 32.6 °C and 32.0 °C was observed in midday time from 6am to 6pm, giving a 12 h in each day. In midnight time from 6pm to 6am, that was while at approximately 29.1 °C, 29.5 °C, 29.5 °C and 29.4 °C, respectively.

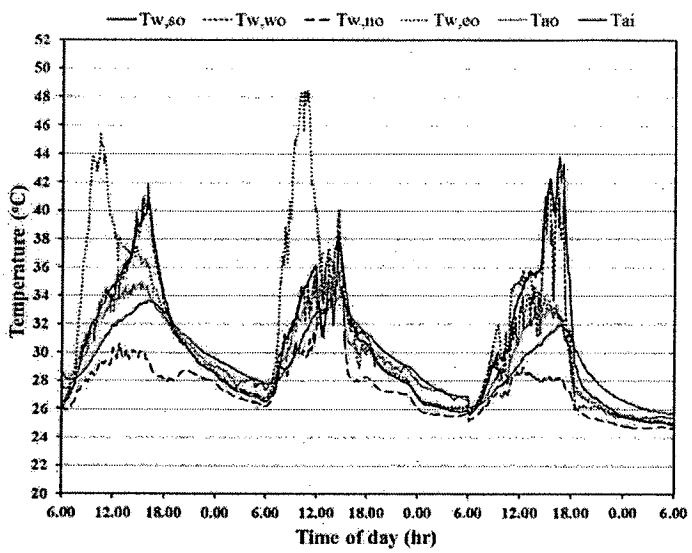

Figure 127 The temperature variation of exterior autoclaved aerated concrete wall surfaces.

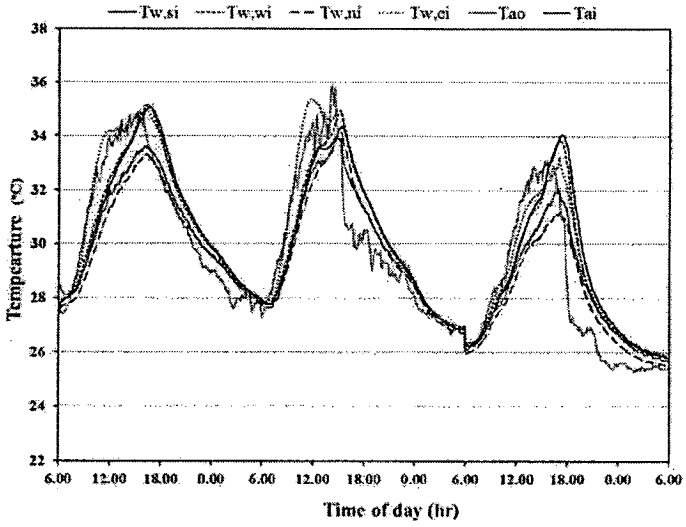

Figure 128 The temperature variation of interior autoclaved aerated concrete wall surfaces.

Northerly aspect wall surfaces

The temperature fluctuation of Northerly aspect interior and exterior surface temperature of the commercial autoclaved aerated concrete house is shown in Figure 129. The maximum value of ambient temperature (Tao) was observed at about 34.5 °C at the day time around 3-3.30pm. The exterior wall temperature of the Northerly aspect rapidly heated to as high as approximately 31.5 °C at around 3pm while peak temperatures of the interior surface reached its maximum value of approximately 33.0 °C at around 4-4.30pm. The maximum room temperature (Tai) as approximately 33.2 °C was found at the day time around 4-4.30pm.

Southerly aspect wall surfaces

The temperature fluctuation of Southerly aspect interior and exterior surface temperature of the commercial autoclaved aerated concrete house is shown in Figure 130. The maximum value of ambient temperature (Tao) was observed at about 34.5 °C at the day time around 3-3.30pm. The exterior wall temperature of the Southerly aspect rapidly heated to as high as approximately 41 °C at around 4-4.30pm while peak temperatures of the interior surface reached its maximum value of approximately 34.4 °C at around 4.30-5pm. The maximum room temperature (Tai) as approximately 33.2 °C was found at the day time around 4-4.30pm.

Easterly aspect wall surfaces

The temperature variation of Easterly aspect interior and exterior surface temperature of the commercial autoclaved aerated concrete house is shown in Figure 131. The maximum value of ambient temperature (Tao) was observed at about 34.5 °C at the day time around 3-3.30pm. The exterior wall temperature of the Easterly aspect rapidly heated to as high as approximately 43 °C at around 10.30-11am while peak temperatures of the interior surface reached its maximum value of approximately 34.2 °C at around 4.30-5pm. The maximum room temperature (Tai) as approximately 33.2 °C was found at the day time around 4-4.30pm.

Westerly aspect wall surfaces

The temperature fluctuation of Westerly aspect interior and exterior surface temperature of the commercial autoclaved aerated concrete house is shown in Figure 132. The maximum value of ambient temperature (Tao) was observed at about 34.5 °C at the day time around 3-3.30pm. The exterior wall temperature of the Westerly aspect rapidly heated to as high as approximately 41.6 °C at around 3-4.30pm while peak temperatures of the interior surface reached its maximum value of approximately 35.0 °C at around 4.30-5pm. The maximum room temperature (Tai) as approximately 33.2 °C was found at the day time around 4-4.30pm.

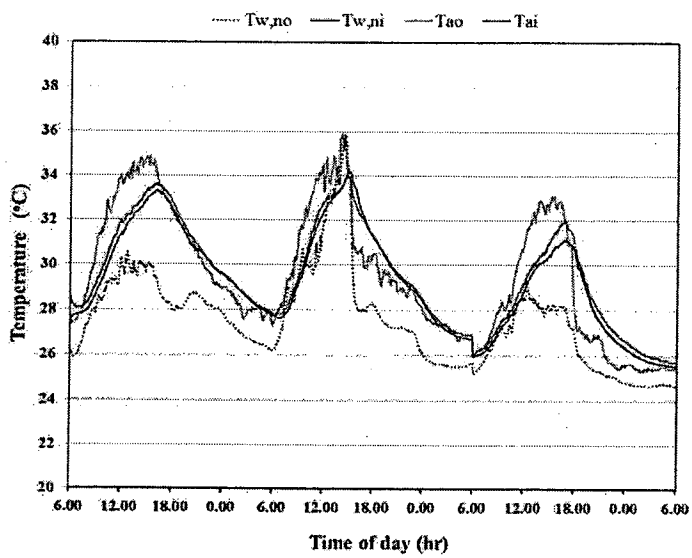

Figure 129 The temperature change of northerly aspect exterior and interior autoclaved aerated concrete wall surfaces.

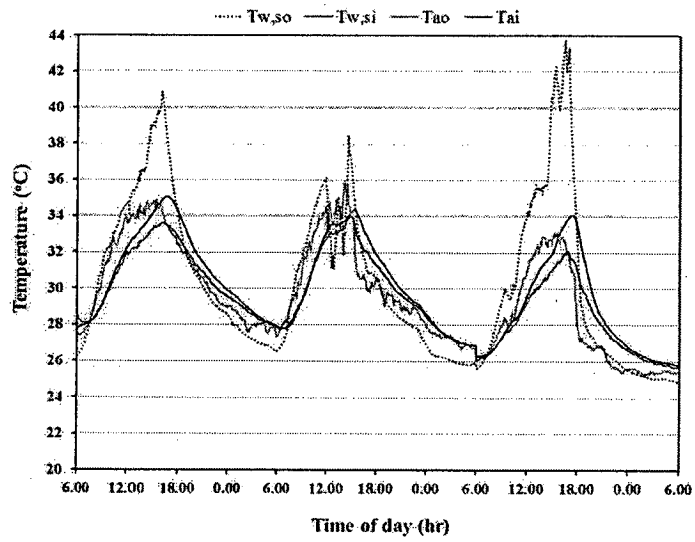

Figure 130 The temperature change of southerly aspect exterior and interior autoclaved aerated concrete wall surfaces.

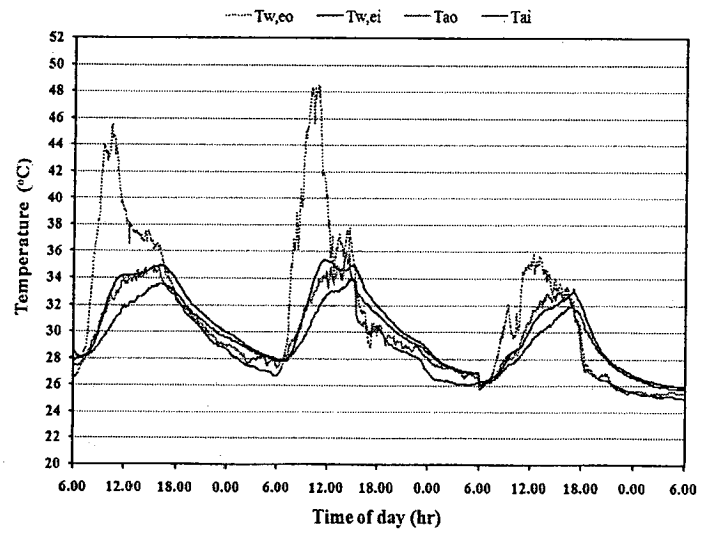

Figure 131 The temperature change of easterly aspect exterior and interior autoclaved aerated concrete wall surfaces.

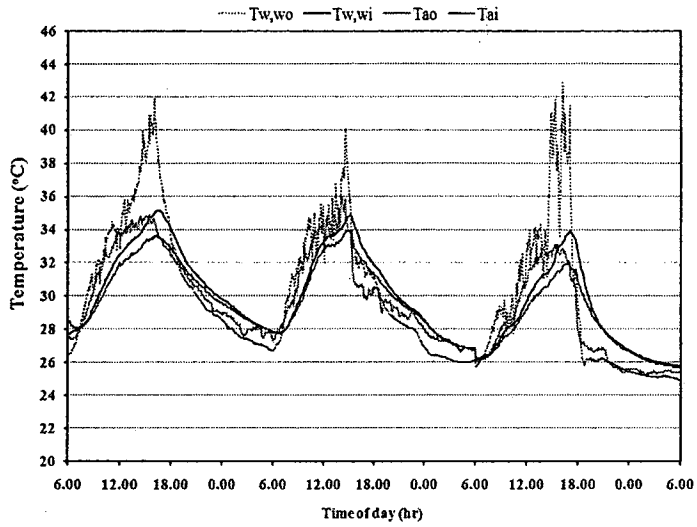

Figure 132 The temperature change of westerly aspect exterior and interior autoclaved aerated concrete wall surfaces.

The brick wall

External wall surfaces

The temperature evolution of the exterior surface temperature of the brick house wall in all sides is shown in Figure 133. The maximum exterior wall temperature of the north, south, east and west surfaces reached as high as 33 °C, 40.2 °C, 39.6 °C and 35.0 °C at around 3-3.30pm, 4-4.30pm, 11am and 3-4pm respectively and then dropped in value over time passed after each those times. The average exterior surface temperature in all of the north, south, east and west surfaces was at approximately 30.8 °C, 33.1 °C, 35.4 °C and 30.3 °C was observed in midday time from 6am to 6pm, giving a 12 h in each day. In midnight time from 6pm to 6am, that was at approximately 28.7 °C, 29.3 °C, 29.0 °C and 28.7 °C, respectively.

Internal wall surfaces

The temperature evolution of the interior surface temperature of the brick house wall in all sides is shown in Figure 134. The maximum interior wall temperature of the north, south, east and west surfaces peaked as high as 33.4 °C, 36.7 °C, 35.4 °C and 34.8 °C at the same time, around 4.30-5pm and then dropped in value over time passed after each those times. The average exterior surface temperature in all of the north, south, east and west surfaces was at approximately 31.4 °C, 32.2 °C, 33.4 °C and

31.1 °C was observed in midday time from 6am to 6pm, giving a 12 h in each day. In midnight time from 6pm to 6am, that was while at approximately 29.3 °C, 30.0 °C, 29.5 °C and 29.3 °C, respectively.

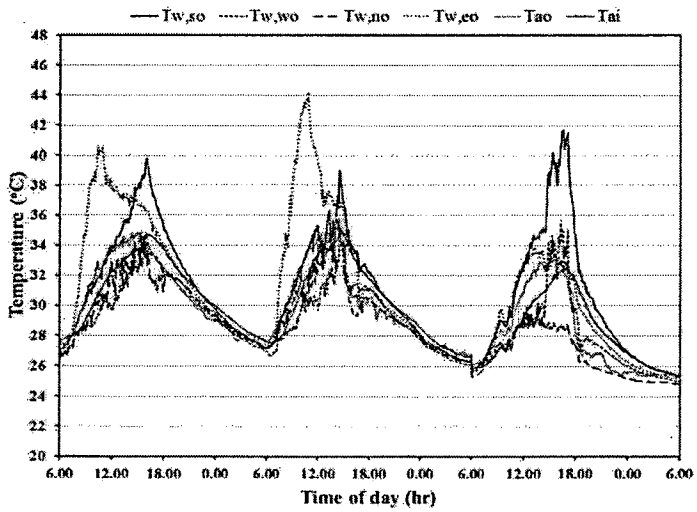

Figure 133 The temperature variation of exterior brick house wall surfaces.

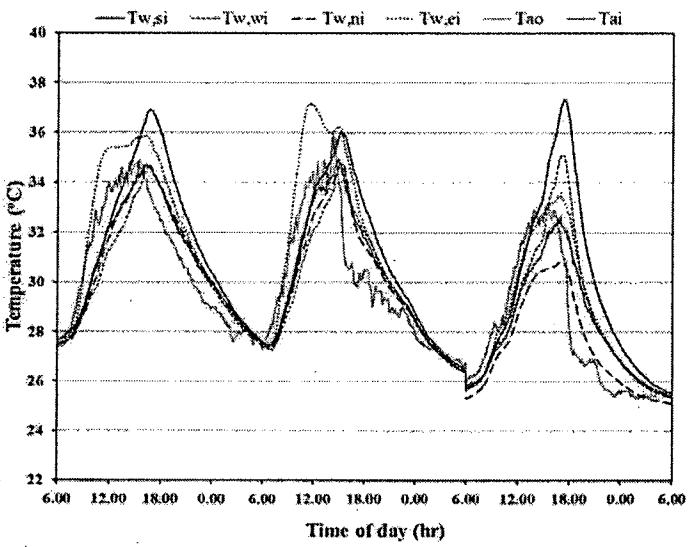

Figure 134 The temperature variation of interior surface of brick house wall.

Northerly aspect wall surfaces

The temperature fluctuation of Northerly aspect interior and exterior surface temperature of the brick house is shown in Figure 135. The maximum value of ambient temperature (Tao) was observed at about 34.5 °C at the day time around 3-3.30pm. The exterior wall temperature of the Northerly aspect rapidly heated to as high as approximately 33 °C at around 3-3.30pm while peak temperatures of the interior surface reached its maximum value of approximately 33.4 °C at around 4-4.30pm. The maximum room temperature (Tai) as approximately 34.0 °C was found at the day time around 4-4.30pm.

Southerly aspect wall surfaces

The temperature fluctuation of Southerly aspect interior and exterior surface temperature of the brick house is shown in Figure 136. The maximum value of ambient temperature (Tao) was observed at about 34.5 °C at the day time around 3-3.30pm. The exterior wall temperature of the Southerly aspect rapidly heated to as high as approximately 40.2 °C at around 4-4.30pm while peak temperatures of the interior surface reached its maximum value of approximately 36.7 °C at around 4.30-5.30pm. The maximum room temperature (Tai) as approximately 34.0 °C was found at the day time around 4-4.30pm.

Easterly aspect wall surfaces

The temperature variation of Easterly aspect interior and exterior surface temperature of the brick house is shown in Figure 137. The maximum value of ambient temperature (Tao) was observed at about 34.5 °C at the day time around 3-3.30pm. The exterior wall temperature of the Easterly aspect rapidly heated to as high as approximately 39.6 °C at around 11am while peak temperatures of the interior surface reached its maximum value of approximately 35.4 °C at around 4-5pm. The maximum room temperature (Tai) as approximately 34.0 °C was found at the day time around 4-4.30pm.

Westerly aspect wall surfaces

The temperature fluctuation of Westerly aspect interior and exterior surface temperature of the brick house is shown in Figure 138. The maximum value of ambient temperature (Tao) was observed at about 34.5 °C at the day time around 3-3.30pm. The exterior wall temperature of the Westerly aspect rapidly heated to as

high as approximately 35.0 °C at around 3-4pm while peak temperatures of the interior surface reached its maximum value of approximately 34.8 °C at around 4.30-5pm. The maximum room temperature (Tai) as approximately 34.0 °C was found at the day time around 4-4.30pm.

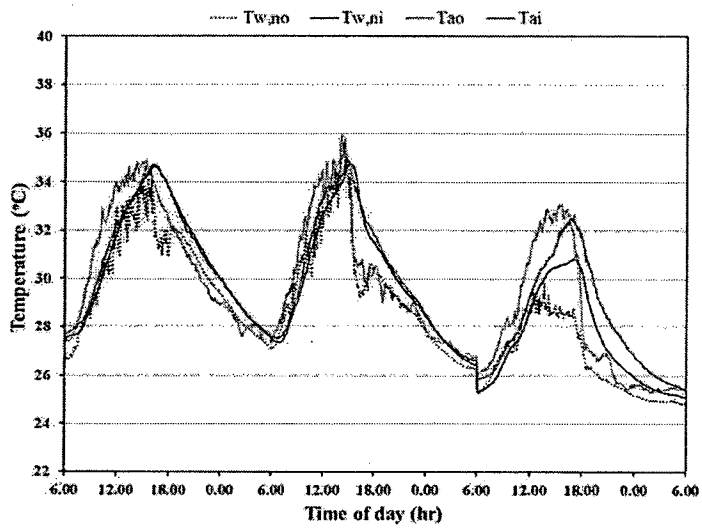

Figure 135 The temperature change of northerly aspect exterior and interior brick wall surfaces.

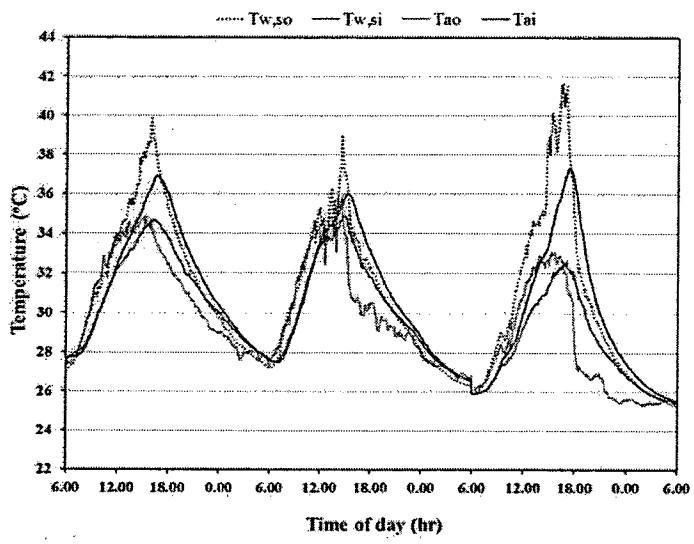

Figure 136 The temperature change of southerly aspect exterior and interior brick wall surfaces.

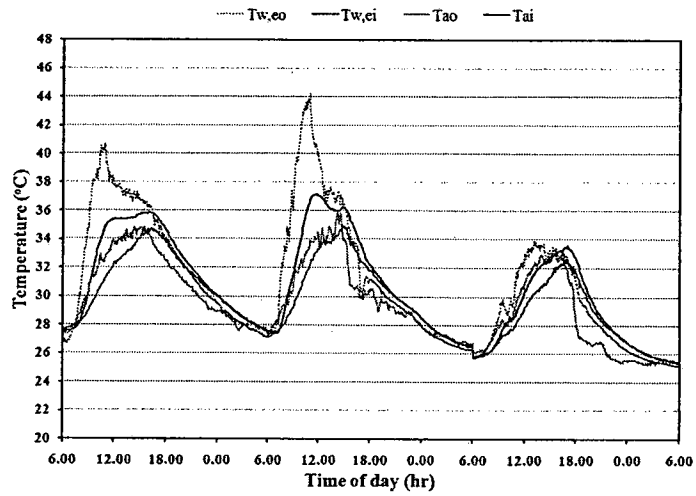

Figure 137 The temperature change of easterly aspect exterior and interior brick wall surfaces.

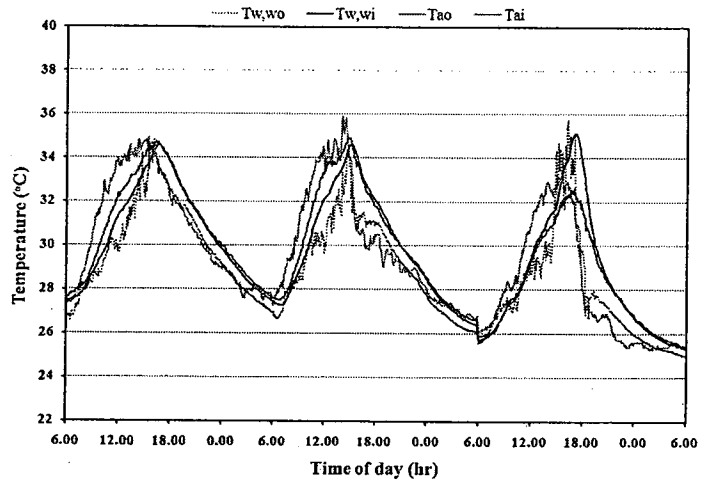

Figure 138 The temperature change of westerly aspect exterior and interior brick wall surfaces.

Comparison of exterior and interior, room temperature and relative humidity and heat flux revolution

Northerly aspect external wall surfaces

Figure 139 illustrates the northerly aspect exterior surfaces temperature of the four houses. The maximum exterior wall temperature of the houses with cement block, brick, AAC and PCM-coated AAC reached as high as 30.8, 33.0, 31.5 and 31.3 °C respectively at the same time around 2.30-3.30pm.

Northerly aspect internal wall surfaces

Figure 140 shows the north interior surface temperature of the four houses. The maximum interior wall temperature of cement block, brick, AAC and PCM coated AAC reached as high as 32.5 °C, 33.4 °C, 33.1 °C and 32 °C repectively for each material at the same time, around 4-4.30pm. It is noteworthy that the maximum interior wall temperature of the PCM coated AAC house was about 0.5 °C –1.5 °C lower than that of the uncoated wall materials, presumably due to the higher insulative property of the AAC material.

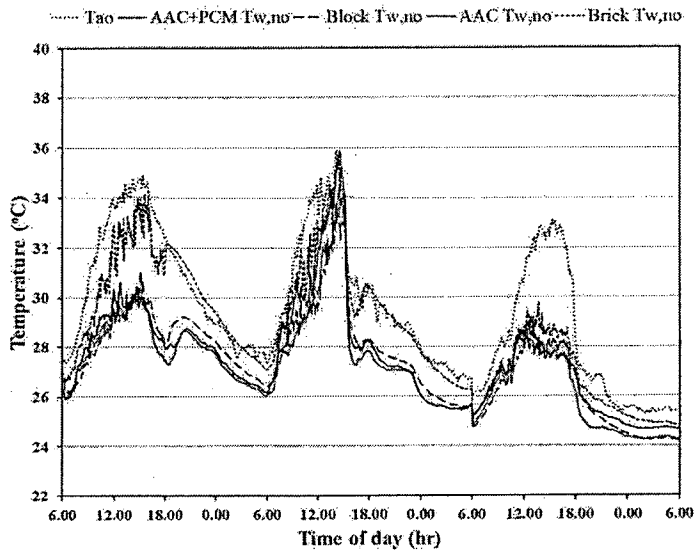

Figure 139 Comparison of northerly aspect exterior wall surface temperature of the 4 houses.

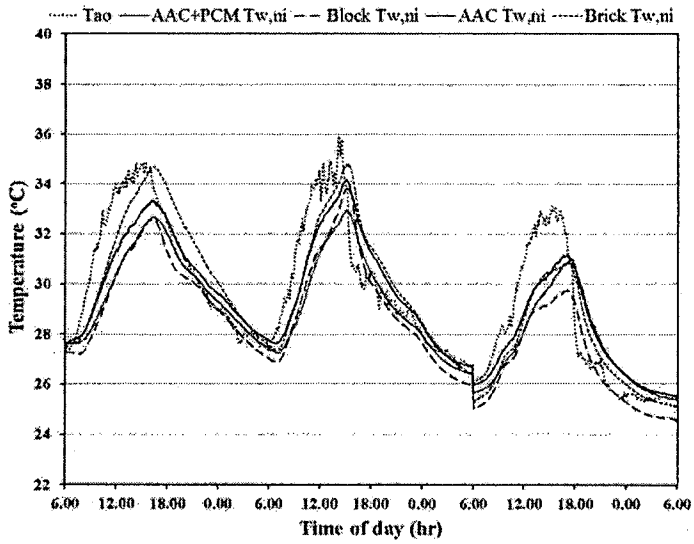

Figure 140 Comparison of northerly aspect interior wall temperature surface of the 4 houses.

Southerly aspect external wall surfaces

Figure 141 illustrates the southerly aspect exterior surfaces temperature of the four houses. The maximum exterior wall temperature of PCM coated AAC peaked as high as 38.5 °C at around 2.30pm while that of the cement block, brick, AAC and were at approximately 40.6 °C, 40.2 °C and 41.0 °C respectively at around 4-4.30pm.

Southerly aspect internal wall surfaces

Figure 142 exhibits the south interior surface temperature of the four houses. The maximum interior wall temperature of cement block wall peaked as high as 36.8 °C at around 4.30-5pm while that of brick, AAC and PCM coated AAC was at approximately 36.7 °C, 34.4 °C and 32.8 °C at around the time of 4.30-5.30pm. So the maximum interior wall temperature of the PCM coated AAC house was about 1.5 °C – 4 °C lower than that of the uncoated wall materials (the cement block, brick and AAC). This may be due to the higher insulative property of the AAC material not allowing the temperature to be transferred to the interior wall.

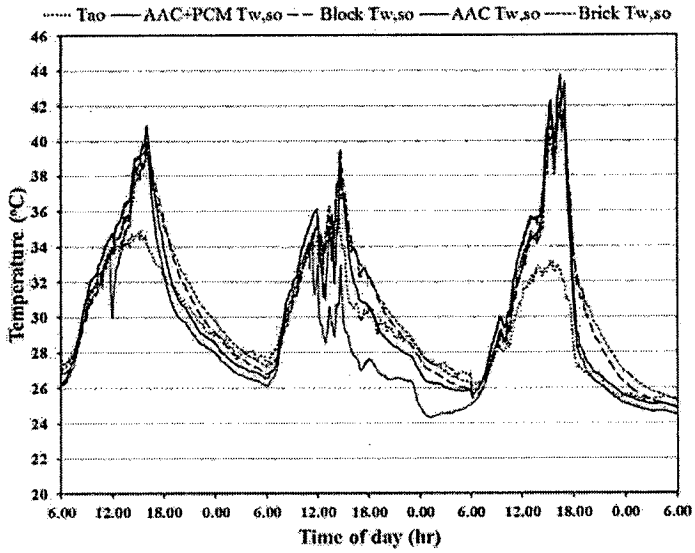

Figure 141 Comparison of southerly aspect exterior wall surface temperature of the 4 houses.

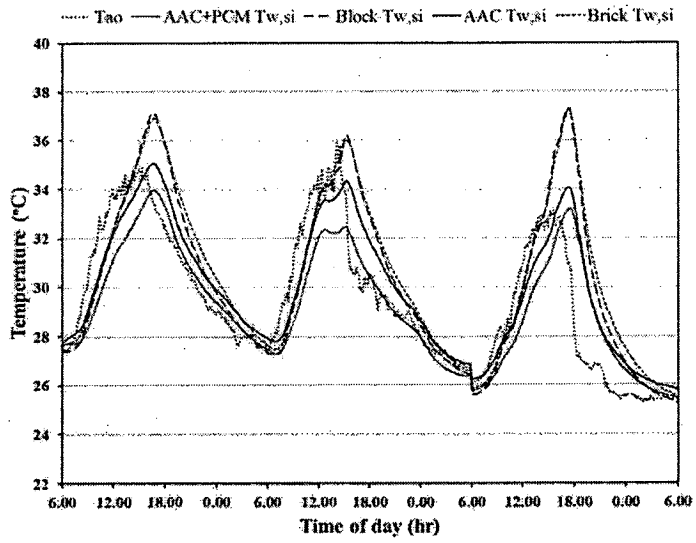

Figure 142 Comparison of southerly aspect interior wall surface temperature of the 4 houses.

Easterly aspect external wall surfaces

Figure 143 shows the east exterior surface temperature of the four houses. The exterior wall temperature of the PCM coated AAC house rapidly heated to as high as 42.3 °C at around 10.30am while peak temperatures of the untreated AAC, cement block and brick walls were approximately 43.0 °C at ~ 10.30-11am, 39.2 °C at ~ 11am and 39.6 °C at 11am, respectively, showing different rates of temperature rise over time.

Easterly aspect internal wall surfaces

Figure 144 exhibits the east interior surface temperature of the four houses. The maximum interior wall temperature of the cement block wall house rapidly peaked as high as 34.6 °C at around 4.30-5pm while that of brick, AAC and PCM coated AAC houses were approximately 35.4 °C, 34.2 °C and 33.3 °C respectively, at the time around 4-5pm. So the maximum interior wall temperature of the PCM coated AAC house was about 1 °C –2 °C lower than that of the uncoated wall materials. This may be due to the higher insulative property of the AAC material not allowing the temperature to be transferred to the interior wall.

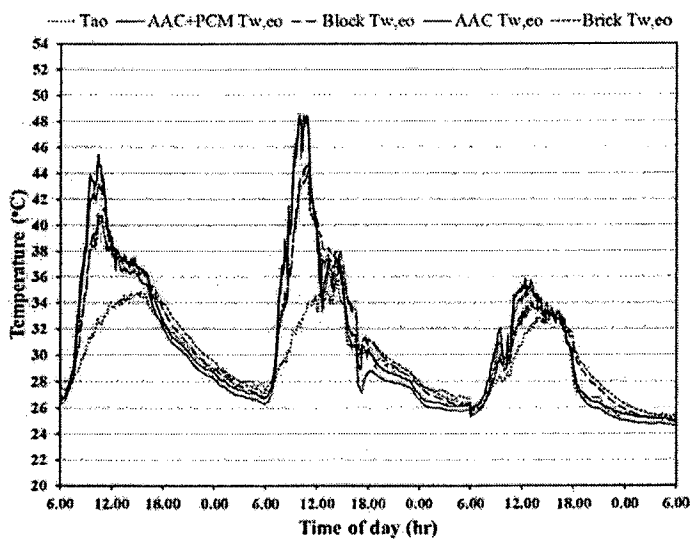

Figure 143 Comparison of easterly aspect exterior wall surface temperature of the 4 houses.

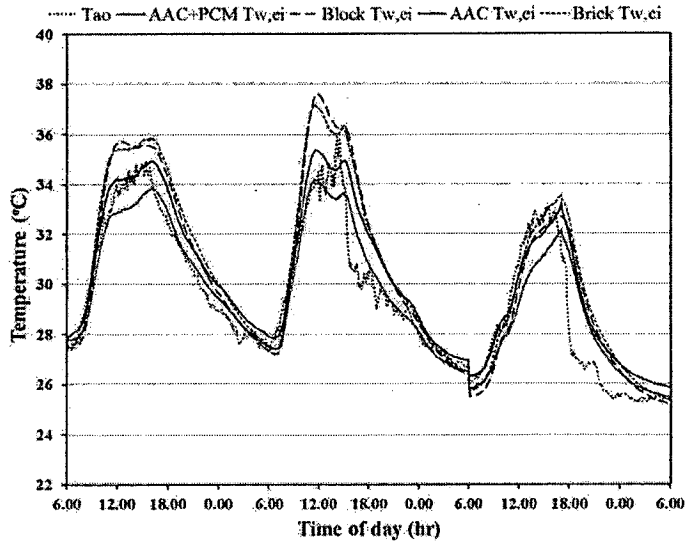

Figure 144 Comparison of easterly aspect interior wall surface temperature of the 4 houses.

Westerly aspect external wall surfaces

Figure 145 illustrates the west exterior surface temperature of the four houses. The maximum exterior wall temperature of cement block peaked as high as 34.0 °C at around 3-3.30pm while that of the brick, AAC and PCM coated AAC were at approximately 35 °C, 41.6 °C and 38.5 °C respectively at around 3-4.30pm.

Westerly aspect internal wall surfaces

Figure 146 exhibits the west interior surface temperature of the four houses. The maximum interior wall temperature of cement block peaked as high as 34 °C at around 4.30-5pm while that of brick, AAC and PCM coated AAC was at approximately 34.8 °C, 35.0 °C and 33 °C respectively, also at around 4.30-5pm. It is noteworthy that the maximum interior wall temperature of the PCM coated AAC around 2 °C was lower than that of the untreated AAC, while being about 1-2 °C lower than that of the cement brick and block materials (also uncoated) at 4.30-5pm. Again, this is presumed to be due to the more effective heat transfer characteristics of the AAC material.

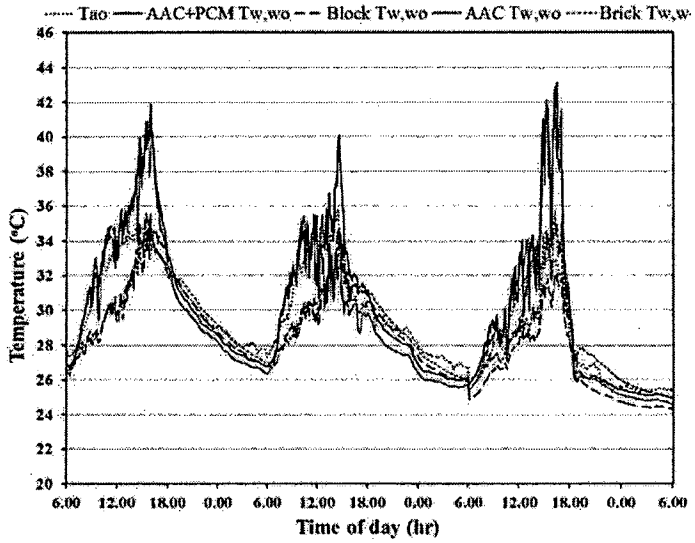

Figure 145 Comparison of westerly aspect exterior wall surface temperature of the 4 houses.

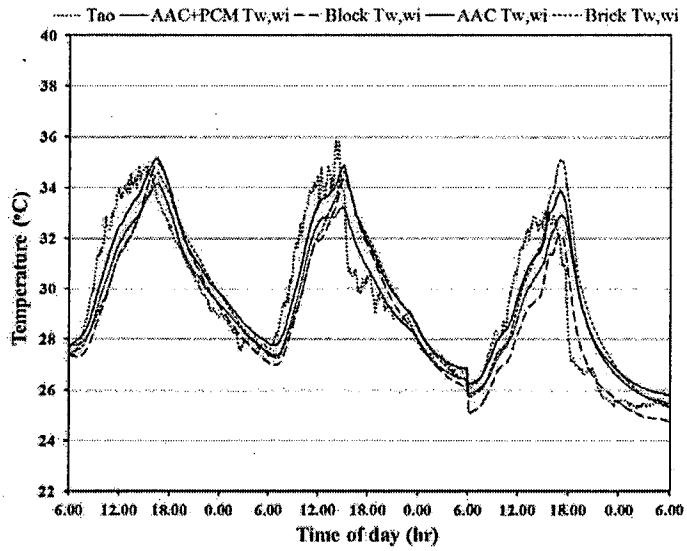

Figure 146 Comparison of westerly aspect interior wall surface temperature of the 4 houses.

Comparison of flux evolution and room temperature

Heat fluxes on both the interior and exterior surfaces of the easterly and westerly aspects walls of the four houses were investigated, as illustrated in Figure 147-148. Heat flux on the wall surface is positive when the heat wave propagates from

the outer surface to the inner surface (That is, when the exterior surface temperature is higher than the interior surface temperature) while heat flux on the wall surface is negative when heat wave propagates from the inside surface to the outside surface (exterior surface temperature is less than interior surface temperature).

With the cement block house, positive heat fluxes in all of the east and west surfaces were first increased and reached its maximum value of approximately 46.7 and 8.65 W/m^2 at around 10am and 3.30pm the east and west surfaces respectively and then dropped in value over time passed after each those times. It was found that the negative heat fluxes of the east and west surfaces began at around 4pm and 4.30pm, respectively. The highest value of the heat fluxes were about 14.8 and 18.6 W/m^2 at around 7pm and 6.30pm for the east and west surfaces respectively, then dropped for day time below these values.

For the heat fluxes of the brick house walls, the maximum positive value for the east and west surfaces was observed at about 34.7 and 10.5 W/m^2 at around 9.30-10.30am and 3pm, respectively. While, the maximum negative value in the part of the east and west surfaces was observed at about 12.1 and 21.1 W/m^2 at around 5-6pm and 6-6.30pm, respectively.

For the heat fluxes of the AAC house wall, the maximum positive value for each of the east and west surfaces was observed at about 19 and 13.5 W/m^2 at around 9.30-10.30 am and 3.30pm, respectively. The maximum negative values were observed at about 5 and 5 W/m^2 at the same time around 6.30-7pm, respectively.

For the heat fluxes of AAC with PCM house wall, the maximum positive value in the part of the east and west surfaces was observed at about 17.1 and 12.0 W/m^2 at around 10am and 3.30pm, respectively. The maximum negative value for each of the east and west surfaces was observed at about 5 and 5.3 W/m^2 at around 7pm and 6.30-7pm, respectively.

This shows that the maximum positive heat flux of the PCM coated AAC house wall in the east and west sides had the least positive heat flux value, while that of cement block house wall in all sides had the maximum value. The maximum positive heat flux of the PCM coated AAC wall on the east surfaces was less than that of the uncoated AAC wall of around 2 W/m^2, that of brick wall of around 17.6 W/m^2 and that of cement block wall of around 29.6 W/m^2. That of the PCM coated AAC

wall on the west surfaces was less than that of the uncoated AAC wall of around 1.5 W/m^2. While, that of the PCM coated AAC wall on the west surfaces higher than that of brick wall of around 1.5 W/m^2 and that of cement block wall of around 3 W/m^2.

The average positive heat flux values of the PCM coated AAC house on the east and west wall surfaces were around 8.5 and 5.0 W/m^2, respectively. The average positive heat flux values of the uncoated AAC wall surfaces were around 9.0 and 4.1 W/m^2, respectively. For the cement block house walls the values were around 20.2 and 2.8 W/m^2, respectively, and for the brick house walls were around 14.7 and 1.5 W/m^2, respectively. Although the average positive heat flux values of the AAC and PCM coated AAC houses on the east and west wall surfaces are higher than that of cement block and brick houses, almost heat flux on the west wall surface in midday time is negative (exterior surface temperature is less than interior surface temperature).

These average positive heat flux values corresponded to the Overall Thermal Transfer Value (OTTV). OTTV is a measure of heat gain into the building through the building envelope, which can be controlled as a means of enhancing the energy efficiency of buildings [92]. OTTV in Thailand is stated in building codes as to not exceed a statutory limit by 45 W/m^2 [93]. In the comparison of OTTV of the 4 houses, it was found that the PCM coated AAC house walls had the lowest OTTV, on the east and west sides, of all the test houses and did not exceed the statutory limit in any case. This demonstrates that the utilization of PCM on the exterior surfaces of a building using Autoclaved Aerated Concrete (AAC) can reduce the heat transfer through the building envelop and lead to an improvement in the insulative efficiency of buildings.

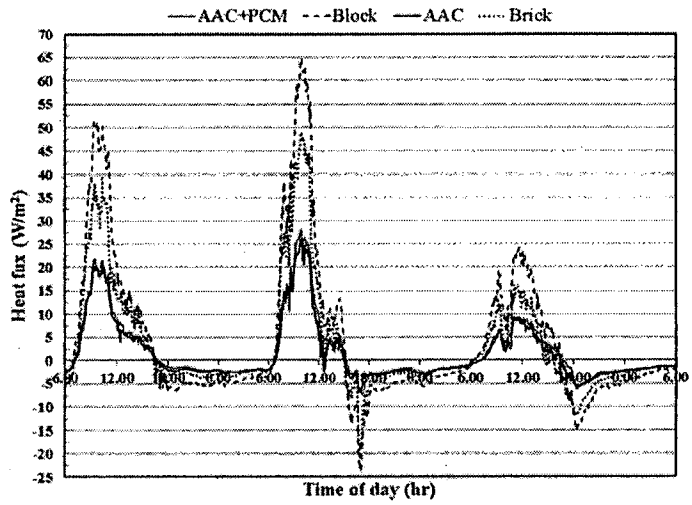

Figure 147 Heat flux Comparison of easterly aspect wall surface of the 4 houses.

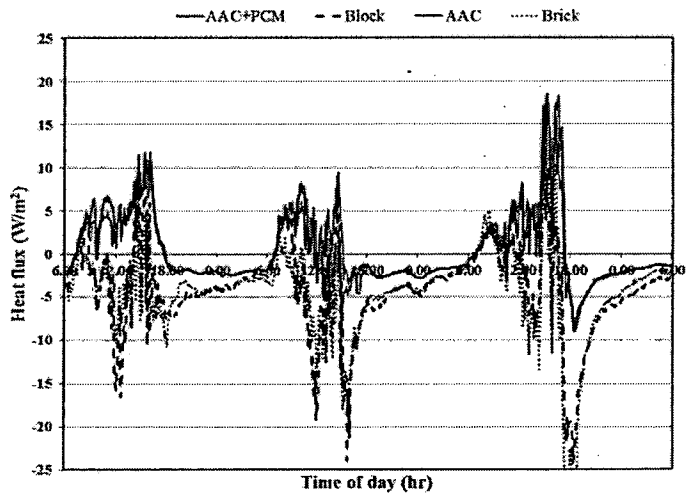

Figure 148 Heat flux Comparison of westerly aspect wall surface of the 4 houses.

Room temperatures in the four houses between 6am and 6pm are shown in Figure 149. The effect of the fluctuating nature of solar radiation, ambient temperature, heat flux transfer and exterior and interior surface temperature evolution of the house walls on each side on the room temperature of each house varied over the course of the day. It can be seen that the room temperatures of the four houses was approximately equal between the times of 6am and 9.30am. After that time, different peak temperatures were reached in each test house at different times. By 11.30am the

PCM coated AAC building room temperature was between 0.5 °C and 1.5 °C lower than the other 3 houses. After 11.30am the temperature readings diverged. The room temperature of the cement block and brick houses rose more rapidly, and achieved the highest peak value of all the houses; 34.7 °C and 34.5 at about 3-4pm. The AAC houses had the slowest temperature rise. The uncoated AAC house reached a peak temperature of 33.8 °C at 3-4pm, and the PCM coated AAC house had the lowest peak temperature, 32.8 °C, reached at 3-4pm.

These readings indicate that the utilization of AAC with PCM coating significantly attenuates the daily room temperature fluctuation of partitions. The daily room temperature swing was reduced from 7.0 °C (cement block house), 6.5 °C (brick house) and 5.5 °C (uncoated AAC house) to only 5 °C in the PCM coated house.

The relative humidity in the four houses was measured from 6am of day to 6am of the following day are shown in Figure 150. The fluctuating nature of relative humidity in the tropics occurs because of the evolution of solar radiation, ambient temperature, heat flux transfer and exterior and interior surface temperature evolution of the house walls on each side on the relative humidity of each house varied over the course of the day. It can be seen that the relative humidity of the four houses was nearly the same level during the daily period of 6am to 6am.

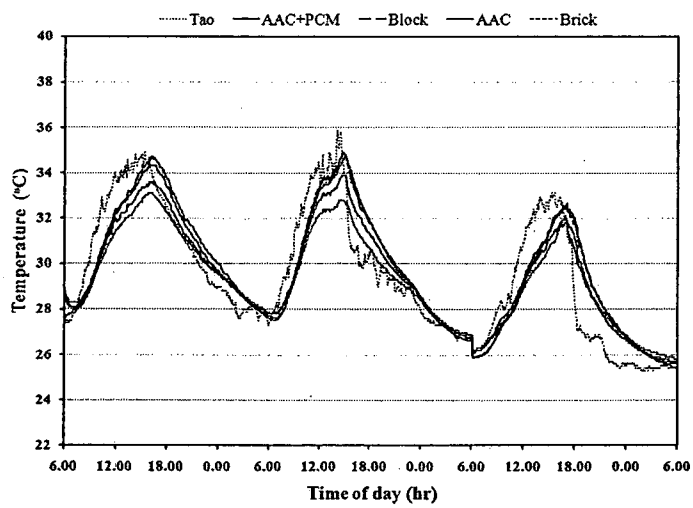

Figure 149 Comparison of room temperature of the 4 houses.

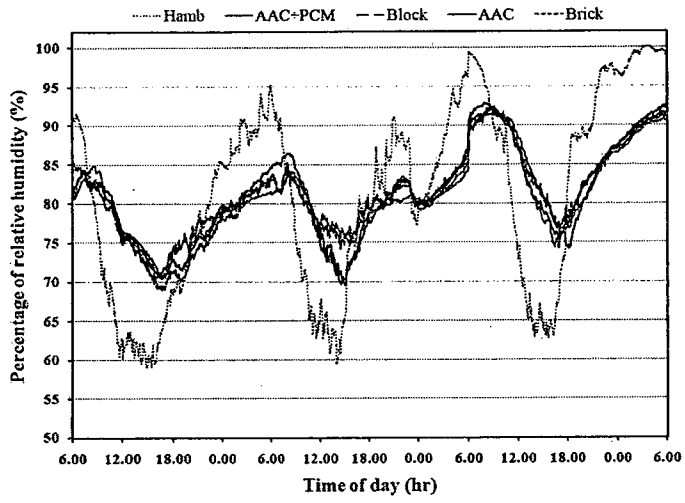

Figure 150 Comparison of interior relative humidity of the 4 houses.

Comparison of cooling load

The cooling load on the air conditioners in the four houses was only measured and compared in the summer. The measurements are shown in Table 17. All the houses were tested first with closed windows and doors for the 3 days and 14 h daily period (from 8am to 10pm). It was found that the cooling load in the cement block wall house started to increase the soonest, and continued to increase over the 42 h 8am to 10pm for 3 days. The cooling load on the air conditioner in this house was around 16.8 units of electrical consumption. The cooling load in the brick, AAC and PCM coated houses had a similar trend to the cement block wall house. At the end of the 42 h period, the cooling loads in the brick, AAC and PCM coated AAC houses were around 14.4, 12.5 and 8.8 units of electrical consumption, respectively. This is say the savings in electrical consumption PCM coated AAC house was lower than the other houses approximately 29.6% (uncoated AAC), 38.9% (brick) and 47.6% (cement block) respectively. Again this demonstrates the ability of the Phase Change Material to significantly reduce the cooling load and electrical consumption of air conditioning plants. Hence, autoclaved aerated concrete with PCM coating on the outside surface could be seriously considered as an important adjunct component in construction material.

Economic analysis

The four houses with different wall materials were constructed to investigate the thermal and energy performance. The different wall materials exhibited also the various thermo-physical properties. Therefore, the details of the thermo-physical properties of these building materials are given in Table 16.

Table 16 The characterized properties of construction materials.

Construction materials	Thermal conductivity (W/m·°C)	Specific heat (kJ/kg ·°C)	Density (kg/m^3)
AAC	0.133	0.84	610
AAC-SS	0.098	0.80	600
Cement block	0.519	0.92	2210
Brick	0.473	0.79	1800
Plaster cement	0.720	0.84	1860
PCM S32	0.510	186	1460
PCM S44	0.430	105	1584

The part of the consumer

In addition to the investigation on the thermal and energy performance of PCM coated AAC, an economic evaluation was done for assessing the further potential benefits from this work. Both capital cost of PCM and electricity tariff are crucial factors affecting the successful application of PCM coating with respect to economic return.

The reduction in the cooling load on air conditioning plants or on the unconditioned internal ambient temperature, and hence electric power consumption, by enhancing the insulative properties of autoclaved aerated concrete, provides a significant economic benefit for the building occupier and power consumer. In this study, the operating hours of air conditioner in the four houses was tested for the 3 days and 14 h daily period as shown in Table 17. The cooling load on the air conditioner in the PCM coated AAC, AAC, brick and cement block houses were

around 8.8, 12.5, 14.4 and 16.8 units of electrical consumption, respectively. If the electrical consumption of the four houses is assumed as being for 30 days or 1 month, the cooling loads in the PCM coated AAC, AAC, brick and cement block houses were around 88, 125, 144 and 168 units of electrical consumption, respectively. If the electrical consumption of the four houses is assumed as being for 12 months or 1 year in the calculation, the cooling loads in the PCM coated AAC, AAC, brick and cement block houses were around 1056, 1500, 1728 and 2016 units of electrical consumption as shown in Table 19. As demonstrated this reduction is in the order of 29.6% to 47.6% when compared against uncoated AAC, brick or concrete block. With considering the monthly electricity tariff as following the Provincial Electricity Authority of Thailand as listed in Table 18-Table 19 [94], the electricity charge of the cement block, brick, AAC and PCM-coated AAC houses were 3060, 4482, 5219 and 6259 Bath. This reduction can be stated in economic terms as a saving of up to 3200 Baht per year. With comparing the brick house, the energy consumption of the houses saved in the order of 14.1% and 41.4% for the AAC house and the PCM coated AAC house as shown in Table 19. When this figure is extrapolated over a year, for larger buildings, the annual possible cost saving can be seen to be very substantial.

Table 17 Electricity consumption of cooling load in the air condition system of the 4 houses.

Date	Time	Electricity consumption (Unit)			
		AAC+PCM	AAC	Brick	Cement block
July 12, 2013	8.00	0.0	0.0	0.0	0.0
	10.00	0.3	0.5	0.5	0.7
	12.00	0.4	0.5	0.6	0.7
	14.00	0.6	0.8	0.8	1.0
	16.00	0.6	0.8	1.0	1.2
	18.00	0.5	0.7	0.9	1.0
	20.00	0.5	0.6	0.8	0.8
	22.00	0.3	0.6	0.6	0.7
Total		3.2	4.5	5.2	6.1

Table 17 (cont.)

Date	Time	Electricity consumption (Unit)			
		AAC+PCM	AAC	Brick	Cement block
July 13, 2013	8.00	0.0	0.0	0.0	0.0
	10.00	0.3	0.4	0.5	0.5
	12.00	0.4	0.5	0.5	0.7
	14.00	0.5	0.8	0.8	0.9
	16.00	0.5	0.7	0.9	1.0
	18.00	0.5	0.7	0.9	1.1
	20.00	0.4	0.6	0.7	0.8
	22.00	0.3	0.6	0.5	0.6
Total		2.9	4.3	4.8	5.6
July 14, 2013	8.00	0.0	0.0	0.0	0.0
	10.00	0.2	0.3	0.4	0.5
	12.00	0.4	0.5	0.5	0.6
	14.00	0.5	0.7	0.8	0.9
	16.00	0.5	0.7	0.8	1.0
	18.00	0.5	0.6	0.7	0.8
	20.00	0.4	0.5	0.7	0.7
	22.00	0.2	0.4	0.5	0.6
Total		2.7	3.7	4.4	5.1

Table 18 Rate of electricity consumption for the residency [94]

Electricity usage (Unit)	Electricity charges (Bath/Unit)	Service fee (Bath/Month)
1-15	1.8632	8.19
16-25	2.5026	
26-35	2.7549	
36-100	3.1381	
101-150	3.2315	
151-400	3.7362	
>400	3.9361	

Table 19 Electricity consumption, electric charge including the service fee and percent energy saving of each house.

Type of the houses	Electricity consumption (Unit)			Charges (Including the service fee) (bath)		Percentage of energy saving per year (%)
	3 days	30 days	1 year	1month	1 year	Compare with brick
AAC+PCM	8.8	88	1056	255.03	3060.39	41.36
AAC	12.5	125	1500	373.48	4481.73	14.12
Brick	14.4	144	1728	434.88	5218.51	0.00
Block	16.8	168	2016	521.52	6258.19	-

From information collected from the suppliers of PCM, it is found that the material and installation cost of PCM is 78 Bath/m^2. The wall area in each side of the house composed of 5.52 m^2 in this study or around 20 m^2 for a house. This was not included the door and window area. The total cost of construction (including only wall material cost and wage) of the PCM coated AAC, AAC, brick and cement block houses were 8,860, 7,300, 7,400 and 5,700 Bath, respectively. As demonstrated in Table 20, the difference in construction of the PCM coated AAC, AAC, and cement block houses is 1,460, -100 and -1,700 Bath when compared against the brick house.

This collected information was calculated to investigate the payback period (PBP), net present value (NPV) and internal rate of return (IRR) as exhibited in Table 21. From this calculation, the energy payback period for the PCM coating and AAC houses was estimated at 4.11 and 9.91 year. The net present value of PCM coated AAC, AAC and cement block houses was at around 14,678, 736 and -17,040 bath within life cycle of 25 years. The internal rate of return of the PCM coated AAC house and AAC house was approximately 13.568 and 9.290%, respectively.

Table 20 The cost for each house construction (Considered only the wall material cost).

Type of the houses	Material cost (bath/m^2)	Wage (Bath/m^2)	Area of wall (m^2)	Total cost (Bath)	Different cost of construction (bath)
AAC+PCM	323	120	20	8,860	1,460
AAC	245	120	20	7,300	-100
Brick	230	230	20	7,400	0
Block	155	155	20	5,700	-1,700

Table 21 Comparison of the payback period (PBP), net present value (NPV) and internal rate of return (IRR) with brick wall construction cost.

Type of the houses	A_0 (Bath)	A_s (Bath)	PBP (year)	NPV (Bath)	IRR (%)
AAC+PCM	8,860	2158.12	-4.11	14,678.05	13.568
AAC	7,300	736.78	9.91	735.87	9.290
Brick	7,400	0.00	-	-7,400	-
Block	5,700	-1039.7	-	-17,039.5	-

Where A_o = Wall construction cost (bath)

A_s = Electrical charge saving when compared with the brick house (bath)

i = Discount rate (%); (Loan Rates of Bank of Ayudhya as of 25 April 2014 = 7.75%)

n = Life cycle (yr); (n = 25 years)

The part of the manufacturer

When comparing the two mixtures AAC-S0 and AAC-SSR0, only sand and lime were included. However, sugar sediment was also included to replace some of the sand and some of the lime content. Usually, sand and lime were included in the

mixture of AAC-S0 as 62.517 and 17.17 weight %, respectively. However, the mixture of AAC-SSR0 included sand and lime in the proportions of 43.762 and 15.882 weight % respectively, with sugar sediment replacing 30 weight % of the sand content.

Further, currently, the usual composition of the AAC-S0 per $1m^2$ is sand (31.767 kg) and lime (8.725 kg). The composition of the AAC-SSR0 in the $1m^2$ use area is sand (22.237 kg), lime (8.070 kg) and sugar sediment (9.530 kg). Sand content was therefore reduced by 9.530 kg sugar sediment. Lime was also decreased by 0.655 kg.

By including sugar sediment as an alternate material in the composition of autoclaved aerated concrete, the savings in sand and lime usage in the national construction industry in Thailand can be calculated. Approximately 28,000,000 m^2 of autoclaved aerated concrete was used in 2012. If the new composition of AAC-SSR0 is used in the calculation, it can be seen that Thailand can reduce the volume of sand and lime used by about 267 million kgs of sand, and 18.3 million kgs of lime per year. Thereby approximately 267 million kgs of otherwise waste sugar sediment would be used, approximately 36% of total annual volume produced. This is an essentially free component input. The raw material cost saving implied in these calculations, saved by the production of autoclaved aerated concrete on this scale, must also have other costs factored in, such as the energy saving on obtaining sand and producing and obtaining lime. Not only this, but the mitigation of the significant environmental and human use impacts occasioned by the disposal of waste sugar sediment in landfills, and the quarrying and mining for sand and lime material, must be seen as substantial.

If the of quantity of autoclaved aerated concrete in 2012 of the Insee superblock industry was considered. The raw material cost saving implied in these calculations, saved by the production of autoclaved aerated concrete on this scale, must also have other costs factored in, such as the energy and fuel saving on digging sand (751.77 Litre or approximately $3.27x10^{-5}$ Litre/piece) and ball milling (285,671.23 kWh or approximately 12.42 Wh/piece) as illustrated in Table 22.

Table 22 Energy saving from the dig and milling procedure of sand.

Conditions	Dig	Ball milling	Energy saving
Time (h)	840	6720	-
Fuel usage(L/h)	12	-	-
Electricity usage (kWh)	-	570	-
Total fuel usage (L)	10,080.00	-	751.77
Total electricity usage (kWh)	-	3,830,400.00	285,671.23

Environmental analysis

This section aimed to evaluate and compare the environmental impacts of the life cycle of autoclaved aerated concrete used in the Thai industry. The improved composition of autoclaved aerated concrete with phase change material coating, commercial autoclaved aerated concrete and average database of autoclaved aerated concrete used in Thailand were discussed. Two major patterns of Life-cycle assessment were considered, firstly in regard to the evaluation of the impact from the obtaining of raw materials stage, manufacture stage, distribution stage, use stage and disposal stage (landfill) (Cradle-to-grave) and secondly the assessment of the impact from the obtaining of raw materials stage, manufacture stage, distribution stage and use stage. This case was also investigated because building walls in Thailand have not been taken to the disposal stage (landfill) yet.

Impact from the obtaining of raw materials stage, manufacture stage, distribution stage, use stage and disposal stage

Life cycle impact of improved autoclaved aerated concrete

The inputs and outputs of the studied alternatives in the life cycle inventory (LCI) were quantified by taking into the account of the information available from the industry, from the suppliers, the customers and other sources to ensure the data reliability and validity.

The Eco-indicator 99 method was applied with the SimaPro software. The eleven impact categories of this indicator were evaluated using characterization, weightings and single score based on the hierarchist cultural perspective [97]. These impact categories are divided into three categories of damages: human health,

ecosystem quality and resources [95, 96, 97]. The category of damage to human health includes the impact categories of carcinogenesis, respiratory effects of organic compounds, respiratory effects of inorganic compounds, climate change, radiation and ozone layer. The category ecosystem quality includes ecotoxicity, acidification/ eutrophication and land use while the resources category includes mineral resources and fossil fuels.

Characterization results

Damage to human health is expressed in DALY (Disability Adjusted Life Years), which is the number of disability years caused by exposing to toxic material multiplied by the "disability factor". DALY (Disability Adjusted Life Years) is a number between 0 and 1 that describes the severity of the damage (0 for being perfectly healthy and 1 for being fatal).

Damages of ecosystem quality include eco toxicity, acidification, eutrophication and land use. They are expressed as a percentage of the species that are threatened or have disappeared in a certain area due to the environmental load during a year. The eco toxicity is characterized in Potentially Affected Fraction (PAF) of species in relation to concentration of the toxic materials. The PAF expressed in the percentage of the species that are exposed to toxic emission. The higher concentration affected the larger number of species. Acidification and Eutrophication are characterized in Potentially Disappeared Fraction (PDF), which is a probability of the plants species to disappear from the area as a result of acidification and eutrophication. Since it is not possible to determine whether the damage is caused by changes in the nutrient level or by acidity, these two impact categories are combined. Land use is also characterized by PDF, which refers to the change in the numbers of all species on the occupied land and at the natural area in the surroundings. The total units of the Ecosystem Quality are PDF times area times year [PDF×m^2×year].

Resources such as minerals and fossil fuels are analyzed by the Eco-indicator 99 methodology. It models the decrease of the concentration of the mineral resources in the Earth's crust and calculates the amount of energy needed to extract the mineral in a future in relation to the concentration. The units of resources damage category are "surplus energy" in MJ per kg extracted material, and it is related to the expected increase of extraction energy per kg of extracted material.

The characterization results of the life cycle of improved autoclaved aerated concrete are exhibited in Figure 151 and Table 23. The obtaining of raw materials stage, manufacture stage, distribution stage, use stage and disposal (landfill) stages are emphasized by the impact category of carcinogenesis, respiratory effects of organic compounds, respiratory effects of inorganic compounds, climate change, radiation, ozone layer, ecotoxicity, acidification/eutrophication, land use, mineral resources and fossil fuels. These harmful impacts are associated with air emissions, water and soil of some organic and inorganic compounds for example diesel, silica sand, aluminium hydroxide, gypsum, light fuel, coal, titanium dioxide and disposal. Moreover, they caused from the process of transportation, and the production and consumption of electricity and stream.

The main pollutants of obtaining of raw materials, manufacture, distribution and use stages are largely caused to the respiratory effects of organic compounds, respiratory effects of inorganic compounds, climate change, radiation, ozone layer, acidification/eutrophication, land use, mineral resources and fossil fuels as shown in Figure 151 and Table 23. The major pollutants of disposal (landfill) are largely produced the effects on carcinogenesis, ecotoxicity, respiratory effects of organic compounds and climate change as exibited in Figure 151 and Table 23.

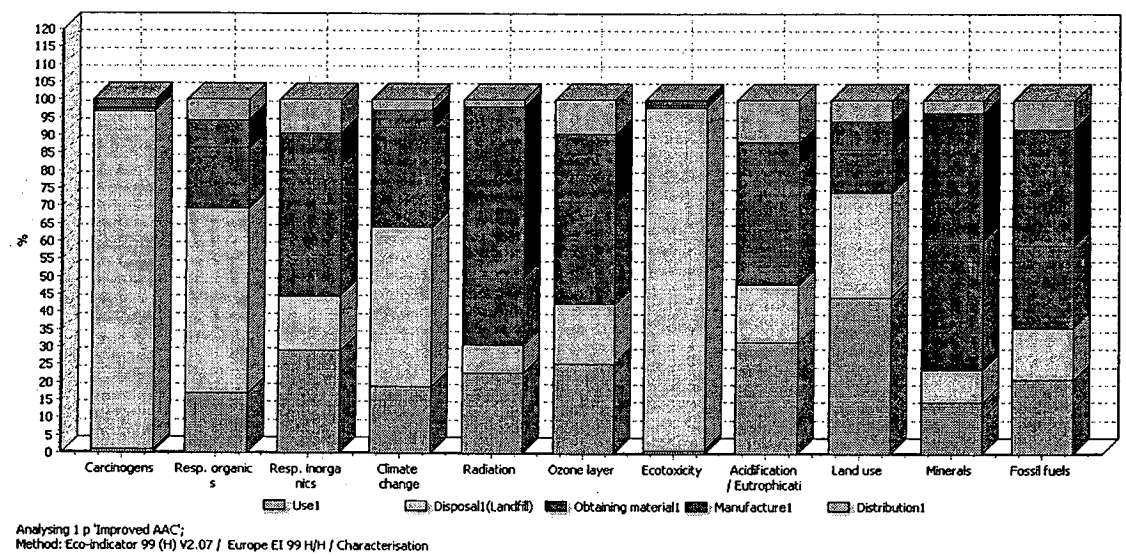

Figure 151 Impact assessment of the improved AAC.

Table 23 Impact assessment of the improved AAC

Impact category	Unit	Total	Use1	Disposal1 (Landfill)	Obtaining material1	Manufacture1	Distribution1
Carcinogens	DALY	2.20E-06	1.95E-08	2.10E-06	2.47E-08	4.98E-08	4.17E-09
Resp. organics	DALY	1.59E-09	2.73E-10	8.28E-10	2.77E-10	1.23E-10	9.44E-11
Resp. inorganics	DALY	6.64E-07	1.92E-07	1.03E-07	2.47E-07	5.95E-08	6.31E-08
Climate change	DALY	4.99E-07	9.50E-08	2.24E-07	1.41E-07	2.47E-08	1.45E-08
Radiation	DALY	7.33E-09	1.66E-09	5.75E-10	1.41E-09	3.56E-09	1.28E-10
Ozone layer	DALY	1.21E-10	3.06E-11	2.07E-11	3.44E-11	2.38E-11	1.13E-11
Ecotoxicity	PAF*m^2·yr	5.48E+00	4.94E-02	5.31E+00	5.50E-02	5.56E-02	1.51E-02
Acidification/ Eutrophication	PDF*m^2·yr	2.51E-02	7.95E-03	4.07E-03	8.51E-03	1.61E-03	2.92E-03
Land use	PDF*m^2·yr	1.81E-02	7.99E-03	5.41E-03	2.18E-03	1.44E-03	1.06E-03
Minerals	MJ surplus	2.58E-02	3.80E-03	2.33E-03	9.44E-03	9.36E-03	8.69E-04
Fossil fuels	MJ surplus	1.70	0.36	0.24	0.40	0.56	0.14

Weighting results by impact categories

In the perspective of physics, the standard Eco-indicator values are dimensionless, which are the same as the units of currency. The unit of measurement is called the Eco-indicator Point (Pt) in the Eco- indicator 99 system. The Eco-indicator Point is divided into 1000 millipoints (mPt). The size of the Pt unit was obviously chosen by Eco indicator -99 to represent one thousandth of the yearly environmental load of an average citizen in Europe.

Figure 152 and Table 24 exhibit the weighting results of the life cycle of improved autoclaved aerated concrete by impact categories, observing that the fossil fuels has the highest harmful environmental impact from the obtaining of raw materials, manufacture, distribution, use and disposal (landfill) stages, justified by the emission of remaining substances, stream, aluminium paste and the consumption of electricity, bituminous coal and diesel fuel as the main pollutants. Therefore, a disadvantage of these stages contributes to also damage to human health and the decrease of the concentration of the mineral resources in the Earth's crust. In addition, the harmful impact of the disposal (landfill) stage is emphasized by the impact category of carcinogenesis, eco toxicity, climate change, respiratory effects of inorganic compounds, and acidification/Eutrophication due to remaining substances emissions, solid waste and polluting emission during the transportation.

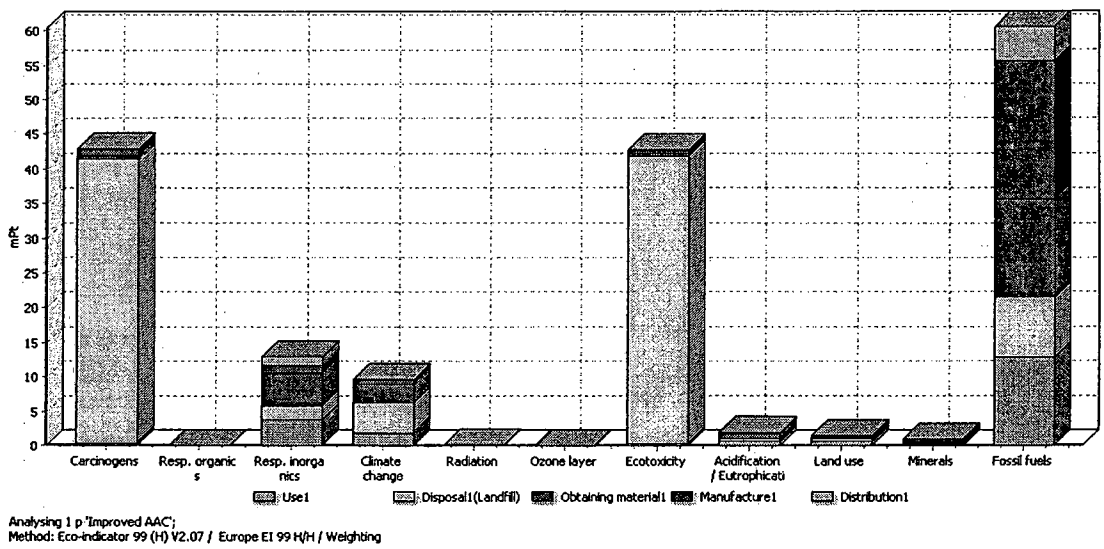

Figure 152 Impact assessment of the improved AAC.

Table 24 Impact assessment of the improved AAC

Impact category	Unit	Total	Use1	Disposal1 (Landfill)	Obtaining material1	Manufacture1	Distribution1
Total	Pt	1.73E-01	2.06E-02	9.83E-02	2.38E-02	2.37E-02	6.93E-03
Carcinogens	Pt	4.29E-02	3.80E-04	4.10E-02	4.83E-04	9.73E-04	8.14E-05
Resp. organics	Pt	3.11E-05	5.33E-06	1.62E-05	5.40E-06	2.40E-06	1.84E-06
Resp. inorganics	Pt	1.30E-02	3.75E-03	2.01E-03	4.82E-03	1.16E-03	1.23E-03
Climate change	Pt	9.75E-03	1.85E-03	4.37E-03	2.76E-03	4.83E-04	2.83E-04
Radiation	Pt	1.43E-04	3.25E-05	1.12E-05	2.75E-05	6.95E-05	2.49E-06
Ozone layer	Pt	2.36E-06	5.98E-07	4.05E-07	6.71E-07	4.65E-07	2.21E-07
Ecotoxicity	Pt	4.28E-02	3.85E-04	4.14E-02	4.29E-04	4.34E-04	1.18E-04
Acidification/ Eutrophication	Pt	1.96E-03	6.20E-04	3.18E-04	6.64E-04	1.25E-04	2.28E-04
Land use	Pt	1.41E-03	6.23E-04	4.22E-04	1.70E-04	1.12E-04	8.30E-05
Minerals	Pt	9.21E-04	1.36E-04	8.30E-05	3.37E-04	3.34E-04	3.10E-05
Fossil fuels	Pt	6.05E-02	1.28E-02	8.68E-03	1.42E-02	2.00E-02	4.87E-03

Single score results by damages categories

Single score results of the life cycle of improved autoclaved aerated concrete by damages categories are shown in Figure 153 and Table 25 for all stages. The disposal stage contributes to the greatest environmental load where the damages to the human health and ecosystem quality show the highest value, about 56.7% of the total impact at this stage. This behavior is largely produced the effect of carcinogens and eco toxicity (about 41.7% of the carcinogens and approximately 42% of eco toxicity).

The obtaining material stage shows the highest contribution to the fossil fuels category with an emphasis on diesel consumption. The manufacture stage illustrates also the highest result in the fossil fuels category with an emphasis on electrical and coal consumption. The use stage exhibits also the highest contribution to the fossil fuels category with an emphasis on diesel consumption. Lastly, the distribution stage shows the lowest results in all categories in comparison with the rest of the stages.

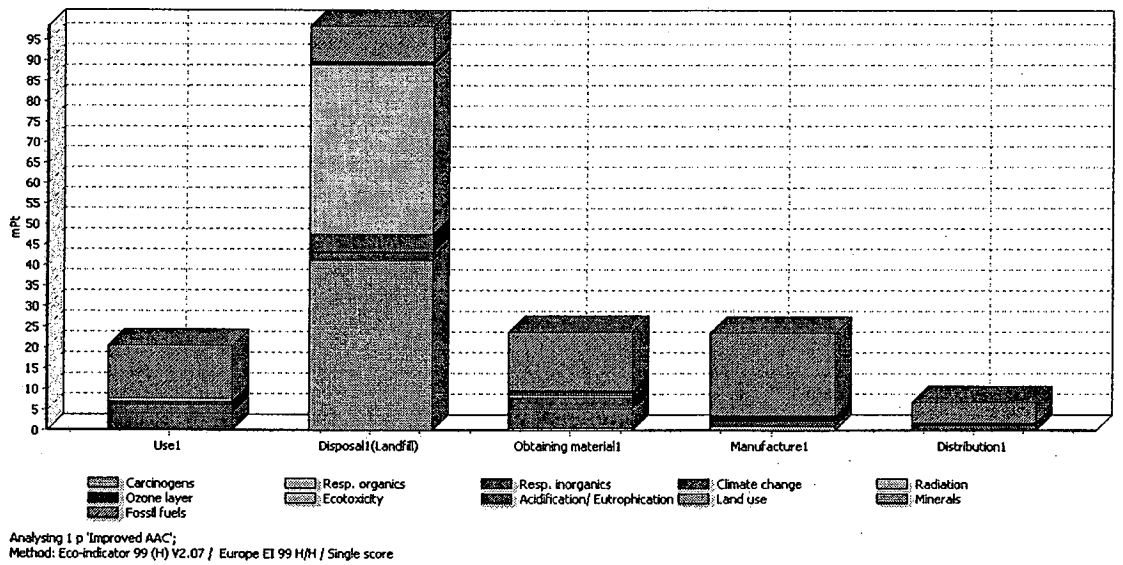

Figure 153 Impact assessment of the improved AAC in the each procedure.

Table 25 Single value of the improved AAC in the each procedure

Impact category	Unit	Total	Use1	Disposal1 (Landfill)	Obtaining material1	Manufacture1	Distribution1
Total	Pt	1.73E-01	2.06E-02	9.83E-02	2.38E-02	2.37E-02	6.93E-03
Carcinogens	Pt	4.29E-02	3.80E-04	4.10E-02	4.83E-04	9.73E-04	8.14E-05
Resp. organics	Pt	3.11E-05	5.33E-06	1.62E-05	5.40E-06	2.40E-06	1.84E-06
Resp. inorganics	Pt	1.30E-02	3.75E-03	2.01E-03	4.82E-03	1.16E-03	1.23E-03
Climate change	Pt	9.75E-03	1.85E-03	4.37E-03	2.76E-03	4.83E-04	2.83E-04
Radiation	Pt	1.43E-04	3.25E-05	1.12E-05	2.75E-05	6.95E-05	2.49E-06
Ozone layer	Pt	2.36E-06	5.98E-07	4.05E-07	6.71E-07	4.65E-07	2.21E-07
Ecotoxicity	Pt	4.28E-02	3.85E-04	4.14E-02	4.29E-04	4.34E-04	1.18E-04
Acidification/ Eutrophication	Pt	1.96E-03	6.20E-04	3.18E-04	6.64E-04	1.25E-04	2.28E-04
Land use	Pt	1.41E-03	6.23E-04	4.22E-04	1.70E-04	1.12E-04	8.30E-05
Minerals	Pt	9.21E-04	1.36E-04	8.30E-05	3.37E-04	3.34E-04	3.10E-05
Fossil fuels	Pt	6.05E-02	1.28E-02	8.68E-03	1.42E-02	2.00E-02	4.87E-03

Life cycle impact of commercial autoclaved aerated concrete

Characterization results

Figure 154 and Table 26 exhibit the characterization results of the life cycle of commercial autoclaved aerated concrete. The impact category of carcinogenesis, respiratory effects of organic compounds, respiratory effects of inorganic compounds, climate change, radiation, ozone layer, ecotoxicity, acidification/eutrophication, land use, mineral resources and fossil fuels associated with the obtaining of raw materials stage, manufacture stage, distribution stage, use stage and disposal (landfill) stages. These harmful impacts are emphasized by air emissions, water and soil of some organic and inorganic compounds for example diesel, silica sand, aluminium paste, gypsum, light fuel, coal, titanium dioxide and disposal. Moreover, the process of transportation, and the production and consumption of electricity and stream produced the effect on these problems.

The main pollutants of obtaining of raw materials, manufacture, distribution and use stages are largely caused to the respiratory effects of organic compounds, respiratory effects of inorganic compounds, climate change, radiation, ozone layer, acidification/eutrophication, land use, mineral resources and fossil fuels as shown in Figure 154 and Table 26. Carcinogenesis, ecotoxicity, respiratory effects of organic compounds and climate change caused from disposal (landfill) as the major pollutants as exhibited in Figure 154 and Table 26.

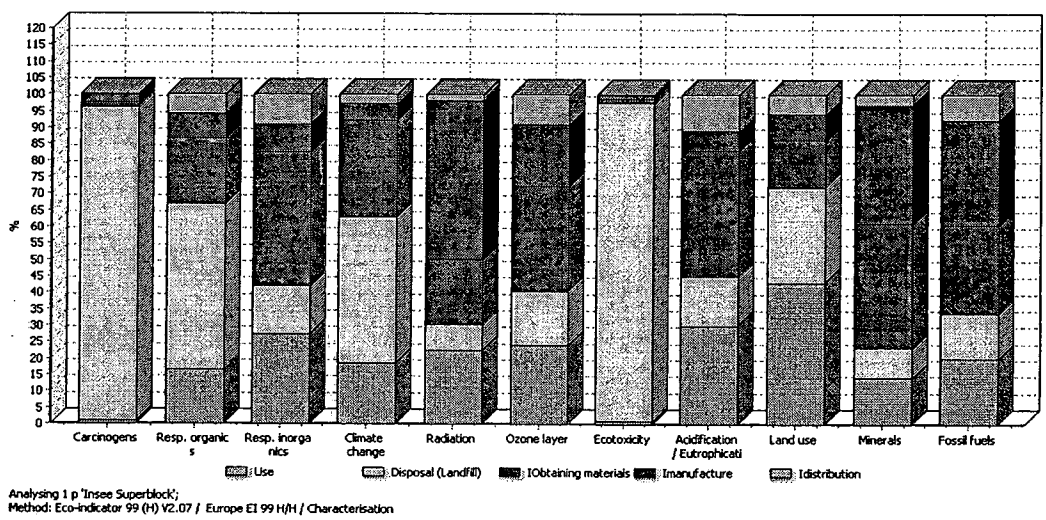

Figure 154 Impact assessment of Insee superblock AAC.

Table 26 Impact assessment of Insee superblock AAC

Impact category	Unit	Total	Use	Disposal (Landfill)	IObtaining materials	Imanufacture	Idistribution
Carcinogens	DALY	2.20E-06	1.95E-08	2.10E-06	2.68E-08	4.98E-08	4.17E-09
Resp. organics	DALY	1.65E-09	2.73E-10	8.28E-10	3.29E-10	1.23E-10	9.44E-11
Resp. inorganics	DALY	6.99E-07	1.92E-07	1.03E-07	2.82E-07	5.95E-08	6.31E-08
Climate change	DALY	5.08E-07	9.50E-08	2.24E-07	1.49E-07	2.47E-08	1.45E-08
Radiation	DALY	7.42E-09	1.66E-09	5.75E-10	1.49E-09	3.56E-09	1.28E-10
Ozone layer	DALY	1.27E-10	3.06E-11	2.07E-11	4.08E-11	2.38E-11	1.13E-11
Ecotoxicity	PAF*m^2·yr	5.49	0.05	5.31	0.06	0.06	0.02
Acidification/ Eutrophication	PDF*m^2·yr	2.66E-02	7.95E-03	4.07E-03	1.01E-02	1.61E-03	2.92E-03
Land use	PDF*m^2·yr	1.86E-02	7.99E-03	5.41E-03	2.70E-03	1.44E-03	1.06E-03
Minerals	MJ surplus	2.62E-02	3.80E-03	2.33E-03	9.89E-03	9.35E-03	8.69E-04
Fossil fuels	MJ surplus	1.77	0.36	0.24	0.47	0.56	0.14

Weighting results by impact categories

The weighting results of the life cycle of commercial autoclaved aerated concrete by impact categories are shown in Figure 155 and Table 27. The fossil fuels has the highest harmful environmental impact from the obtaining of raw materials, manufacture, distribution, use and disposal (landfill) stages, which concerned with the emission of remaining substances, stream, aluminium paste and the consumption of electricity, bituminous coal and diesel fuel as the main pollutants. Hence, a disadvantage of these stages contributes to also damage to human health and the decrease of the concentration of the mineral resources in the Earth's crust. Furthermore, the harmful impact of the disposal (landfill) stage is emphasized by the impact category of carcinogenesis, eco toxicity, climate change, respiratory effects of inorganic compounds, and acidification/Eutrophication due to remaining substances emissions, solid waste and polluting emission during the transportation.

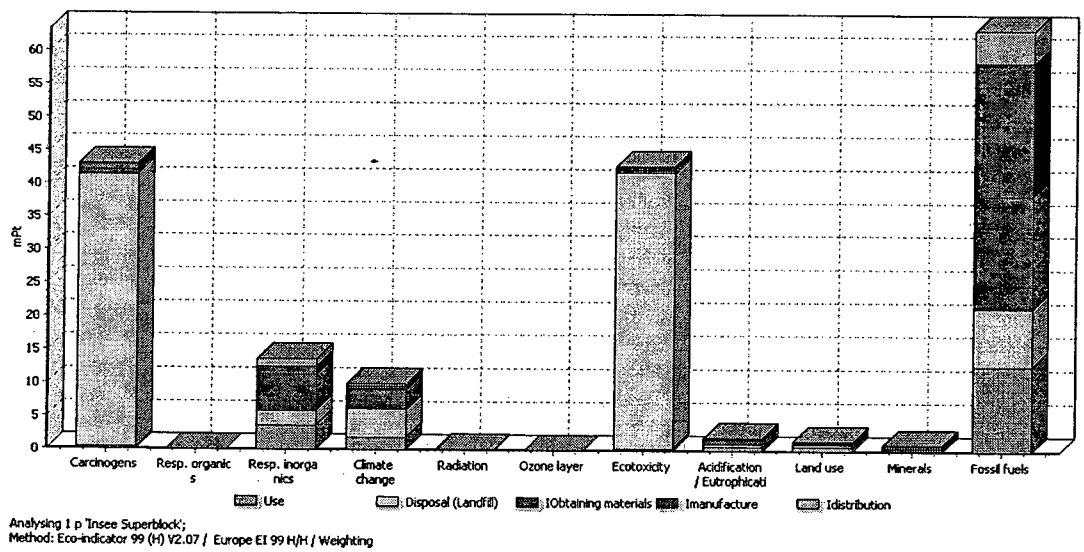

Figure 155 Impact assessment of Insee superblock AAC.

Table 27 Impact assessment of Insee superblock AAC

Impact category	Unit	Total	Use	Disposal (Landfill)	Obtaining materials	Manufacture	Distribution
Total	Pt	1.77E-01	2.06E-02	9.83E-02	2.78E-02	2.37E-02	6.93E-03
Carcinogens	Pt	4.30E-02	3.80E-04	4.10E-02	5.24E-04	9.73E-04	8.14E-05
Resp. organics	Pt	3.22E-05	5.33E-06	1.62E-05	6.43E-06	2.40E-06	1.84E-06
Resp. inorganics	Pt	1.37E-02	3.75E-03	2.01E-03	5.50E-03	1.16E-03	1.23E-03
Climate change	Pt	9.91E-03	1.85E-03	4.37E-03	2.92E-03	4.83E-04	2.83E-04
Radiation	Pt	1.45E-04	3.25E-05	1.12E-05	2.91E-05	6.95E-05	2.49E-06
Ozone layer	Pt	2.49E-06	5.98E-07	4.05E-07	7.97E-07	4.65E-07	2.21E-07
Ecotoxicity	Pt	4.28E-02	3.85E-04	4.14E-02	4.92E-04	4.33E-04	1.18E-04
Acidification/ Eutrophication	Pt	2.08E-03	6.20E-04	3.18E-04	7.87E-04	1.25E-04	2.28E-04
Land use	Pt	1.45E-03	6.23E-04	4.22E-04	2.11E-04	1.12E-04	8.30E-05
Minerals	Pt	9.37E-04	1.36E-04	8.30E-05	3.53E-04	3.34E-04	3.10E-05
Fossil fuels	Pt	6.33E-02	1.28E-02	8.68E-03	1.69E-02	2.00E-02	4.87E-03

Single score results by damages categories

Single score results of the life cycle of commercial autoclaved aerated concrete by damages categories in all stages are shown in Figure 156 and Table 28. The disposal stage contributes to the greatest environmental load where the damages to the human health and ecosystem quality show the highest value, about 55.5 % of the total impact at this stage. This behavior is largely produced the effect of carcinogens and eco toxicity (about 41.7% of the carcinogens and approximately 42.1% of eco toxicity).

The obtaining material stage exhibits the highest contribution to the fossil fuels category with an emphasis on diesel consumption. The manufacture stage illustrates also the highest result in the fossil fuels category with an emphasis on electrical and coal consumption. The use stage exhibits also the highest contribution to the fossil fuels category with an emphasis on diesel consumption. Finally, the distribution stage illustrates the lowest results in all categories in comparison with the rest of the stages.

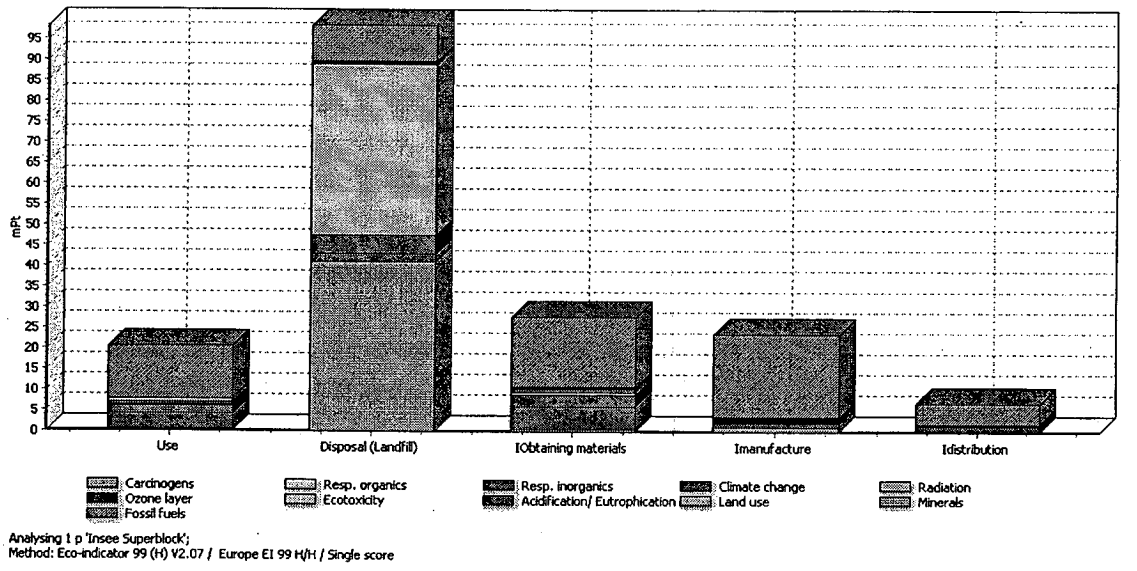

Figure 156 Impact assessment of Insee superblock AAC in the each procedure.

Table 28 Single value of Insee superblock AAC in the each procedure

Impact category	Unit	Total	Use	Disposal (Landfill)	Obtaining materials	Manufacture	Distribution
Total	Pt	1.77E-01	2.06E-02	9.83E-02	2.78E-02	2.37E-02	6.93E-03
Carcinogens	Pt	4.30E-02	3.80E-04	4.10E-02	5.24E-04	9.73E-04	8.14E-05
Resp. organics	Pt	3.22E-05	5.33E-06	1.62E-05	6.43E-06	2.40E-06	1.84E-06
Resp. inorganics	Pt	1.37E-02	3.75E-03	2.01E-03	5.50E-03	1.16E-03	1.23E-03
Climate change	Pt	9.91E-03	1.85E-03	4.37E-03	2.92E-03	4.83E-04	2.83E-04
Radiation	Pt	1.45E-04	3.25E-05	1.12E-05	2.91E-05	6.95E-05	2.49E-06
Ozone layer	Pt	2.49E-06	5.98E-07	4.05E-07	7.97E-07	4.65E-07	2.21E-07
Ecotoxicity	Pt	4.28E-02	3.85E-04	4.14E-02	4.92E-04	4.33E-04	1.18E-04
Acidification/ Eutrophication	Pt	2.08E-03	6.20E-04	3.18E-04	7.87E-04	1.25E-04	2.28E-04
Land use	Pt	1.45E-03	6.23E-04	4.22E-04	2.11E-04	1.12E-04	8.30E-05
Minerals	Pt	9.37E-04	1.36E-04	8.30E-05	3.53E-04	3.34E-04	3.10E-05
Fossil fuels	Pt	6.33E-02	1.28E-02	8.68E-03	1.69E-02	2.00E-02	4.87E-03

Life cycle impact of average database of autoclaved aerated concrete

Characterization results

The characterization results of the life cycle of average database of autoclaved aerated concrete are exhibited in Figure 157 and Table 29. The obtaining of raw materials stage, manufacture stage, distribution stage, use stage and disposal (landfill) stages are emphasized by the impact category of carcinogenesis, respiratory effects of organic compounds, respiratory effects of inorganic compounds, climate change, radiation, ozone layer, ecotoxicity, acidification/eutrophication, land use, mineral resources and fossil fuels. These harmful impacts are associated with air emissions, water and soil of some organic and inorganic compounds for example diesel, silica sand, aluminium paste, gypsum, light fuel, coal, titanium dioxide and disposal. Moreover, they caused from the process of transportation, and the production and consumption of electricity and stream.

The main pollutants of obtaining of raw materials, manufacture, distribution and use stages are largely caused to the respiratory effects of organic compounds, respiratory effects of inorganic compounds, climate change, radiation, ozone layer, acidification/eutrophication, land use, mineral resources and fossil fuels. The major pollutants of disposal (landfill) are largely caused carcinogenesis, ecotoxicity, respiratory effects of organic compounds and climate change as exhibited in Figure 157 and Table 29.

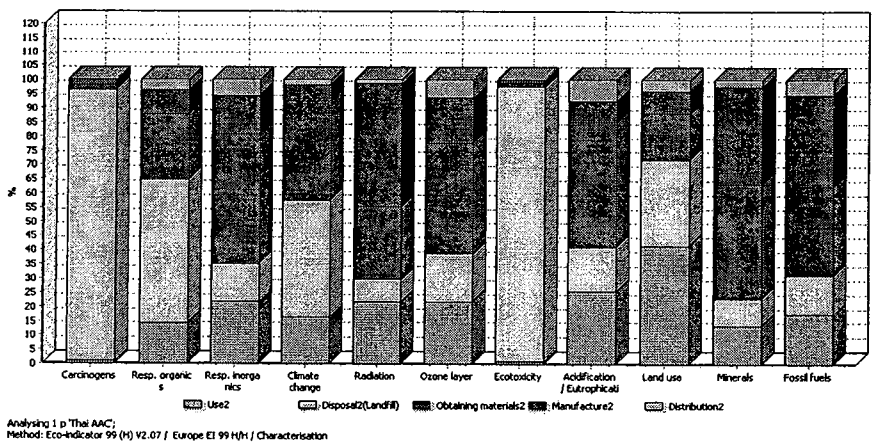

Figure 157 Impact assessment of average AAC in Thailand.

Table 29 Impact assessment of average database of AAC in Thailand

Impact category	Unit	Total	Use2	Disposal2 (Landfill)	Obtaining materials2	Manufacture2	Distribution2
Carcinogens	DALY	2.20E-06	1.77E-08	2.10E-06	3.12E-08	4.57E-08	2.78E-09
Resp. organics	DALY	1.64E-09	2.34E-10	8.28E-10	3.80E-10	1.35E-10	6.29E-11
Resp. inorganics	DALY	7.67E-07	1.66E-07	1.03E-07	3.49E-07	1.07E-07	4.20E-08
Climate change	DALY	5.47E-07	8.97E-08	2.24E-07	1.93E-07	3.05E-08	9.64E-09
Radiation	DALY	7.36E-09	1.60E-09	5.75E-10	1.89E-09	3.20E-09	8.51E-11
Ozone layer	DALY	1.21E-10	2.65E-11	2.07E-11	4.70E-11	1.96E-11	7.54E-12
Ecotoxicity	PAF*m^2·yr	5.49	0.04	5.31	0.07	0.05	0.01
Acidification/ Eutrophication	PDF*m^2·yr	2.66E-02	6.79E-03	4.07E-03	1.17E-02	2.00E-03	1.95E-03
Land use	PDF*m^2·yr	1.80E-02	7.50E-03	5.41E-03	3.00E-03	1.42E-03	7.10E-04
Minerals	MJ surplus	2.51E-02	3.44E-03	2.33E-03	1.02E-02	8.61E-03	5.79E-04
Fossil fuels	MJ surplus	1.76	0.31	0.24	0.54	0.58	0.09

Weighting results by impact categories

Figure 158 and Table 30 exhibit the weighting results of the life cycle of average database of autoclaved aerated concrete in Thailand by impact categories, observing that the fossil fuels has the highest harmful environmental impact from the obtaining of raw materials, manufacture, distribution, use and disposal (landfill) stages, justified by the emission of remaining substances, stream, aluminium paste and the consumption of electricity, bituminous coal and diesel fuel as the main pollutants. Therefore, a disadvantage of these stages contributes to also damage to human health and the decrease of the concentration of the mineral resources in the Earth's crust. In addition, the harmful impact of the disposal (landfill) stage is emphasized by the impact category of carcinogenesis, eco toxicity, climate change, respiratory effects of inorganic compounds, and acidification/eutrophication due to remaining substances emissions, solid waste and polluting emission during the transportation.

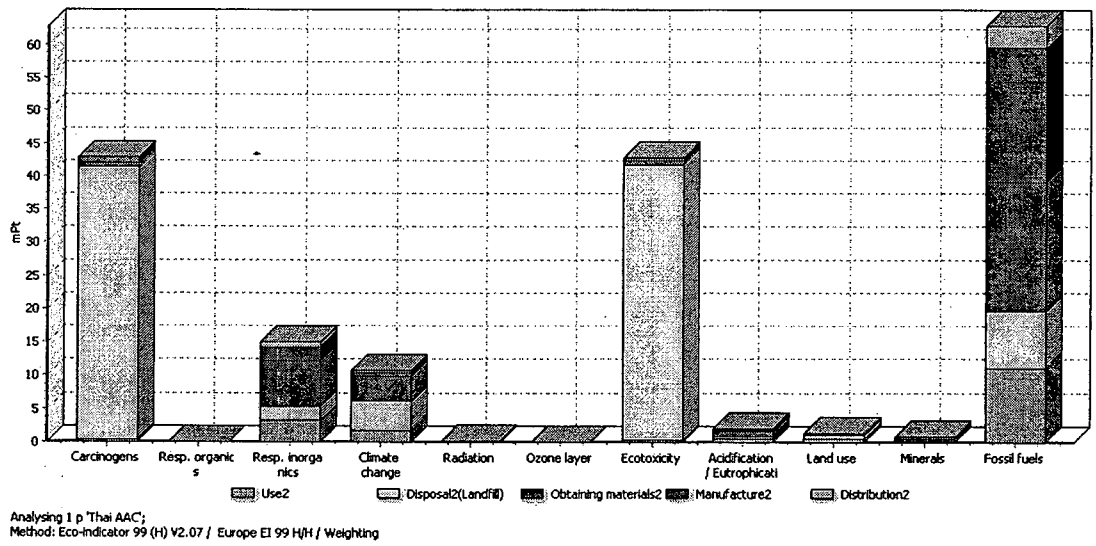

Figure 158 Impact assessment of average database of AAC in Thailand.

Table 30 Impact assessment of average database of AAC in Thailand

Impact category	Unit	Total	Use2	Disposal2 (Landfill)	Obtaining materials2	Manufacture2	Distribution2
Total	Pt	1.79E-01	1.80E-02	9.83E-02	3.27E-02	2.52E-02	4.62E-03
Carcinogens	Pt	4.29E-02	3.46E-04	4.10E-02	6.09E-04	8.92E-04	5.43E-05
Resp. organics	Pt	3.20E-05	4.57E-06	1.62E-05	7.42E-06	2.63E-06	1.23E-06
Resp. inorganics	Pt	1.50E-02	3.24E-03	2.01E-03	6.82E-03	2.09E-03	8.21E-04
Climate change	Pt	1.07E-02	1.75E-03	4.37E-03	3.77E-03	5.95E-04	1.88E-04
Radiation	Pt	1.44E-04	3.13E-05	1.12E-05	3.69E-05	6.25E-05	1.66E-06
Ozone layer	Pt	2.37E-06	5.18E-07	4.05E-07	9.18E-07	3.83E-07	1.47E-07
Ecotoxicity	Pt	4.28E-02	3.38E-04	4.14E-02	5.76E-04	4.05E-04	7.88E-05
Acidification/ Eutrophication	Pt	2.07E-03	5.30E-04	3.18E-04	9.15E-04	1.56E-04	1.52E-04
Land use	Pt	1.41E-03	5.85E-04	4.22E-04	2.34E-04	1.10E-04	5.54E-05
Minerals	Pt	8.97E-04	1.23E-04	8.30E-05	3.63E-04	3.07E-04	2.07E-05
Fossil fuels	Pt	6.29E-02	1.10E-02	8.68E-03	1.93E-02	2.06E-02	3.25E-03

Single score results by damages categories

Single score results of the life cycle of average database of autoclaved aerated concrete by damages categories in all stages are shown in Figure 159 and Table 31. The disposal stage contributes to the greatest environmental load where the damages to the human health and ecosystem quality show the highest value, about 55.0 % of the total impact at this stage. This behavior is largely produced the effect of carcinogens and eco toxicity (about 41.7% of the carcinogens and approximately 42.1% of eco toxicity).

The obtaining material stage shows the maximum contribution to the fossil fuels category with an emphasis on diesel consumption. The manufacture stage illustrates also the maximum result in the fossil fuels category with an emphasis on electrical and coal consumption. The use stage exhibits also the highest contribution to the fossil fuels category with an emphasis on diesel consumption. Lastly, the distribution stage shows the lowest results in all categories in comparison with the rest of the stages.

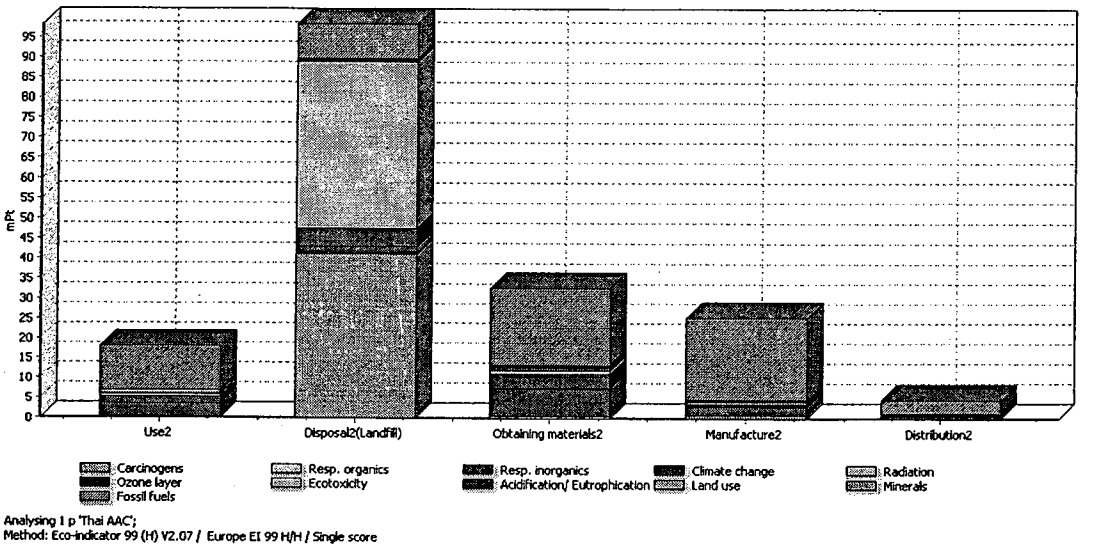

Figure 159 Impact assessment of average AAC of the each procedure in Thailand.

Table 31 Single score of the average database of AAC used in Thailand

Impact category	Unit	Total	Use2	Disposal2 (Landfill)	Obtaining materials2	Manufacture2	Distribution2
Total	Pt	1.79E-01	1.80E-02	9.83E-02	3.27E-02	2.52E-02	4.62E-03
Carcinogens	Pt	4.29E-02	3.46E-04	4.10E-02	6.09E-04	8.92E-04	5.43E-05
Resp. organics	Pt	3.20E-05	4.57E-06	1.62E-05	7.42E-06	2.63E-06	1.23E-06
Resp. inorganics	Pt	1.50E-02	3.24E-03	2.01E-03	6.82E-03	2.09E-03	8.21E-04
Climate change	Pt	1.07E-02	1.75E-03	4.37E-03	3.77E-03	5.95E-04	1.88E-04
Radiation	Pt	1.44E-04	3.13E-05	1.12E-05	3.69E-05	6.25E-05	1.66E-06
Ozone layer	Pt	2.37E-06	5.18E-07	4.05E-07	9.18E-07	3.83E-07	1.47E-07
Ecotoxicity	Pt	4.28E-02	3.38E-04	4.14E-02	5.76E-04	4.05E-04	7.88E-05
Acidification/ Eutrophication	Pt	2.07E-03	5.30E-04	3.18E-04	9.15E-04	1.56E-04	1.52E-04
Land use	Pt	1.41E-03	5.85E-04	4.22E-04	2.34E-04	1.10E-04	5.54E-05
Minerals	Pt	8.97E-04	1.23E-04	8.30E-05	3.63E-04	3.07E-04	2.07E-05
Fossil fuels	Pt	6.29E-02	1.10E-02	8.68E-03	1.93E-02	2.06E-02	3.25E-03

Comparison of weighting results of autoclaved aerated concrete in the three conditions

The weighting results of the life cycle of autoclaved aerated concrete in the three conditions are illustrated in Figure 160 and Table 32. These observed that the fossil fuels in the life cycle of autoclaved aerated concrete in the three conditions has the highest harmful environmental impact from the obtaining of raw materials, manufacture, distribution, use and disposal (landfill) stages. These activities corresponded to the emission of remaining substances, stream, aluminium paste and the consumption of electricity, bituminous coal and diesel fuel as the main pollutants. Therefore, a difficulty of these stages contributes to also damage to human health and the decrease of the concentration of the mineral resources in the Earth's crust. Moreover, the harmful impact of the disposal (landfill) stage is emphasized by the impact category of carcinogenesis, eco toxicity, climate change, respiratory effects of inorganic compounds, and acidification/eutrophication due to remaining substances emissions, solid waste and polluting emission during the transportation.

The weighting results of the life cycle of autoclaved aerated concrete in the three conditions are the similar except for fossil fuels, respiratory effects of inorganic compounds and climate change. With comparing in the part of fossil fuels, the life cycle of average database of commercial autoclaved aerated concrete has the highest harmful impact while that of improved autoclaved aerated concrete has the least harmful impact. These results may be associated with different electrical consumption in the part of the manufacturer because of the ancient machines and different distance of transportation. With comparing in the part of respiratory effects of inorganic compounds and climate change, the life cycle of average database of autoclaved aerated concrete has the highest harmful impact while that of improved autoclaved aerated concrete has the least harmful impact. Lower harmful impact in the part of respiratory effects of inorganic compounds and climate change of life cycle of improved autoclaved aerated concrete has the cause from the raw material replacement by sugar sediment waste.

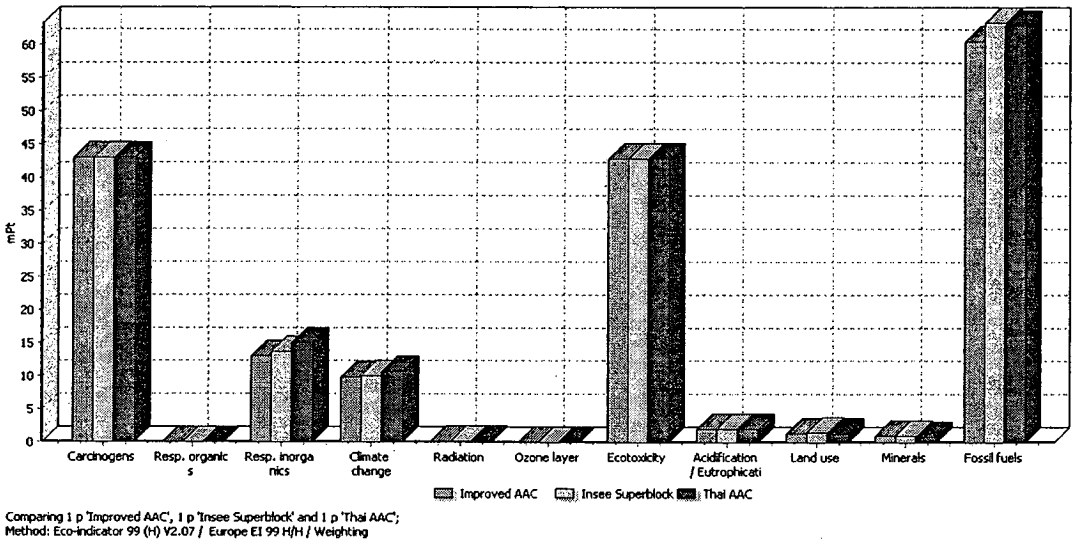

Figure 160 Impact assessment of average AAC of the each procedure in Thailand.

Table 32 Impact assessment of AAC in the three conditions

Impact category	Unit	Improved AAC	Insee Superblock AAC	Thai AAC
Total	Pt	1.73E-01	1.77E-01	1.79E-01
Carcinogens	Pt	4.29E-02	4.30E-02	4.29E-02
Resp. organics	Pt	3.11E-05	3.22E-05	3.20E-05
Resp. inorganics	Pt	1.30E-02	1.37E-02	1.50E-02
Climate change	Pt	9.75E-03	9.91E-03	1.07E-02
Radiation	Pt	1.43E-04	1.45E-04	1.44E-04
Ozone layer	Pt	2.36E-06	2.49E-06	2.37E-06
Ecotoxicity	Pt	4.28E-02	4.28E-02	4.28E-02
Acidification/ Eutrophication	Pt	1.96E-03	2.08E-03	2.07E-03
Land use	Pt	1.41E-03	1.45E-03	1.41E-03
Minerals	Pt	9.21E-04	9.37E-04	8.97E-04
Fossil fuels	Pt	6.05E-02	6.33E-02	6.29E-02

Impact from the obtaining of raw materials stage, manufacture stage, distribution stage and use stage

Life cycle impact of improved autoclaved aerated concrete

Characterization results

The characterization results of the life cycle of improved autoclaved aerated concrete are illustrated in Figure 151 and Table 23. The impact category of carcinogenesis, respiratory effects of organic compounds, respiratory effects of inorganic compounds, climate change, radiation, ozone layer, ecotoxicity, acidification/ eutrophication, land use, mineral resources and fossil fuels were considered from the process of the obtaining of raw materials stage, manufacture stage, distribution stage and use stage. These harmful impacts corresponded to air emissions, water and soil of some organic and inorganic compounds for example diesel, silica sand, aluminum paste, gypsum, light fuel, coal, titanium dioxide and disposal. Furthermore, these harmful impacts were also resulted from the process of transportation, and the production and consumption of electricity and stream.

The main pollutants of obtaining of raw materials, manufacture, distribution and use stages are largely caused to the respiratory effects of organic compounds, respiratory effects of inorganic compounds, climate change, radiation, ozone layer, acidification/eutrophication, land use, mineral resources and fossil fuels as shown in Figure 151 and Table 23.

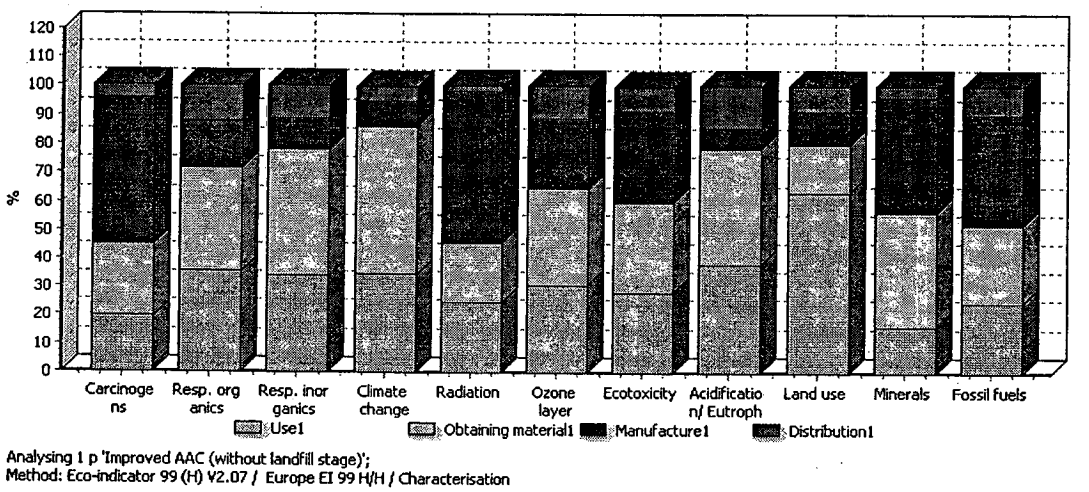

Figure 161 Impact assessment of the improved AAC.

Table 33 Impact assessment of the improved AAC

Impact category	Unit	Total	Obtaining material1	Manufacture1	Distribution1	Use1
Carcinogens	DALY	9.81E-08	2.47E-08	4.98E-08	4.17E-09	1.95E-08
Resp. organics	DALY	7.67E-10	2.77E-10	1.23E-10	9.44E-11	2.73E-10
Resp. inorganics	DALY	5.61E-07	2.47E-07	5.95E-08	6.31E-08	1.92E-07
Climate change	DALY	2.75E-07	1.41E-07	2.47E-08	1.45E-08	9.50E-08
Radiation	DALY	6.76E-09	1.41E-09	3.56E-09	1.28E-10	1.66E-09
Ozone layer	DALY	1.00E-10	3.44E-11	2.38E-11	1.13E-11	3.06E-11
Ecotoxicity	PAF*m^2·yr	1.75E-01	5.50E-02	5.56E-02	1.51E-02	4.94E-02
Acidification/ Eutrophication	PDF*m^2·yr	2.10E-02	8.51E-03	1.61E-03	2.92E-03	7.95E-03
Land use	PDF*m^2·yr	1.27E-02	2.18E-03	1.44E-03	1.06E-03	7.99E-03
Minerals	MJ surplus	2.35E-02	9.44E-03	9.36E-03	8.69E-04	3.80E-03
Fossil fuels	MJ surplus	1.45E+00	3.96E-01	5.61E-01	1.36E-01	3.58E-01

Weighting results by impact categories

The weighting results of the life cycle of improved autoclaved aerated concrete by impact categories are shown in Figure 162 and Table 24, which were observed that the fossil fuels has the highest harmful environmental impact from the obtaining of raw materials, manufacture, distribution, and use stages, justified by the emission of remaining substances, stream, aluminium paste and the consumption of electricity, bituminous coal and diesel fuel as the main pollutants. So, a disadvantage of these stages contributes to also damage to human health and the decrease of the concentration of the mineral resources in the Earth's crust.

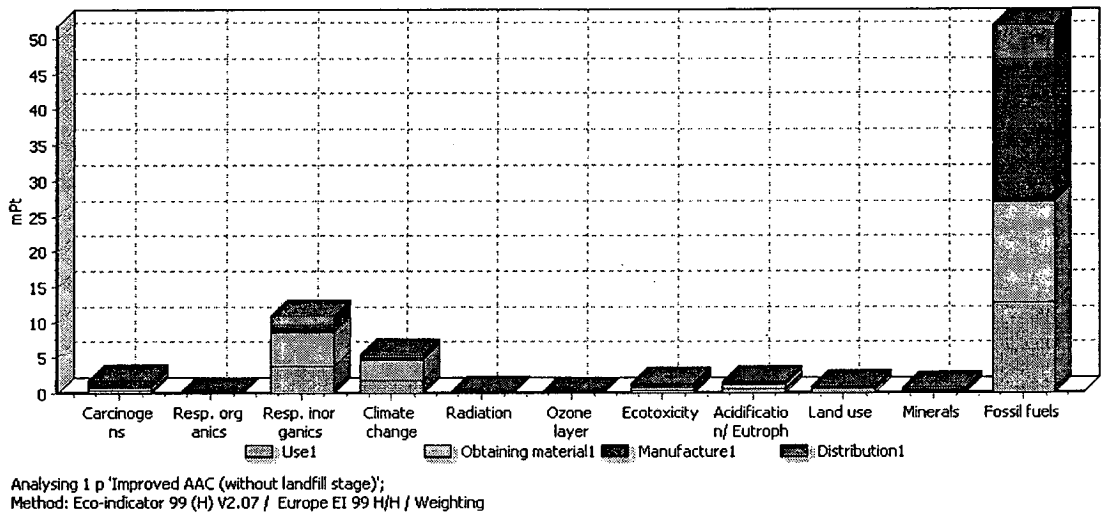

Figure 162 Impact assessment of the improved AAC.

Table 34 Impact assessment of the improved AAC

Impact category	Unit	Total	Obtaining material1	Manufacture1	Distribution1	Use1
Total	Pt	7.51E-02	2.38E-02	2.37E-02	6.93E-03	2.06E-02
Carcinogens	Pt	1.92E-03	4.83E-04	9.73E-04	8.14E-05	3.80E-04
Resp. organics	Pt	1.50E-05	5.40E-06	2.40E-06	1.84E-06	5.33E-06
Resp. inorganics	Pt	1.10E-02	4.82E-03	1.16E-03	1.23E-03	3.75E-03
Climate change	Pt	5.38E-03	2.76E-03	4.83E-04	2.83E-04	1.85E-03
Radiation	Pt	1.32E-04	2.75E-05	6.95E-05	2.49E-06	3.25E-05
Ozone layer	Pt	1.96E-06	6.71E-07	4.65E-07	2.21E-07	5.98E-07
Ecotoxicity	Pt	1.37E-03	4.29E-04	4.34E-04	1.18E-04	3.85E-04
Acidification/ Eutrophication	Pt	1.64E-03	6.64E-04	1.25E-04	2.28E-04	6.20E-04
Land use	Pt	9.89E-04	1.70E-04	1.12E-04	8.30E-05	6.23E-04
Minerals	Pt	8.38E-04	3.37E-04	3.34E-04	3.10E-05	1.36E-04
Fossil fuels	Pt	5.18E-02	1.42E-02	2.00E-02	4.87E-03	1.28E-02

Single score results by damages categories

Figure 153 and Table 25 exhibit the single score results of the life cycle of improved autoclaved aerated concrete in all stages by damages categories. The obtaining material stage contributes to the greatest environmental load where the damages to the human health and ecosystem quality show the highest value, about 31.8% of the total impact at this stage. This behavior is largely produced the effect of the fossil fuels and respiratory effects of inorganic compounds (about 59.4% of the fossil fuels and approximately 20% of respiratory effects of inorganic compounds).

The manufacture stage displays the highest contribution to the fossil fuels category with an emphasis on diesel consumption. The manufacture stage illustrates the highest result in the fossil fuels category with an emphasis on electrical and coal consumption. The use stage exhibits also the highest contribution to the fossil fuels category with an emphasis on diesel consumption. Lastly, the distribution stage shows the lowest results in all categories in comparison with the rest of the stages.

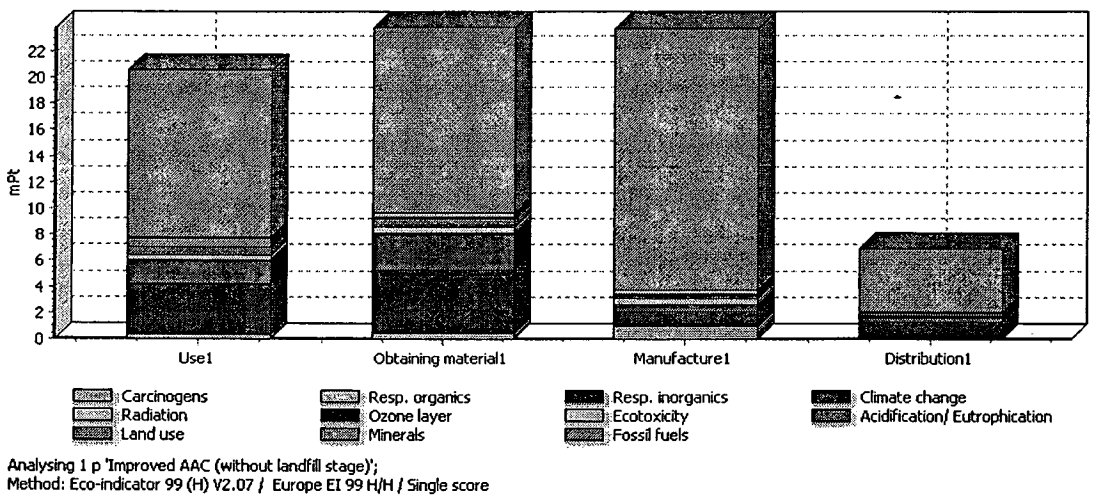

Figure 163 Impact assessment of the improved AAC in the each procedure.

Table 35 Single value of the improved AAC in the each procedure

Impact category	Unit	Total	Obtaining material1	Manufacture1	Distribution1	Use1
Total	Pt	7.51E-02	2.38E-02	2.37E-02	6.93E-03	2.06E-02
Carcinogens	Pt	1.92E-03	4.83E-04	9.73E-04	8.14E-05	3.80E-04
Resp. organics	Pt	1.50E-05	5.40E-06	2.40E-06	1.84E-06	5.33E-06
Resp. inorganics	Pt	1.10E-02	4.82E-03	1.16E-03	1.23E-03	3.75E-03
Climate change	Pt	5.38E-03	2.76E-03	4.83E-04	2.83E-04	1.85E-03
Radiation	Pt	1.32E-04	2.75E-05	6.95E-05	2.49E-06	3.25E-05
Ozone layer	Pt	1.96E-06	6.71E-07	4.65E-07	2.21E-07	5.98E-07
Ecotoxicity	Pt	1.37E-03	4.29E-04	4.34E-04	1.18E-04	3.85E-04
Acidification/ Eutrophication	Pt	1.64E-03	6.64E-04	1.25E-04	2.28E-04	6.20E-04
Land use	Pt	9.89E-04	1.70E-04	1.12E-04	8.30E-05	6.23E-04
Minerals	Pt	8.38E-04	3.37E-04	3.34E-04	3.10E-05	1.36E-04
Fossil fuels	Pt	5.18E-02	1.42E-02	2.00E-02	4.87E-03	1.28E-02

Life cycle impact of commercial autoclaved aerated concrete

Characterization results

Figure 154 and Table 26 exhibit the characterization results of the life cycle of commercial autoclaved aerated concrete. The obtaining of raw materials stage, manufacture stage, distribution stage, and use stage affected to the impact category of carcinogenesis, respiratory effects of organic compounds, respiratory effects of inorganic compounds, climate change, radiation, ozone layer, ecotoxicity, acidification/ eutrophication, land use, mineral resources and fossil fuels. These harmful impacts are emphasized by air emissions, water and soil of some organic and inorganic compounds for example diesel, silica sand, aluminium paste, gypsum, light fuel, coal, titanium dioxide and disposal. Moreover, the effect on these problems was produced from the process of transportation, and the production and consumption of electricity and stream.

The main pollutants of obtaining of raw materials, manufacture, distribution and use stages are largely caused to the respiratory effects of organic compounds, respiratory effects of inorganic compounds, climate change, radiation, ozone layer, acidification/eutrophication, land use, mineral resources and fossil fuels as exhibited in Figure 154 and Table 26.

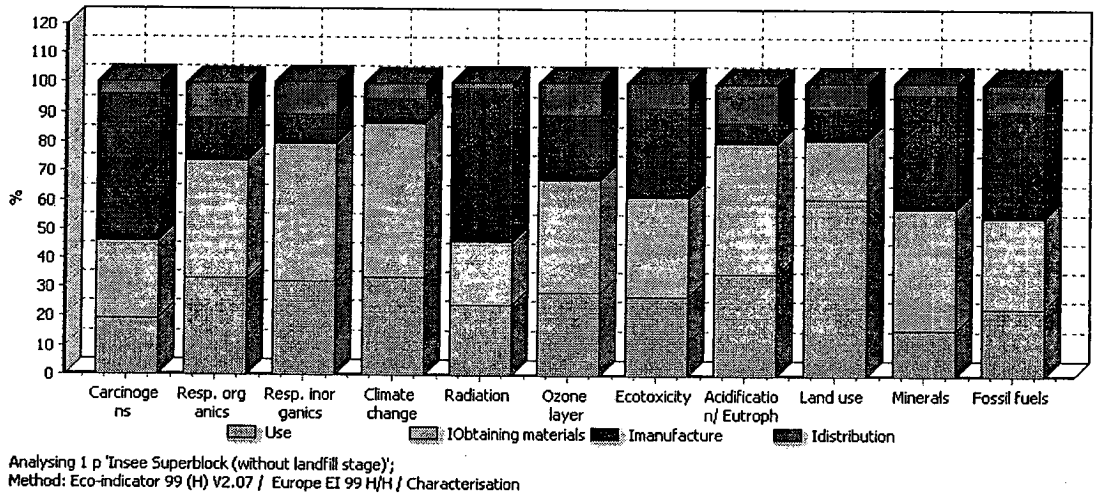

Figure 164 Impact assessment of Insee superblock AAC.

Table 36 Impact assessment of Insee superblock AAC

Impact category	Unit	Total	IObtaining materials	Imanufacture	Idistribution	Use
Carcinogens	DALY	1.00E-07	2.68E-08	4.98E-08	4.17E-09	1.95E-08
Resp. organics	DALY	8.19E-10	3.29E-10	1.23E-10	9.44E-11	2.73E-10
Resp. inorganics	DALY	5.96E-07	2.82E-07	5.95E-08	6.31E-08	1.92E-07
Climate change	DALY	2.84E-07	1.49E-07	2.47E-08	1.45E-08	9.50E-08
Radiation	DALY	6.84E-09	1.49E-09	3.56E-09	1.28E-10	1.66E-09
Ozone layer	DALY	1.07E-10	4.08E-11	2.38E-11	1.13E-11	3.06E-11
Ecotoxicity	PAF*m^2·yr	1.83E-01	6.31E-02	5.56E-02	1.51E-02	4.94E-02
Acidification/ Eutrophication	PDF*m^2·yr	2.26E-02	1.01E-02	1.61E-03	2.92E-03	7.95E-03
Land use	PDF*m^2·yr	1.32E-02	2.70E-03	1.44E-03	1.06E-03	7.99E-03
Minerals	MJ surplus	2.39E-02	9.89E-03	9.35E-03	8.69E-04	3.80E-03
Fossil fuels	MJ surplus	1.53E+00	4.74E-01	5.61E-01	1.36E-01	3.58E-01

Weighting results by impact categories

The weighting results of the life cycle of commercial autoclaved aerated concrete by impact categories are exhibited in Figure 155 and Table 27. The fossil fuels has the highest harmful environmental impact from the obtaining of raw materials, manufacture, distribution and use stages, which concerned with the emission of remaining substances, stream, aluminium paste and the consumption of electricity, bituminous coal and diesel fuel as the main pollutants. Therefore, a difficulty of these stages contributes to also damage to human health and the decrease of the concentration of the mineral resources in the Earth's crust.

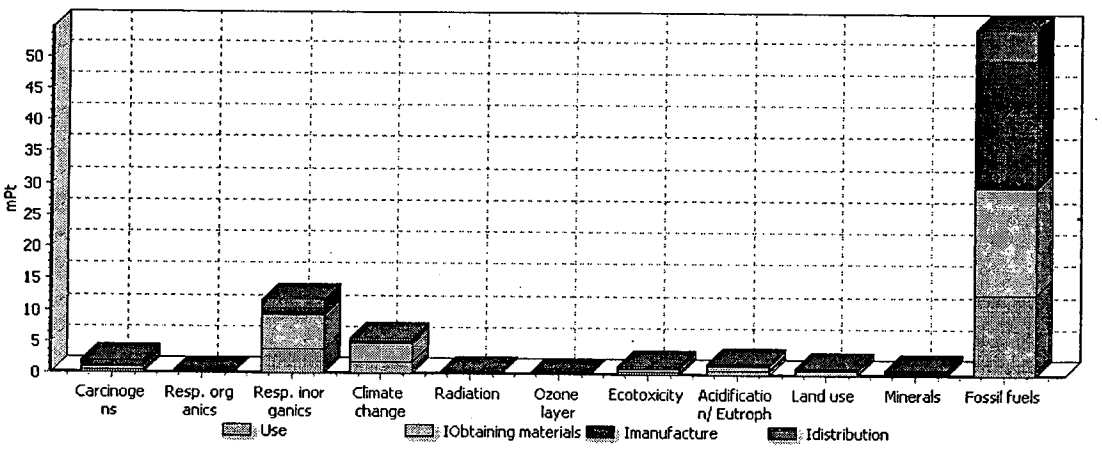

Figure 165 Impact assessment of Insee superblock AAC.

Table 37 Impact assessment of Insee superblock AAC

Impact category	Unit	Total	IObtaining materials	Imanufacture	Idistribution	Use
Total	Pt	7.90E-02	2.78E-02	2.37E-02	6.93E-03	2.06E-02
Carcinogens	Pt	1.96E-03	5.24E-04	9.73E-04	8.14E-05	3.80E-04
Resp. organics	Pt	1.60E-05	6.43E-06	2.40E-06	1.84E-06	5.33E-06
Resp. inorganics	Pt	1.16E-02	5.50E-03	1.16E-03	1.23E-03	3.75E-03
Climate change	Pt	5.54E-03	2.92E-03	4.83E-04	2.83E-04	1.85E-03
Radiation	Pt	1.34E-04	2.91E-05	6.95E-05	2.49E-06	3.25E-05
Ozone layer	Pt	2.08E-06	7.97E-07	4.65E-07	2.21E-07	5.98E-07
Ecotoxicity	Pt	1.43E-03	4.92E-04	4.33E-04	1.18E-04	3.85E-04
Acidification/ Eutrophication	Pt	1.76E-03	7.87E-04	1.25E-04	2.28E-04	6.20E-04
Land use	Pt	1.03E-03	2.11E-04	1.12E-04	8.30E-05	6.23E-04
Minerals	Pt	8.54E-04	3.53E-04	3.34E-04	3.10E-05	1.36E-04
Fossil fuels	Pt	5.46E-02	1.69E-02	2.00E-02	4.87E-03	1.28E-02

Single score results by damages categories

Single score results of the life cycle of commercial autoclaved aerated concrete by damages categories in all stages are shown in Figure 156 and Table 28. The obtaining materials stage contributes to the greatest environmental load where the damages to the human health and ecosystem quality show the highest value, about 35.2 % of the total impact at this stage. This behavior is largely produced the effect of the fossil fuels and respiratory effects of inorganic compounds (about 61% of the fossil fuels and approximately 19.8% of respiratory effects of inorganic compounds).

The obtaining material stage exhibits the highest contribution to the fossil fuels category with an emphasis on diesel consumption. The manufacture stage illustrates also the highest result in the fossil fuels category with an emphasis on electrical and coal consumption. The use stage exhibits also the highest contribution to the fossil fuels category with an emphasis on diesel consumption. Finally, the distribution stage illustrates the lowest results in all categories in comparison with the rest of the stages.

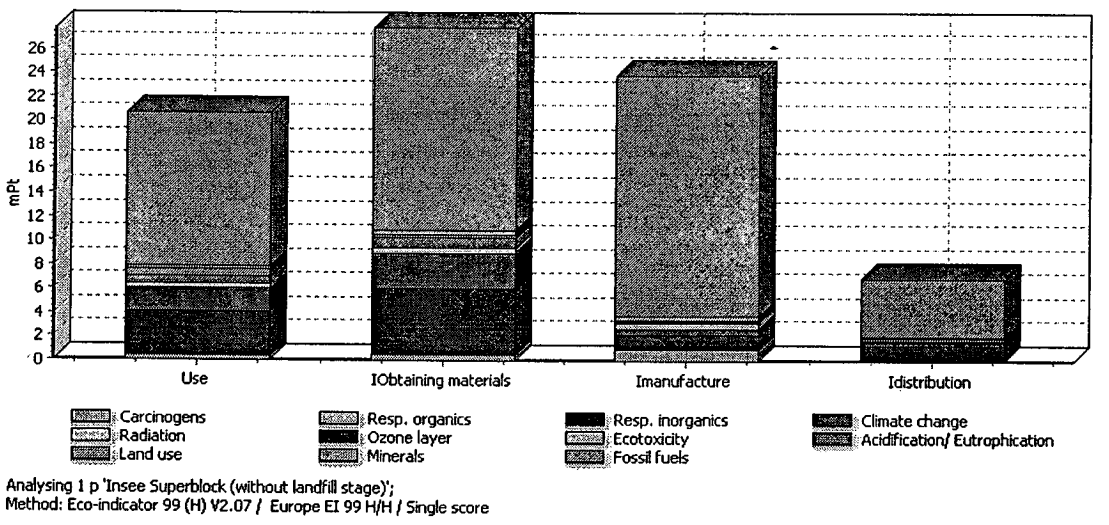

Figure 166 Impact assessment of Insee superblock AAC in the each procedure.

Table 38 Single value of Insee superblock AAC in the each procedure

Impact category	Unit	Total	IObtaining materials	Imanufacture	Idistribution	Use
Total	Pt	7.90E-02	2.78E-02	2.37E-02	6.93E-03	2.06E-02
Carcinogens	Pt	1.96E-03	5.24E-04	9.73E-04	8.14E-05	3.80E-04
Resp. organics	Pt	1.60E-05	6.43E-06	2.40E-06	1.84E-06	5.33E-06
Resp. inorganics	Pt	1.16E-02	5.50E-03	1.16E-03	1.23E-03	3.75E-03
Climate change	Pt	5.54E-03	2.92E-03	4.83E-04	2.83E-04	1.85E-03
Radiation	Pt	1.34E-04	2.91E-05	6.95E-05	2.49E-06	3.25E-05
Ozone layer	Pt	2.08E-06	7.97E-07	4.65E-07	2.21E-07	5.98E-07
Ecotoxicity	Pt	1.43E-03	4.92E-04	4.33E-04	1.18E-04	3.85E-04
Acidification/ Eutrophication	Pt	1.76E-03	7.87E-04	1.25E-04	2.28E-04	6.20E-04
Land use	Pt	1.03E-03	2.11E-04	1.12E-04	8.30E-05	6.23E-04
Minerals	Pt	8.54E-04	3.53E-04	3.34E-04	3.10E-05	1.36E-04
Fossil fuels	Pt	5.46E-02	1.69E-02	2.00E-02	4.87E-03	1.28E-02

Life cycle impact of average database of autoclaved aerated concrete

Characterization results

The characterization results of the life cycle of average database of autoclaved aerated concrete are shown in Figure 157 and Table 29. The obtaining of raw materials stage, manufacture stage, distribution stage and use stage are emphasized by the impact category of carcinogenesis, respiratory effects of organic compounds, respiratory effects of inorganic compounds, climate change, radiation, ozone layer, ecotoxicity, acidification/eutrophication, land use, mineral resources and fossil fuels. These harmful impacts are associated with air emissions, water and soil of some organic and inorganic compounds for example diesel, silica sand, aluminium paste, gypsum, light fuel, coal, titanium dioxide and disposal. Moreover, they caused from the process of transportation, and the production and consumption of electricity and stream.

The main pollutants of obtaining of raw materials, manufacture, distribution and use stages are largely caused to the respiratory effects of organic compounds, respiratory effects of inorganic compounds, climate change, radiation, ozone layer, acidification/eutrophication, land use, mineral resources and fossil fuels.

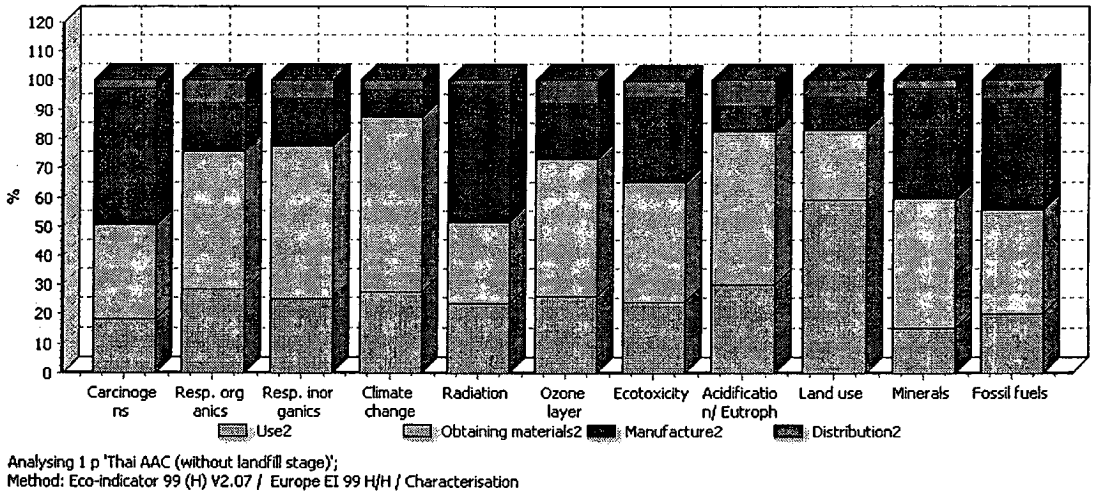

Figure 167 Impact assessment of average AAC in Thailand.

Table 39 Impact assessment of average database of AAC in Thailand

Impact category	Unit	Total	Obtaining materials2	Manufacture2	Distribution2	Use2
Carcinogens	DALY	9.74E-08	3.12E-08	4.57E-08	2.78E-09	1.77E-08
Resp. organics	DALY	8.11E-10	3.80E-10	1.35E-10	6.29E-11	2.34E-10
Resp. inorganics	DALY	6.64E-07	3.49E-07	1.07E-07	4.20E-08	1.66E-07
Climate change	DALY	3.23E-07	1.93E-07	3.05E-08	9.64E-09	8.97E-08
Radiation	DALY	6.78E-09	1.89E-09	3.20E-09	8.51E-11	1.60E-09
Ozone layer	DALY	1.01E-10	4.70E-11	1.96E-11	7.54E-12	2.65E-11
Ecotoxicity	PAF*m^2·yr	1.79E-01	7.39E-02	5.19E-02	1.01E-02	4.34E-02
Acidification/ Eutrophication	PDF*m^2·yr	2.25E-02	1.17E-02	2.00E-03	1.95E-03	6.79E-03
Land use	PDF*m^2·yr	1.26E-02	3.00E-03	1.42E-03	7.10E-04	7.50E-03
Minerals	MJ surplus	2.28E-02	1.02E-02	8.61E-03	5.79E-04	3.44E-03
Fossil fuels	MJ surplus	1.52E+00	5.42E-01	5.76E-01	9.10E-02	3.09E-01

Table 39 Impact assessment of average database of AAC in Thailand

Impact category	Unit	Total	Obtaining materials2	Manufacture2	Distribution2	Use2
Carcinogens	DALY	9.74E-08	3.12E-08	4.57E-08	2.78E-09	1.77E-08
Resp. organics	DALY	8.11E-10	3.80E-10	1.35E-10	6.29E-11	2.34E-10
Resp. inorganics	DALY	6.64E-07	3.49E-07	1.07E-07	4.20E-08	1.66E-07
Climate change	DALY	3.23E-07	1.93E-07	3.05E-08	9.64E-09	8.97E-08
Radiation	DALY	6.78E-09	1.89E-09	3.20E-09	8.51E-11	1.60E-09
Ozone layer	DALY	1.01E-10	4.70E-11	1.96E-11	7.54E-12	2.65E-11
Ecotoxicity	PAF*m^2·yr	1.79E-01	7.39E-02	5.19E-02	1.01E-02	4.34E-02
Acidification/ Eutrophication	PDF*m^2·yr	2.25E-02	1.17E-02	2.00E-03	1.95E-03	6.79E-03
Land use	PDF*m^2·yr	1.26E-02	3.00E-03	1.42E-03	7.10E-04	7.50E-03
Minerals	MJ surplus	2.28E-02	1.02E-02	8.61E-03	5.79E-04	3.44E-03
Fossil fuels	MJ surplus	1.52E+00	5.42E-01	5.76E-01	9.10E-02	3.09E-01

Weighting results by impact categories

Figure 158 and Table 30 exhibit the weighting results of the life cycle of average database of autoclaved aerated concrete in Thailand by impact categories, observing that the fossil fuels has the highest harmful environmental impact from the obtaining of raw materials, manufacture, distribution and use stages, justified by the emission of remaining substances, stream, aluminum paste and the consumption of electricity, bituminous coal and diesel fuel as the main pollutants. Therefore, a disadvantage of these stages contributes to also damage to human health and the decrease of the concentration of the mineral resources in the Earth's crust.

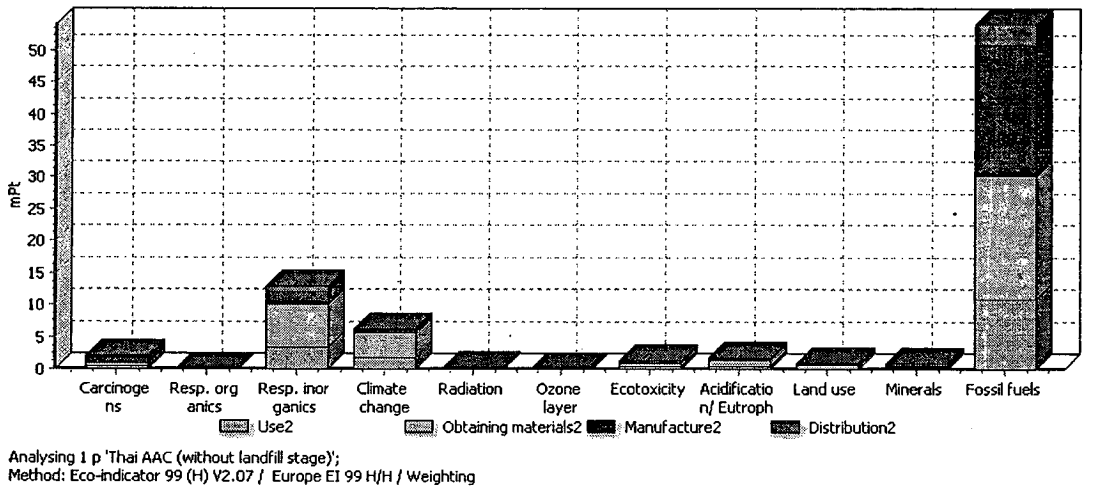

Figure 168 Impact assessment of average database of AAC in Thailand.

Table 40 Impact assessment of average database of AAC in Thailand

Impact category	Unit	Total	Obtaining materials2	Manufacture2	Distribution2	Use2
Total	Pt	8.05E-02	3.27E-02	2.52E-02	4.62E-03	1.80E-02
Carcinogens	Pt	1.90E-03	6.09E-04	8.92E-04	5.43E-05	3.46E-04
Resp. organics	Pt	1.58E-05	7.42E-06	2.63E-06	1.23E-06	4.57E-06
Resp. inorganics	Pt	1.30E-02	6.82E-03	2.09E-03	8.21E-04	3.24E-03
Climate change	Pt	6.31E-03	3.77E-03	5.95E-04	1.88E-04	1.75E-03
Radiation	Pt	1.32E-04	3.69E-05	6.25E-05	1.66E-06	3.13E-05
Ozone layer	Pt	1.97E-06	9.18E-07	3.83E-07	1.47E-07	5.18E-07
Ecotoxicity	Pt	1.40E-03	5.76E-04	4.05E-04	7.88E-05	3.38E-04
Acidification/ Eutrophication	Pt	1.75E-03	9.15E-04	1.56E-04	1.52E-04	5.30E-04
Land use	Pt	9.85E-04	2.34E-04	1.10E-04	5.54E-05	5.85E-04
Minerals	Pt	8.14E-04	3.63E-04	3.07E-04	2.07E-05	1.23E-04
Fossil fuels	Pt	5.42E-02	1.93E-02	2.06E-02	3.25E-03	1.10E-02

Single score results by damages categories

Figure 159 and Table 31 exhibit the single score results of the life cycle of average database of autoclaved aerated concrete by damages categories in all stages. The obtaining materials stage contributes to the greatest environmental load where the damages to the human health and ecosystem quality show the highest value, about 40.6.0 % of the total impact at this stage. This behavior is largely produced the effect of the fossil fuels and respiratory effects of inorganic compounds (about 59.2% of the fossil fuels and approximately 20.9% of respiratory effects of inorganic compounds).

The obtaining material stage exhibits the maximum contribution to the fossil fuels category with an emphasis on diesel consumption. The manufacture stage illustrates the maximum result in the fossil fuels category with an emphasis on electrical and coal consumption. The use stage shows the highest contribution to the fossil fuels category with an emphasis on diesel consumption. Lastly, the distribution stage shows the lowest results in all categories in comparison with the rest of the stages.

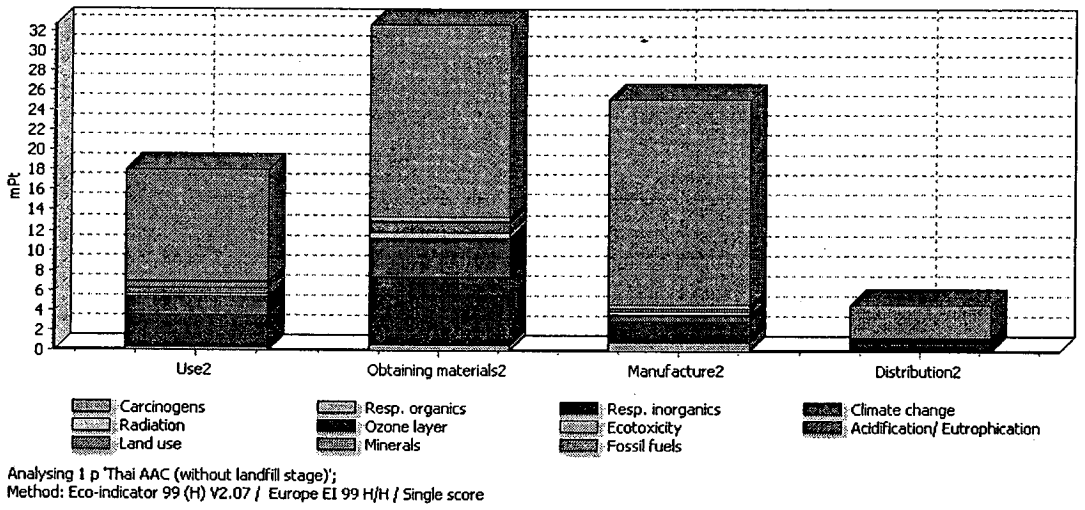

Figure 169 Impact assessment of average AAC of the each procedure in Thailand.

Table 41 Single score of the average database of AAC used in Thailand

Impact category	Unit	Total	Obtaining materials2	Manufacture2	Distribution2	Use2
Total	Pt	8.05E-02	3.27E-02	2.52E-02	4.62E-03	1.80E-02
Carcinogens	Pt	1.90E-03	6.09E-04	8.92E-04	5.43E-05	3.46E-04
Resp. organics	Pt	1.58E-05	7.42E-06	2.63E-06	1.23E-06	4.57E-06
Resp. inorganics	Pt	1.30E-02	6.82E-03	2.09E-03	8.21E-04	3.24E-03
Climate change	Pt	6.31E-03	3.77E-03	5.95E-04	1.88E-04	1.75E-03
Radiation	Pt	1.32E-04	3.69E-05	6.25E-05	1.66E-06	3.13E-05
Ozone layer	Pt	1.97E-06	9.18E-07	3.83E-07	1.47E-07	5.18E-07
Ecotoxicity	Pt	1.40E-03	5.76E-04	4.05E-04	7.88E-05	3.38E-04
Acidification/ Eutrophication	Pt	1.75E-03	9.15E-04	1.56E-04	1.52E-04	5.30E-04
Land use	Pt	9.85E-04	2.34E-04	1.10E-04	5.54E-05	5.85E-04
Minerals	Pt	8.14E-04	3.63E-04	3.07E-04	2.07E-05	1.23E-04
Fossil fuels	Pt	5.42E-02	1.93E-02	2.06E-02	3.25E-03	1.10E-02

Comparison of weighting results of autoclaved aerated concrete in the three conditions

The weighting results of the life cycle of autoclaved aerated concrete in the three conditions are exhibited in Figure 160 and Table 32. These observed that the fossil fuels in the life cycle of autoclaved aerated concrete in the three conditions have the highest harmful environmental impact from the obtaining of raw materials, manufacture, distribution and use stages. These activities corresponded to the emission of remaining substances, stream, aluminium paste and the consumption of electricity, bituminous coal and diesel fuel as the main pollutants. Therefore, a difficulty of these stages contributes to also damage to human health and the decrease of the concentration of the mineral resources in the Earth's crust.

The weighting results of the life cycle of autoclaved aerated concrete in the three conditions are the similar except for fossil fuels, respiratory effects of inorganic compounds and climate change. With comparing in the part of fossil fuels, the life cycle of commercial autoclaved aerated concrete has the highest harmful impact while that of improved autoclaved aerated concrete has the least harmful impact. These results may be associated with different electrical consumption in the part of the manufacturer because of the ancient machines and different distance of transportation. With comparing in the part of respiratory effects of inorganic compounds and climate change, the life cycle of average database of autoclaved aerated concrete has the highest harmful impact while that of improved autoclaved aerated concrete has the least harmful impact. Lower harmful impact in the part of respiratory effects of inorganic compounds and climate change of life cycle of improved autoclaved aerated concrete has the cause from the raw material replacement by sugar sediment waste.

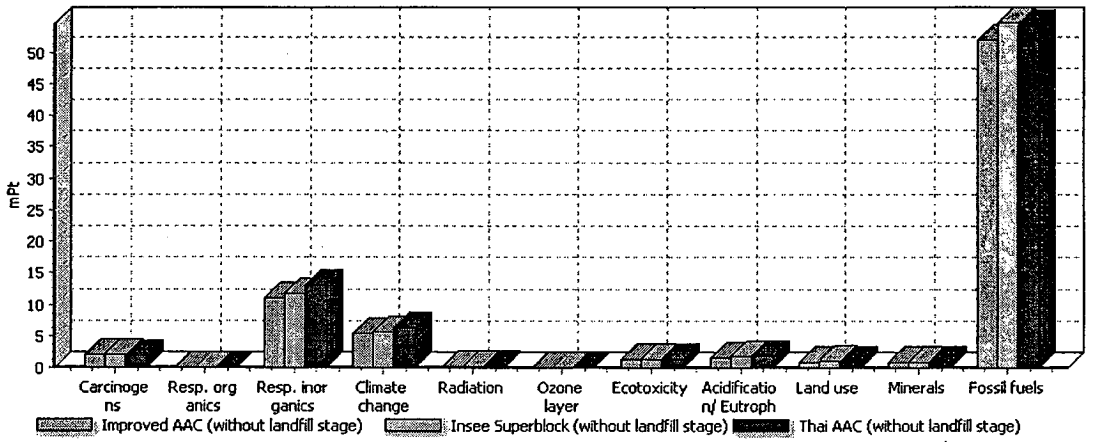

Figure 170 Impact assessment of average AAC of the each procedure in Thailand.

Table 42 Impact assessment of AAC in the three conditions

Impact category	Unit	Improved AAC	Insee Superblock AAC	Thai AAC
Total	Pt	7.51E-02	7.90E-02	8.05E-02
Carcinogens	Pt	1.92E-03	1.96E-03	1.90E-03
Resp. organics	Pt	1.50E-05	1.60E-05	1.58E-05
Resp. inorganics	Pt	1.10E-02	1.16E-02	1.30E-02
Climate change	Pt	5.38E-03	5.54E-03	6.31E-03
Radiation	Pt	1.32E-04	1.34E-04	1.32E-04
Ozone layer	Pt	1.96E-06	2.08E-06	1.97E-06
Ecotoxicity	Pt	1.37E-03	1.43E-03	1.40E-03
Acidification/ Eutrophication	Pt	1.64E-03	1.76E-03	1.75E-03
Land use	Pt	9.89E-04	1.03E-03	9.85E-04
Minerals	Pt	8.38E-04	8.54E-04	8.14E-04
Fossil fuels	Pt	5.18E-02	5.46E-02	5.42E-02